


The Gamma-ray Bursts fundamental plane correlation as a cosmological tool.

M. G. Dainotti^{1,2,3} *, A. Ł. Lenart⁴, A. Chraya⁵, G. Sarracino^{6,7}, S. Nagataki^{8,9}, N. Fraija¹⁰, S. Capozziello^{6,7,11}, M. Bogdan¹²

¹National Astronomical Observatory of Japan, 2 Chome-21-1 Osawa, Mitaka, Tokyo 181-8588, Japan

²The Graduate University for Advanced Studies (SOKENDAI), 2-21-1 Osawa, Mitaka, Tokyo 181-8588, Japan

³Space Science Institute, Boulder, Colorado

⁴Astronomical Observatory, Jagiellonian University, ul. Orła 171, 31-501 Kraków, Poland

⁵Department of Physical Sciences, Indian Institute of Science Education and Research (IISER) Mohali, Sector 81, SAS Nagar, Punjab 140306, India

⁶SDipartimento di Fisica, “E. Pancini” Università “Federico II” di Napoli, Compl. Univ. Monte S. Angelo Ed. G, Via Cinthia, I-80126 Napoli (Italy)

⁷INFN Sez. di Napoli, Compl. Univ. Monte S. Angelo Ed. G, Via Cinthia, I-80126 Napoli (Italy)

⁸Interdisciplinary Theoretical & Mathematical Science Program, RIKEN (iTHEMS), 2-1 Hirosawa, Wako, Saitama, Japan 351-0198

⁹RIKEN Cluster for Pioneering Research, Astrophysical Big Bang Laboratory (ABBL), 2-1 Hirosawa, Wako, Saitama, Japan 351-0198

¹⁰Instituto de Astronomía, Universidad Nacional Autónoma de México, Apdo. Postal 70-264, Cd. Universitaria, Ciudad de México 04510

¹¹Scuola Superiore Meridionale, Università di Napoli Federico II Largo San Marcellino 10, 80138 Napoli (Italy)

¹²University of Wrocław, plac Grunwaldzki 2/4, Wrocław, Lower Silesia Province, 50-384, Poland.

Accepted XXX. Received YYY; in original form ZZZ

ABSTRACT

Cosmological models and their corresponding parameters are widely debated because of the current discrepancy between the results of the Hubble constant, H_0 , obtained by SNe Ia, and the Planck data from the Cosmic Microwave Background Radiation. Thus, considering high redshift probes like Gamma-Ray Bursts (GRBs) is a necessary step. However, using GRB correlations between their physical features to infer cosmological parameters is difficult because GRB luminosities span several orders of magnitude. In our work, we use a 3-dimensional relation between the peak prompt luminosity, the rest-frame time at the end of the X-ray plateau, and its corresponding luminosity in X-rays: the so-called 3D Dainotti fundamental plane relation. We correct this relation by considering the selection and evolutionary effects with a reliable statistical method, obtaining a lower central value for the intrinsic scatter, $\sigma_{int} = 0.18 \pm 0.07$ (47.1 %) compared to previous results, when we adopt a particular set of GRBs with well-defined morphological features, called the platinum sample. We have used the GRB fundamental plane relation alone with both Gaussian and uniform priors on cosmological parameters and in combination with SNe Ia and BAO measurements to infer cosmological parameters like H_0 , the matter density in the universe (Ω_M), and the dark energy parameter w for a w CDM model. Our results are consistent with the parameters given by the Λ CDM model but with the advantage of using cosmological probes detected up to $z = 5$, much larger than the one observed for the furthest SNe Ia.

Key words: Gamma rays: general; Supernovae: general; Distance scale; cosmological parameters

1 INTRODUCTION

Gamma-Ray Bursts (GRBs) are incredibly powerful phenomena: they are the brightest objects after the Big Bang, as well as one of the farthest astrophysical objects ever detected (Paczynski 1986; Piran 2004; Kumar & Zhang 2015). These features allow us to use them as cosmological tools, similar to what has been achieved for Supernovae Type Ia (SNe Ia, Riess et al. (1998)). Because of their high luminosity, GRBs can be observed up to very large distances, corresponding to high redshifts. Indeed, GRBs have been observed up to $z = 8.2$ and $z = 9.4$ (Tanvir et al. 2009; Cucchiara et al. 2011), while SNe Ia has only been observed up to $z = 2.26$ (Rodney et al. 2015). Using GRBs as cosmological tools requires a full understanding of their physical mechanisms. Both their energy emission mechanisms and progenitors are still being studied by the scientific community. For their birth, there is a general consensus on two different main scenarios: the explosion of a very massive star at the end of its lifetime (Narayan et al. 1992; Woosley et al. 1993; MacFadyen & Woosley 1999; Nagataki et al. 2007; Nagataki 2009, 2011), followed by a core-collapse SNe (Staneke et al. 2003; MacFadyen et al. 2001) or the coalescence of two compact objects, like black holes (BHs) or neutron stars (NSs) (Lattimer & Schramm 1976; Eichler et al. 1989; Li & Paczyński 1998; Rowlinson et al. 2014; Rea et al. 2015; Stratta et al. 2018). The most probable frameworks for the central engine that powers the GRB

consider the following astrophysical objects: BHs, NSs, or fast spinning newly born highly magnetized NSs magnetars, (Usov (1992); Liang et al. (2018); Ai et al. (2018); Komissarov and Barkov (2007); Barkov and Komissarov (2008)).

To identify the different possible natures of their origin, it is necessary to classify GRBs according to their observable features. A general paradigm divides GRB light curves (LCs) into a rapid prompt energy emission followed by a longer emission phase called the afterglow. The afterglow is usually detected in X-ray, optical, and also radio wavelengths (Sari et al. 1998; O’Brien et al. 2006; Sakamoto 2007; Perley et al. 2014; Li et al. 2015; Morsony et al. 2016; Warren et al. 2017, 2018). We usually detect the prompt emission of GRBs in high-energy bands, like from X-rays up to ≥ 100 MeV γ -rays, but sometimes they have been observed in the optical band as well (Fraija & Veres 2018; Panaitescu & Vestrand 2011; Fraija et al. 2020b).

A first categorization divides GRBs into Short and Long, depending on the duration of their prompt emission: $T_{90} \leq 2$ s or $T_{90} \geq 2$ s¹, respectively (Mazets et al. 1981; Kouveliotou et al. 1993). There is a very strong association between the prompt duration and the progenitor of GRBs: indeed, the majority of Long GRBs originate from the core collapse of a very massive star, while Short GRBs are born by the merging of two compact objects (Abbott et al. 2017; Troja et al. 2017; Zhang et al. 2006; Ito et al. 2015, 2021). A new classification of GRBs according to their progenitor mechanism has been proposed (Zhang et al. 2006): Type I GRBs are the ones born by the merging of two compact objects, while Type II are the ones born by the core collapse of very massive stars. Their progenitors can be inferred from morphological and physical characteristics.

The plateau phase of GRBs is a flat part of the GRB LC following the prompt phase, and it was discovered by the *Neil Gehrels Swift Observatory* (*Swift*) (O’Brien et al. 2006; Sakamoto 2007; Willingale et al. 2007). The duration of this plateau usually ranges from 10^2 to 10^5 s, after which a power-law (PL) decay phase is observed. Several scenarios describe the plateau, such as the external shock model, according to which the shock front between the ejecta of the emission and the interstellar medium is powered by a long-lasting energy emission from the central engine (Zhang et al. 2006), or due to the spin-down of a new-born magnetar (Stratta et al. 2018; Fraija et al. 2020).

In the past decades many efforts have been performed by the scientific community in order to find possible correlations between physical features of GRBs. Regarding correlations involving only the prompt features we cite, among the others, the relation between the peak in the νF_ν spectrum, E_{peak} the isotropic energy in the prompt emission, E_{iso} (Amati et al. 2002); and the one between E_{peak} and the isotropic prompt luminosity L_{iso} (Yonetoku et al. 2004; Ito et al. 2019). We also mention the correlations between the collimated-corrected energy $E_{jet} = E_{iso} \times (1 - \cos\theta)$ where θ is the jet opening angle and E_{peak} found by Ghirlanda et al. (2004); the one found by Liang & Zhang (2005) between E_p , E_{iso} , and the break time of the optical afterglow LCs, t_b . The last two correlations, even if they involve prompt features, introduce the jet-break time, which can also be inferred from the X-ray afterglow, which in some cases can include a plateau.

Several other correlations directly involving the plateau (Dainotti et al. 2008, 2013b, 2015a, 2016; Liang et al. 2010; Bernardini et al. 2012a; Xu & Huang 2012; Margutti et al. 2013; Zaninoni et al. 2016; Shun-Kun et al. 2018; Tang et al. 2019; Zhao et al. 2019; Srinivasaragavan et al. 2020; Wen et al. 2020) and their applications as cosmological probes (Cardone et al. 2010; Postnikov et al. 2014; Dainotti et al. 2013a; Izzo et al. 2015) have been presented. For a more extensive discussion on the prompt, prompt-afterglow relations, their selection biases and the application as cosmological tools see Dainotti & Del Vecchio (2017); Dainotti & Amati (2018); Dainotti et al. (2018). One of these correlations is the so-called Dainotti relation, which links the time at the end of the plateau emission measured in the rest frame, T_X^* , with the corresponding X-Ray luminosity of the LC, L_X (Dainotti et al. 2008), see Equation 2. This correlation is theoretically supported by the magnetar model (Dall’Osso et al. 2011; Bernardini et al. 2012b; Rowlinson et al. 2014). Its extension in three dimensions has been discovered by adding the prompt peak luminosity, L_{peak} (Dainotti et al. 2016, 2017c) and is known as the fundamental plane correlation or the 3D Dainotti relation.²

To use this relation as a cosmological tool we selected a GRB sample with well-defined morphological properties and almost flat plateaus, called the platinum sample, which was introduced in Dainotti et al. (2020a), and whose properties are detailed in Sec. 2. We clarify that, following a well-established approach in the realm of the SNe Ia cosmology in which only the golden SNe Ia LCs are taken (see Scolnic et al. (2018)), we choose a well-defined sample. This is built in the observer frame and not in the rest-frame - namely, the LCs are in the fluxes versus time parameter space. This means that there is no involvement of cosmological parameters in this selection of the LCs. Therefore there is no circularity problem involved in the application of this sample for cosmological use. We correct this correlation for evolutionary effects due to the redshift and selection biases, as done in Dainotti et al. (2020a), to infer cosmological parameters, such as the Hubble constant H_0 , the current mass density of the universe, Ω_M , and the dark energy parameter, w , for a w CDM model, together with other cosmological probes like the SNe Ia and the Baryon Acoustic Oscillations (BAO). Indeed, the evolution of the cosmological parameters is a vital topic and it has

¹ T_{90} is the time during which a GRB ejects from 5% to 95% of its total measured photons during the prompt phase

² We note that we are referring to the fundamental plane correlation related to GRBs, and not to other definitions of fundamental planes used in astronomy, such as the fundamental plane of elliptical galaxies (Djorgovski & Davis 1987)

been discussed especially in relation to H_0 . It has been highlighted even for the SNe Ia by [Dainotti et al. \(2021a\)](#) and [Dainotti et al. \(2022d\)](#) that there is an evolutionary trend on H_0 as a function of the redshift, which can be possibly explained either with selection biases or with a new physics (i.e., invoking the so-called $f(R)$ -gravity theory). For a general review on the Hubble constant tension see [Abdalla et al. \(2022\)](#).

In Sec. 2 the criteria used for the sample selection of the GRB data are detailed. In Sec. 3 we show the GRB fundamental plane both with and without correcting for evolutionary effects and selection biases. In Sec. 4 we study the evolutionary parameters as a function of cosmology. In Sec. 5 we apply the fundamental plane as a cosmological tool. Our results are shown in Sec. 6. In Sec. 7 we present a comparison between the results obtained using GRBs alone versus the SNe Ia and SNe Ia + BAO sets. In Sec. 8 we discuss the future use of GRBs as standalone probes. Finally, our conclusions are discussed in Sec. 9.

2 SAMPLE SELECTION

We take into account the GRBs which can be described by the [Willingale et al. \(2007\)](#) phenomenological model using the BAT + XRT LCs gathered from the Swift web page repository ([Evans et al. 2009, 2010](#))³. We fit this sample with the Willingale functional form for $f(t)$, which reads as follows:

$$f(t) = \begin{cases} F_i \exp\left(\alpha_i \left(1 - \frac{t}{T_i}\right)\right) \exp\left(-\frac{t}{t_i}\right) & \text{for } t < T_i \\ F_i \left(\frac{t}{T_i}\right)^{-\alpha_i} \exp\left(-\frac{t}{t_i}\right) & \text{for } t \geq T_i, \end{cases} \quad (1)$$

modelled for both the prompt (index ‘i=p’) γ -ray and initial hard X-ray decay and for the afterglow (‘i=X’), so that the complete LC $f_{tot}(t) = f_p(t) + f_X(t)$ contains two sets of four free parameters (T_i, F_i, α_i, t_i), where α_i is the temporal power law (PL) decay index and T_i is the end time of the prompt and the plateau emission, respectively, while the time t_i is the initial rise timescale. The transition from the exponential to PL occurs at the point $(T_i, F_i e^{-T_i/T_i})$, where the two functions have the same value and this point marks the beginning of the plateau. Using these criteria, we fit 222 LCs. The peak prompt luminosity at 1 second, L_{peak} , and the X-ray luminosity measured in the final part of the plateau phase, L_X , have been calculated as follows:

$$L = 4\pi D_L^2(z) F(E_{min}, E_{max}, T_X^*) \cdot K. \quad (2)$$

To calculate L_{peak} one substitutes the flux F with F_{peak} which is the γ -ray flux in 1 s interval ($erg\ cm^{-2}\ s^{-1}$) measured at the peak of the prompt emission, while to calculate L_X , one uses the flux F_X , measured in X-rays at the end of the plateau; $D_L(z)$ is the luminosity distance computed for a particular redshift in the flat Λ CDM cosmological model, according to which we have an energy equation of state $w = -1$, $\Omega_M = 0.3$, and $H_0 = 70\ Km\ s^{-1}\ Mpc^{-1}$; T_X^* is the time measured in the rest frame at the end of the plateau, and K is the K -correction for the cosmic expansion ([Bloom et al. 2001](#)). For GRBs whose spectrum is fitted by a simple PL this correction is given by $K = (1+z)^{(\beta-1)}$, where β is the spectral index of the plateau in the X-ray band ([Evans et al. 2009, 2010](#)).

The Platinum Sample ([Dainotti et al. 2020a](#)) is a subset of the Gold Sample, the latter being defined in [Dainotti et al. \(2016\)](#) and inspired by similar samples presented in the literature ([Xu & Huang 2012; Tang et al. 2019](#)). To define the Gold Sample, we consider the following requirements for the plateau: 1) its beginning, defined by the quantity T_i , must have at least five data points; 2) its inclination must be $< 41^\circ$, this latter criterion is adopted in [Dainotti et al. \(2016\)](#) on the Gold Sample, where a Gaussian distribution fit the plateau angles, and the outliers are beyond the threshold of 41° .

To build the Platinum Sample, we also add the following requirements for the plateau: 3) its end time T_X must not fall within observational gaps of the LCs to allow us the determination of this quantity directly from the data and not from the LC fitting; 4) it should last at least 500 s; and 5) should not present flares at its start or during the entire duration of the plateau itself (refining the idea of [Xu & Huang \(2012\)](#)).

Using these criteria, the platinum sample is composed of 50 GRBs out of the 222 plateaus analyzed. The furthest GRB in this sample is at $z = 5$.

Regarding the SNe Ia data, we use the Pantheon sample ([Scolnic et al. 2018](#)), a set composed of 1048 SNe Ia collected by different surveys spanning from $z = 0.01$ up to $z = 2.26$.

It is important to note that the criteria defining our sample are objectively determined before the construction of the correlations sought; sample cuts are introduced strictly following either data quality or physical class constraints.

³ http://www.swift.ac.uk/burst_analyser. We follow the criteria for the GRB sample selection considered in [Srinivasaragavan et al. \(2020\)](#) and [Dainotti et al. \(2020a\)](#), and we use the platinum sample detailed in [Dainotti et al. \(2020a\)](#).

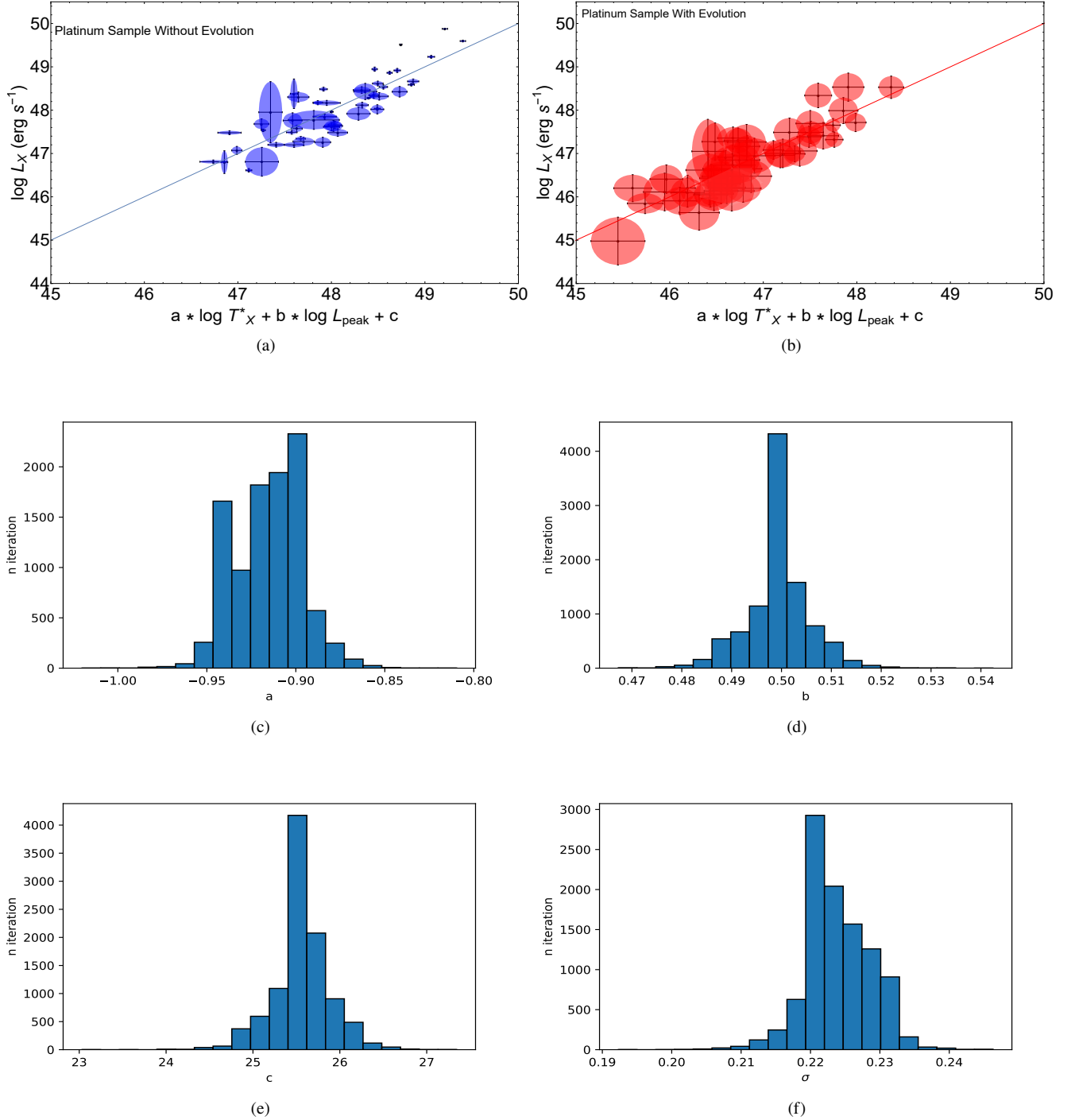


Figure 1. Top panels: the 2D projections of the fundamental plane related to the platinum sample without correcting for redshift evolution (1a), and with the corrections for selection and evolutionary effects (1b). Panels 1c, 1d, 1e and 1f: Histograms of the parameters a , b , c , and σ_{int} evaluated from the simulation of evolutionary coefficients taken from the 1σ range.

3 THE 3D RELATION FOR THE PLATINUM GAMMA-RAY BURSTS

In order to robustly apply any GRB correlation as a cosmological tool we need to have a reliable model supporting the theoretical scenario, like what has been done for SNe Ia. We also have to note that even if there is a very clear idea on the birth of the SNe Ia after the complete disruption of the accreted white dwarf in a binary system, there is still a debate on the particular mechanism that originates the SN explosion (Livio & Mazzali 2018). A possible example of a model that can satisfactorily explain the plateau, which we have pinpointed in Sec. 1, is the magnetar model. Indeed, the intrinsic scatter, σ_{int} , of the correlation, and the errors on the parameters can be derived directly from the values of the periods of the spin and the magnitude of the magnetic

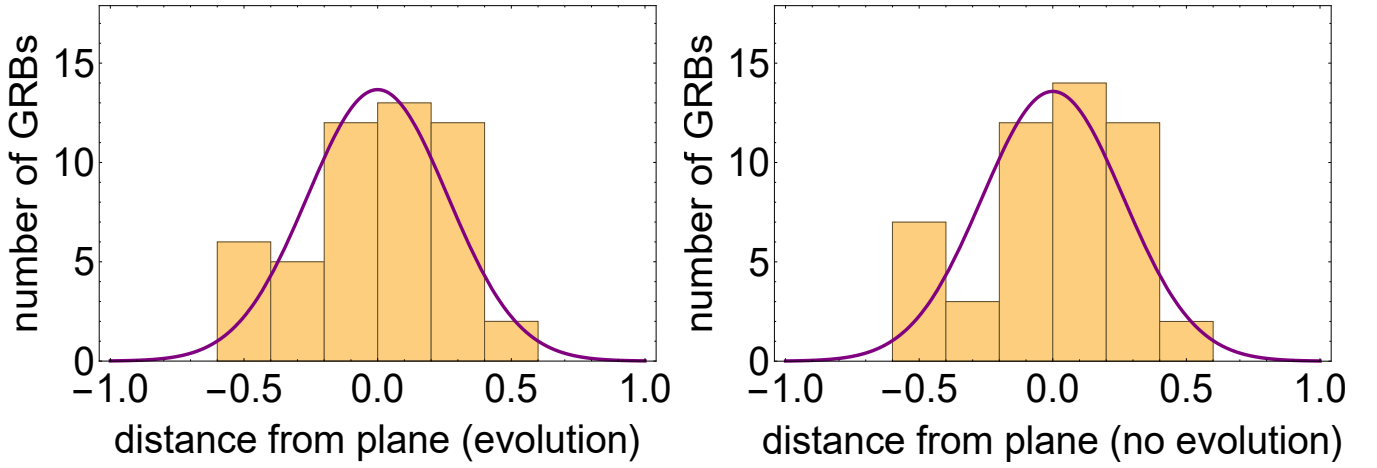


Figure 2. The distributions of distances of the Platinum sample from the 3D fundamental plane with and without correction for evolution with their fitted Gaussian distributions.

fields representative of the magnetar. Thus, the slope and the intercept of the $L_X - T_X^*$ relation are naturally derived from the equation of the magnetar (Rowlinson et al. 2014; Stratta et al. 2018), which links L_X to T_X^* using physical quantities of the astrophysical object, such as the moment of inertia and the spin period through the following equations:

$$L_{0,49} \propto B_{p,15}^2 P_{0,3}^{-4} R_6^6, \quad (3)$$

$$T_{em,3} = 2.05 I_{45} B_{p,15}^2 P_{0,-3}^2 R_6^{-6}. \quad (4)$$

In Equations 3 and 4, $L_{0,49}$ is the plateau luminosity in $10^{49} \text{ erg s}^{-1}$, I_{45} is the moment of inertia in units of 10^{45} g cm^2 , $B_{p,15}$ is the magnetic field strength at the poles in units of 10^{15} G , R_6 is the radius of the neutron star in 10^6 cm and $P_{0,-3}$ is the spin period in milliseconds. If we substitute in Equation 3 the radii from Equation 4 we obtain the following:

$$\log L_0 \propto (\log(10^{52} I_{45}^{-1} P_{0,-3}^2) - \log(T_{em})), \quad (5)$$

where it is possible to see immediately that the first term is a constant for a given fixed period of the magnetar and momentum of inertia, and the luminosity is inversely correlated with the rest frame time at the end of the plateau emission. However, there are additional explanations for the plateau emission and the existence of the $L_{peak} - L_a$ relation, which can be ascribed to the external forward shock model by changing the microphysical parameters (Hascoet et al. 2014). In addition, in Stratta et al. (2018) the properties of the Dainotti 3D relation are explained through the anti-correlation between L_{peak} and the spin period within the model of the pulsar spin-down described in Contopoulos & Spitkovsky (2006).

Having stressed that this correlation and the 3D extension can be supported reliably within the magnetar scenario, we can safely proceed with the description of the procedure for using this correlation as a cosmological tool. We leave the parameters a , b , c of the fundamental plane free to vary and we fit the correlation using the D’Agostini (2005) Bayesian method. In the paper the uncertainties on our computed values are always be quoted in 1σ . The luminosities and times carry error bars which are comparable, namely the $\frac{\Delta_x}{x}$ and $\frac{\Delta_y}{y}$ are of the same order of magnitude, where Δ_x is the error on the x-axis (error on time in our case) and Δ_y is the error on y axis (luminosity at the end of the plateau phase in our case). Thus, it is necessary to adopt methods which take into account both error bars like the D’Agostini (2005). The fundamental plane relation has the following form:

$$\log L_X = c + a \cdot \log T_X^* + b \cdot (\log L_{peak}), \quad (6)$$

where a and b are the best-fit parameters given by the D’Agostini (2005) procedure linked to $\log T_X^*$ and $\log L_{peak}$, respectively, while c is the normalization. The best fit results are: $a = -0.86 \pm 0.13$, $b = 0.56 \pm 0.12$, $c = 21.8 \pm 6.3$, and $\sigma_{int} = 0.34 \pm 0.04$. We stress that if we had an ad hoc choice of the sample we would not have had any outliers from the distribution of the geometric distances of any point from the fundamental plane, while it is clear from the distribution of the distance from the platinum plane that we have several GRBs at distance -0.5 which are outliers from the distribution of the GRBs from the plane itself.

The role of the corrections due to selection biases and evolutionary effects has been studied for the $L_X - T_X^*$ (Dainotti et al. 2013b) and for the $L_X - L_{peak}$ relations (Dainotti et al. 2015b, 2017b). Indeed, each physical feature, L_X , T_X^* and L_{peak} , is affected by selection biases due to instrumental thresholds and redshift evolution of the variables involved in the correlations. To correct these effects for each variable, we employ the Efron & Petrosian (1992) method, which tests the statistical dependence among L_X , T_X^* and L_{peak} , see Dainotti et al. (2013b, 2015b, 2017b); Petrosian et al. (2015).



Figure 3. Paired smoothed histograms of the σ_{int} obtained for cases with and without evolution with different methods using the HyperFit online routine. The thin black horizontal lines indicate the central value of the σ_{int} parameter from the D’Agostini fitting, while the red ones correspond to the 1σ error bars.

The fundamental plane correlation, once the selection effects are considered, becomes:

$$\log L_X - k_{L_a} \log(z+1) = a_{ev} \cdot (\log T_X^* - k_{T_X} \log(z+1)) + b_{ev} \cdot (\log L_{peak} - k_{L_{peak}} \log(z+1)) + c_{ev}, \quad (7)$$

where a_{ev} , b_{ev} , and c_{ev} denote the parameters with redshift evolution. With evolution we define the dependence of the parameters on the redshift. The $k_{L_{peak}}$, k_{T_X} , and k_{L_a} are the evolutionary coefficients computed by us for the whole sample of 222 GRBs: $k_{L_{peak}} = 2.24^{+0.30}_{-0.30}$, $k_{T_X} = -1.25^{+0.28}_{-0.27}$, $k_{L_a} = 2.42^{+0.41}_{-0.74}$. Comparing these results with the ones obtained in the literature, we note that the evolution on L_{peak} is compatible within 1σ , the evolution on T_a^* is compatible within 1.6σ , while the L_a evolution is compatible within 1.8σ with the ones taken from [Dainotti et al. \(2017b\)](#) and used in [Dainotti et al. \(2020a\)](#).

To verify the reliability of our results, we simulated random values of the power-law coefficients of the evolution, $k_{L_{peak}}$, k_{T_X} , k_{L_a} drawn from uniform distributions within the 1σ error range. For our best-fit computations of the Dainotti 3D relation we used the [D’Agostini \(2005\)](#) and [Reichart \(2001\)](#) methods (the latter considers a slightly different likelihood, but still includes σ_{int} , like the D’Agostini one) with the same minimization algorithm. To further ensure the reliability of our results, we repeated this procedure 1000 times finding that the results from these two computations are compatible within 1σ . The results of minimization of the D’Agostini likelihood are shown in the central and bottom panels of Fig. 1. Considering these effects, the new best-fit parameters for the fundamental plane of the platinum sample are $a_{ev} = -0.85 \pm 0.12$, $b_{ev} = 0.49 \pm 0.13$, $c_{ev} = 25.4 \pm 6.9$, and $\sigma_{int} = 0.18 \pm 0.09$. We note that [Rowlinson et al. \(2014\)](#) predicts that the a coefficient of the $\log L_X - \alpha \log(z+1) \propto \log T_X^* - \beta \log(z+1)$ relation should be $a_{theoretical} = -1$, which is compatible with our results within 1.3σ error range. The central value of the intrinsic scatter is 47.1% smaller than the one computed for the original fundamental plane.

We compare the two intrinsic scatters obtained with and without considering the corrections due to the EP method using the following formula, adapted from [Dainotti et al. \(2020a\)](#):

$$x = \frac{\sigma_{int, NoEV} - \sigma_{int, EV}}{\sqrt{\sigma_{\sigma_{int, NoEV}}^2 + \sigma_{\sigma_{int, EV}}^2}}. \quad (8)$$

We obtain $x = 1.98$, meaning that the evolutionary effects do indeed reduce the intrinsic scatter on the platinum fundamental plane correlation in a significant way. We also show in Fig. 2 the distances of each data point belonging to the Platinum sample with respect to the best fit of the fundamental plane, both with the evolutionary effects (left panel) and without them (right panel). The 2D projections of both fundamental planes are shown in the top panels of Fig. 1. These figures allow us to show how the error bars for each GRB shown with the ellipses are placed around the plane when we correct for selection biases and redshift evolution (right upper panel) and when we do not correct for them (left upper panel). We note that when the correction for evolution is

applied, the data points are closer to the plane including the errorbars, and fewer outliers are present compared to the situation in which the evolution is not taken into account. To compare these two relations we computed for both cases the Akaike information criterion (AIC) and the model weight: $B_i = e^{\frac{AIC_{min} - AIC_i}{2}}$ for each relation, where $AIC_{min} = MIN(AIC_{evolution}, AIC_{noev})$, and AIC_i is the AIC value corresponding to the relation for which the B parameter is computed. For each model we computed the “relative likelihood”: $P_i = \frac{B_i}{\sum_j B_j}$, obtaining $P_{evolution} = 0.99$ and $P_{noev} = 0.01$. Thus, the model with evolution is favoured compared to the one without evolution.

To further confirm the reliability of our results and their independence for the particular Bayesian method adopted we performed other best fit procedures for the fundamental plane, both with and without evolution. We also used the Reichart (2001) method, which we recall is another Bayesian approach which takes also into account of both error bars, obtaining best fit results compatible within 1σ to the D’Agostini ones, and an online fitting procedure called “HyperFit” (<https://hyperfit.icrar.org/>) based on Robotham & Obreschkow (2015), built to obtain the best-fit of linear models that consider heteroscedastic errors for multidimensional data using Bayesian inference. The latter tool offers the possibility to employ different algorithms and methods, which we used to compute a smoothed paired histogram of the σ_{int} obtained for each case, with and without evolution, presented in Fig. 3. The values obtained with the D’Agostini (2005) method are consistent with these histograms. Specifically, we add a black line indicating the mean value of σ_{int} and red lines indicating the error on σ_{int} obtained by the D’Agostini (2005) method. We also applied other best fit methods: the Principal Component Analysis, PCA, the PC Regression (PCR, Liu et al. (2003)), and the Partial Least Squares (PLS), where the latter two are regression methods based on PCA. For PCA we found: $a = -1.19$, $b = 0.44$, $c = 28.87$ and $a_{ev} = -1.17$, $b_{ev} = 0.49$, $c_{ev} = 26.75$ for the no evolution and the evolution cases, respectively. When comparing the PCA results with the D’Agostini (2005) ones for the non-evolution case the parameters a , b , and c are within 2.5, 1, and 1.1σ , respectively; for the evolution case b_{ev} and c_{ev} are consistent in 1σ , while a_{ev} is consistent in 2.7σ . The PCA fitting does not account for the error bars, thus does not consider the intrinsic scatter that is instead computed by the Bayesian methods of D’Agostini (2005) and Reichart (2001). This drives the difference in the results. For PCR and PLS we used the bootstrapping technique to infer the errors on the best fit parameters. These methods are consistent with the D’Agostini ones in 1σ , thus giving more reliability to our conclusions.

4 THE STUDY OF THE EVOLUTIONARY PARAMETERS AS A FUNCTION OF COSMOLOGY

The reliability of this procedure has already been proven via Monte Carlo simulations (Dainotti et al. 2013b). To correct for the evolution we use $g(z) = 1/(1+z)^k$, where the k parameter mimics the evolution due to the redshift. As addressed in Dainotti et al. (2015b), the functional form for the evolution can be a power law or a more complex function, and the results for these functions are compatible within 2σ for the luminosities and 1σ for the time evolutions. Here, we detail our results of the EP method for the whole sample of 222 GRBs for the studied parameters. The EP method takes into account these effects by using an adaptation of the Kendall τ test, according to which τ has the following definition:

$$\tau = \frac{\sum_i (\mathcal{R}_i - \mathcal{E}_i)}{\sqrt{\sum_i \mathcal{V}_i}}, \quad (9)$$

where $\mathcal{E}_i = (1/2)(i+1)$ is the expectation value, R_i is the rank, and $\mathcal{V}_i = (1/12)(i^2+1)$ is the variance. To eliminate the impact of the redshift on our data we demand $\tau = 0$. R_i is computed for each data point considering the position of the data in the so-called associated sets, which are samples that include all the objects that can be detected considering a particular observational limit (Dainotti et al. 2013b, 2015b, 2017c). The computations to derive the evolutionary coefficients follow the same procedure for L_{peak} , L_X , and T_X^* . The limiting values for these quantities are shown in the left panels of Fig. 4, while the evolutionary coefficients are shown in the right panels. Here, for simplicity we detail only the computation for L_X , given that for the other parameters is similar. For this luminosity we compute the flux limit at the end of the plateau phase, f_{lim} , and then we compute the correspondent luminosity $L_{min}(z_i)$, that would allow us to detect that object at a given z_i . The associated set for z_i contains all GRBs with $L_{min} \leq L(z_j)$ and $z_j \leq z_i$, where with j and i we denote the objects of the associated set and of the GRB sample, respectively. According to the EP method, the samples used to derive the evolutionary effects should not be less than 90% of the original ones, so conservative choices regarding the limiting values are needed. The chosen coefficients for the evolutionary functions ($g(z)$, $f(z)$, and $h(z)$ for the L_{peak} , L_X and T_X^* , respectively) are the ones for which $\tau = 0$ as shown with the red vertical lines in Fig. 4, while the dashed blue lines correspond to the 1σ for the evolutionary coefficients, which is determined for $\tau \leq 1$. We have used this method on our sample of 222 GRBs to compute new evolutionary parameters, thus updating the values with respect to the ones used in Dainotti et al. (2020a). We also would like to point out that Dainotti et al. (2021b) has shown that this method is reliable regardless of the choice of the limiting values for several sample sizes for Short

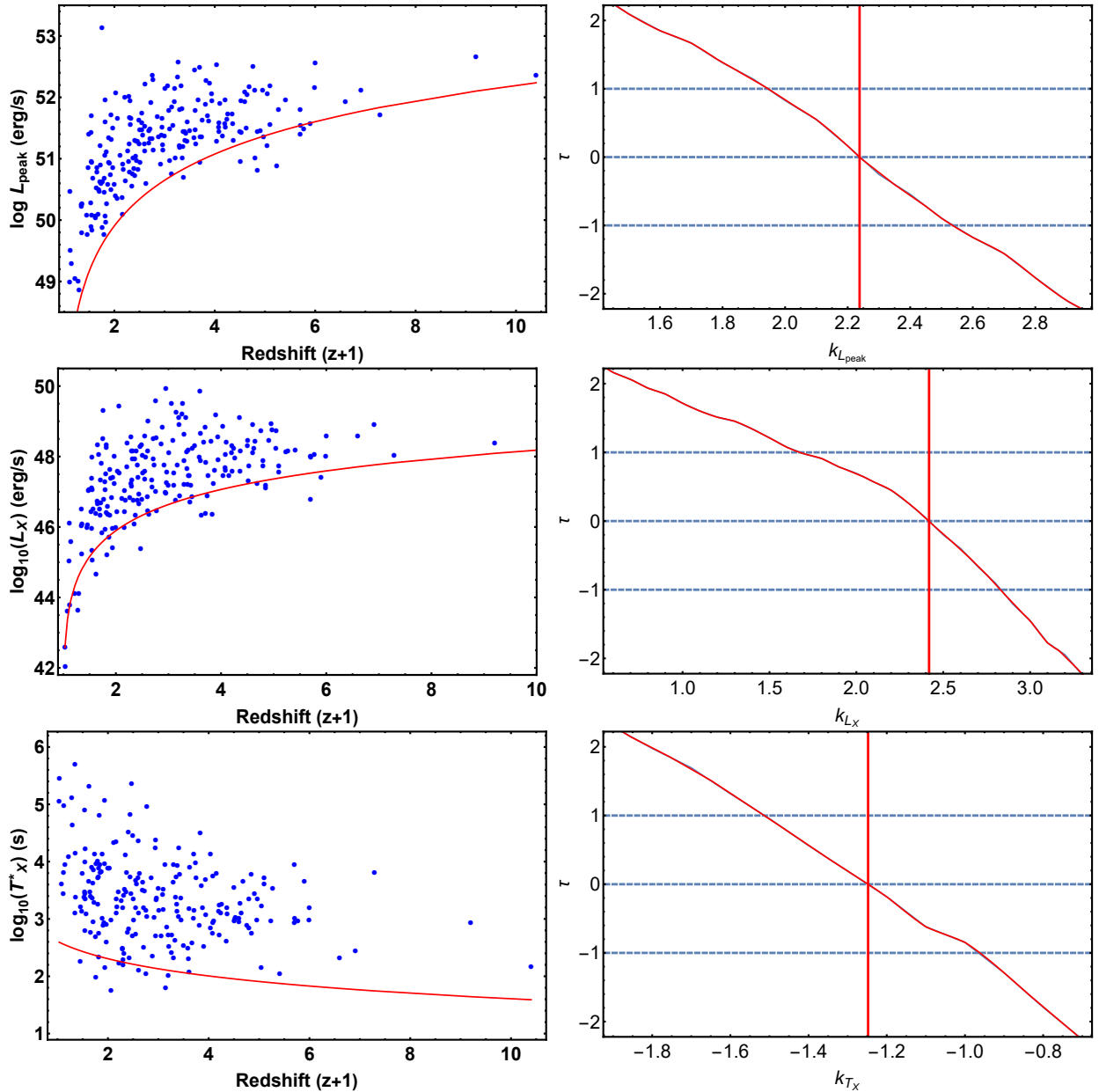


Figure 4. The application of the EP method to our entire sample for the parameters involved in the fundamental plane correlation. The limiting lines chosen for the EP method are visible in red. The left panels show the distribution of studied parameters versus *redshift* + 1, while the right panels show the relation between τ and the evolutionary coefficients in red. The vertical red solid lines indicate the value for which $\tau = 0$ and thus the evolution is removed. The dashed blue lines represent the 1σ for the evolution, which is determined for $\tau \leq 1$.

GRBs (samples of 56, 32 and 34 GRBs). Thus, the discussion of [Bryant, Osborne, & Shahmoradi \(2021\)](#) on the EP method and its applicability are not a concern given the approach and the reliability of the results in [Dainotti et al. \(2021b\)](#).

The previous analysis in this paper fixes the value of an evolutionary parameter at a given Ω_M , H_0 , Ω_k and w . One may wonder how this influences the cosmological results. To verify the impact of the cosmological parameters when k_{L_a} and $k_{L_{\text{peak}}}$ depend on Ω_M , H_0 , Ω_k and w , we repeat the EP method with luminosity distances computed over a grid of different Ω_M , H_0 , Ω_k and w values. Similar analysis of the dependence of evolutionary parameters on cosmology was performed on quasars in [Dainotti et al. \(2022d\)](#). This allows us to determine how the evolutionary functions vary when the cosmological parameters change. The results of this procedure are presented in Fig. 5 and Fig. 6. We note that there are no changes of the evolutionary parameter, k , as H_0 varies. Regarding Ω_M and Ω_k , there is a mild evolution of the evolutionary parameter, although at very low values of Ω_M (between 0 and 0.2) the evolution is noticeable, but still within 1σ when we account for the errorbars. **When we consider the behaviour of the evolutionary slope, k , with Ω_k , it is compatible in $1\text{-}\sigma$ both for k_{L_a} and $k_{L_{\text{peak}}}$ over the whole considered range of Ω_k values. When we consider even a very wide range of the w parameter, all obtained values of the k are**

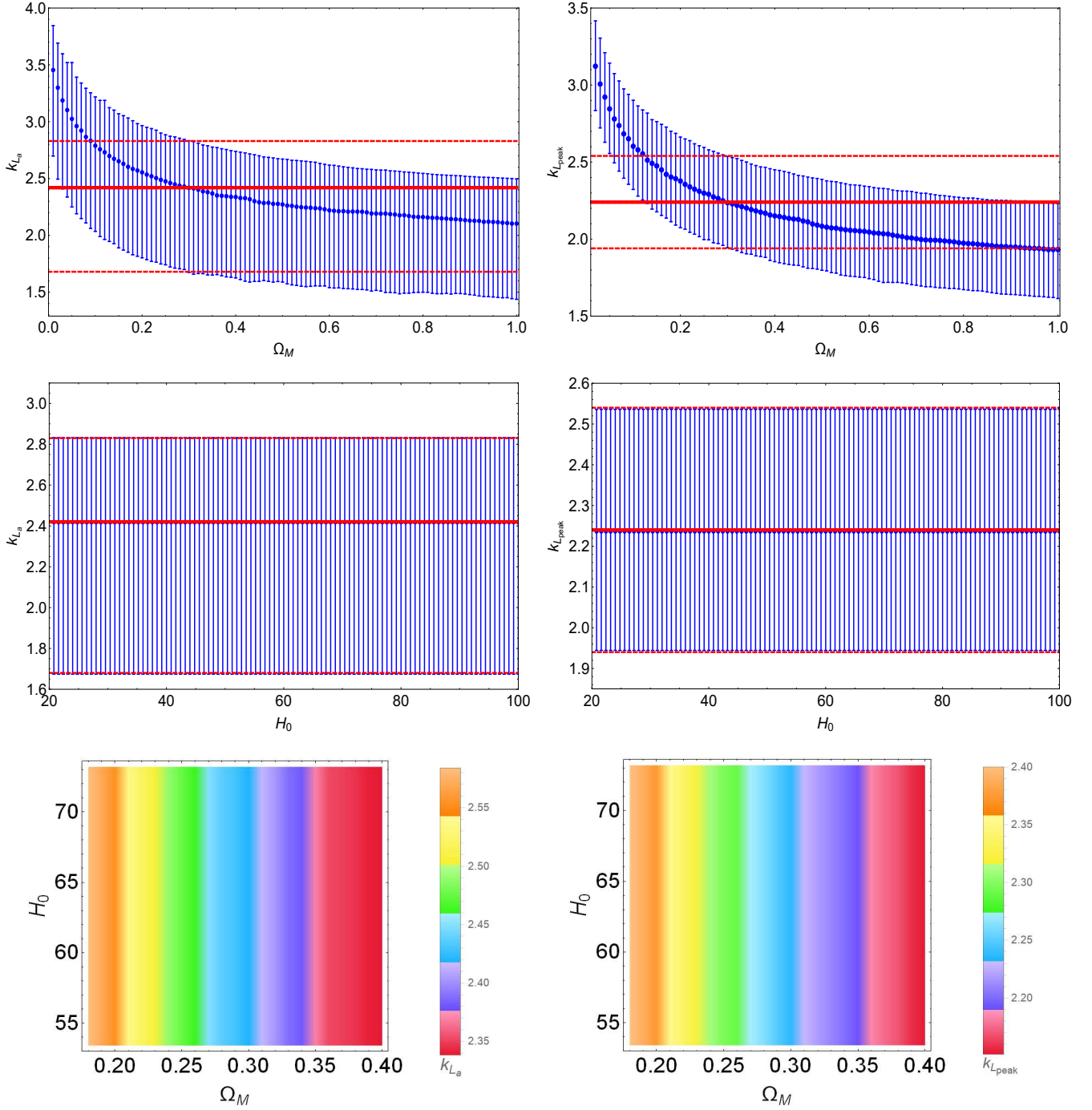


Figure 5. The k_{La} (left) and k_{Lpeak} (right) as a function of Ω_M and H_0 . In the first four pictures the 1- σ error bars are shown with the thin red line together with the thick central line that represents the value of the slope of the function for which the evolution is removed. In the two bottom pictures the contour plots of Ω_M and H_0 as a function of k_{La} (left) and k_{Lpeak} (right). The different colours indicate the different values of the k parameters.

compatible with each other in less than 1- σ , thus again in this case the relation of k with w is negligible. To account for those results, we created a numerical function ($k = k(\Omega_M)$) with a linear interpolation method and varied the values and errors on the k parameters with Ω_M . This is the first time in the literature that such a complete treatment has been performed, which completely overcomes the circularity problem. **In this approach we neglect the k as a function of Ω_k and w because over a reasonable range of parameters the change of k is insignificant.** Dainotti et al. (2022d) showed that the change of k with Ω_M is much more significant for QSOs, this is a result derived using a much larger sample. Thus, in future for a large

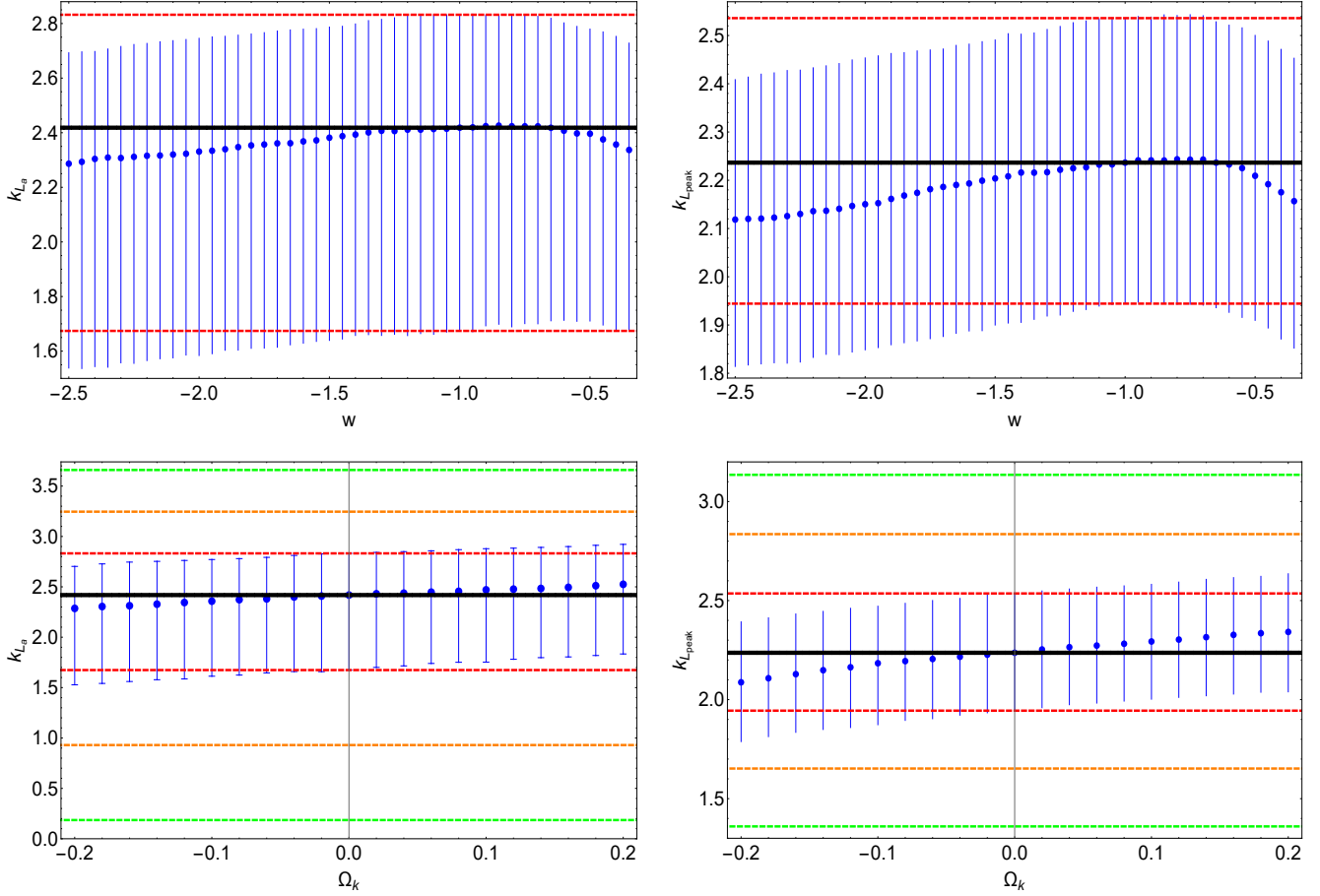


Figure 6. The k_{L_a} (left) and $k_{L_{peak}}$ (right) as a functions of w and Ω_k . In the pictures, the 1- σ , 2- σ and 3- σ error bars are shown with thin red, orange and green lines, respectively. The thick central line represents the value of the slope of the function for which the evolution is removed assuming $w = -1$ and $\Omega_k = 0$.

sample we may encounter a more significant relation of k with Ω_k and w . We postulate that all present cosmological efforts should investigate the impact of selection biases and redshift evolution, contrary to assuming a lack of such effects.

5 THE GRB COSMOLOGY WITH THE FUNDAMENTAL PLANE RELATION

In order to check the reliability of the fundamental plane for cosmological purposes, we here perform a series of tests. First of all we plot for a fixed fiducial cosmology the distance moduli (μ_{GRB}) derived by the fundamental plane relation, with the distance moduli obtained by the SNe Ia, μ_{SNe} in Fig. 6. The left and right panels respectively show GRBs without accounting for selection biases and the right panel the ones accounting for selection biases.

To solve the so-called circularity problem, we compute the cosmological parameters together with the coefficients of the fundamental plane relation, starting from the peak fluxes and the fluxes at the end of the plateau emission which are the observer frame quantities of the corresponding peak prompt luminosity and the luminosity at the end of the plateau emission, respectively. Thus, this procedure does not involve any fixed a priori cosmological models, and the results of this computation leads to the best-fit cosmological parameters together with the coefficients of the fundamental plane correlation using the right hand side of Equation 6 in which the luminosity is defined in Equation 2. More specifically, in our computation we run MCMC simulations using either uniform or Gaussian priors on Ω_M , H_0 and w , and compute the corresponding distance luminosity $D_L(z, \Omega_M, H_0, w)$ and the corresponding L_{peak} , L_X for each value of this grid. Then, for each value of this grid, we compute the best fit parameters of the plane. Thus, this procedure completely avoids the circularity problem. This method does not need any calibration of the fundamental plane relation on other local probes; the correlation's parameters are free to vary following [Dainotti et al. \(2013a\)](#). For the flat Λ CDM cosmological model, in which $w = -1$, and where we neglect the radiation contribution, the luminosity

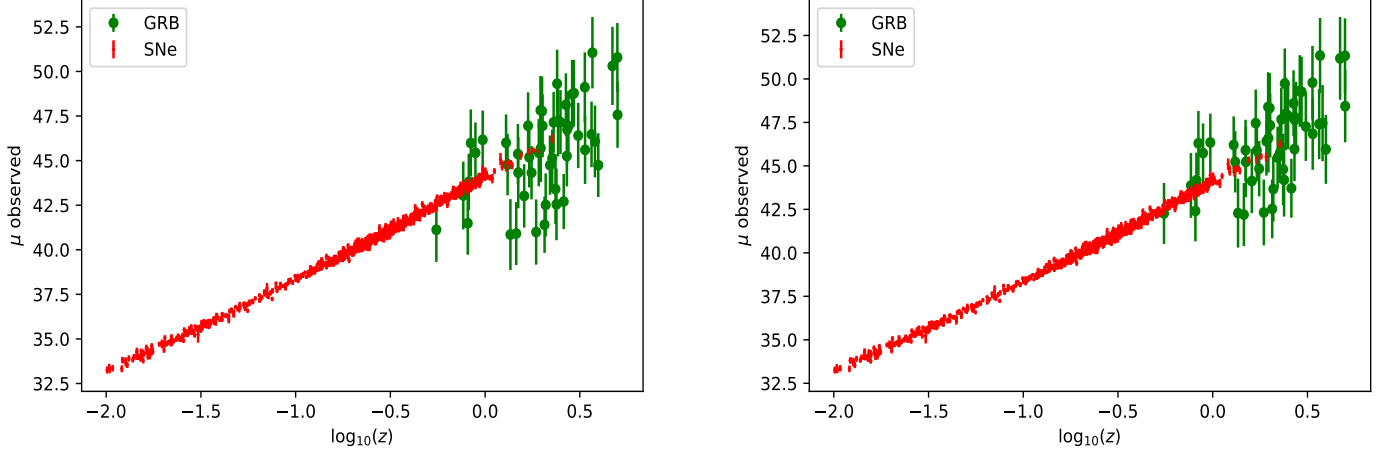


Figure 7. The distance moduli versus logarithm-ed redshift of SNe Ia (μ_{SNe}) and GRBs (μ_{GRB}) belonging to the platinum sample assuming the fundamental plane relation and **assuming** Λ CDM. On the left for the case without correction for evolution, while on the right with correction.

distance used in Equation 2 is :

$$D_L(z) = (1+z) \frac{c}{H_0} \int_0^z \frac{dz'}{\sqrt{\Omega_M (1+z')^3 + (1-\Omega_M)}}, \quad (10)$$

where c is the speed of light. For simplicity we can also write that integrand of Equation 10 as the following:

$$E(z) = \frac{1}{\sqrt{\Omega_M (1+z')^3 + (1-\Omega_M)}}. \quad (11)$$

We combine the GRB Platinum sample, the SNe Ia Pantheon Sample, and the BAO data presented in [Sharov & Vasiliev \(2018\)](#). We note that even if according to [Riess et al. \(1998\)](#) Ω_M and H_0 are kinematically independent, we still have chosen to take into account the separate case of varying both of them together as a check of how the precision reached by us on these quantities depends on the parameter space's dimension. We use the fundamental plane correlation both with and without the correction computed by the EP method to see if this correction may carry a reduction on σ_{int} , and consequently on the cosmological parameters. We derive $\mu_{obs,GRBs}$ in such a way that it is completely independent from the μ_{SNe} , by manipulating the fundamental plane relation corrected for evolution:

$$\mu_{obs,GRBs} = 5(b_1 \log F_{p,cor} + a_1 \log F_{X,cor} + c_1 + d_1 \log T_X^*) + 25, \quad (12)$$

where $\log F_{p,cor}$ and $\log F_{X,cor}$ are the prompt and afterglow emission fluxes, respectively, corrected by the K -correction and the evolutionary functions. We show some of the algebraic computations performed to obtain Equation 6 starting from Equation 2. For the case where we do not take into account the evolutionary effects, considering the relation between fluxes and luminosities given by Equation 2 we obtain:

$$\log_{10}(4\pi d_L^2) + \log_{10} K_X - b \cdot (\log_{10}(4\pi d_L^2) + \log_{10} K_{peak}) = b \cdot \log_{10} F_{peak} + a \cdot \log_{10} T_X^* + C - \log_{10} F_X, \quad (13)$$

where K_{peak} and K_X are the K -corrections computed for the prompt and the afterglow, respectively, and a , b , and C are the coefficients of the fundamental plane correlation. Isolating the luminosity distance from the previous equation we obtain:

$$\log_{10}(d_L) = -\frac{\log_{10} F_X + \log_{10} K_X}{2(1-b)} + \frac{b \cdot (\log_{10} F_{peak} + \log_{10} K_{peak})}{2(1-b)} - \frac{(1-b) \log_{10}(4\pi) + C}{2(1-b)} + \frac{a \log_{10} T_X^*}{2(1-b)}. \quad (14)$$

With new definitions of the coefficients and the fluxes we finally reproduce Equation 12 considering also the relation between luminosity distance and distance modulus.

We compare both $\mu_{obs,GRBs,SNe}$ with the theoretical μ_{th} , defined as:

$$\mu_{th} = 5 \cdot \log D_L(z, \Omega_M, H_0, w) + 25. \quad (15)$$

We now present the constraints given by BAO measurements used in our computations.

The data comes from [Sharov & Vasiliev \(2018\)](#) who refer to the equation for the $d_z(z')$ function defined as:

$$d_z(z') = \frac{r_s(z_d)}{D_V(z')}, \quad (16)$$

$$\text{where } D_V(z') = \frac{c}{H_0} \left[\frac{z'}{E(z')} \times \left(\int_0^{z'} \frac{dz}{E(z)} \right)^2 \right]^{\frac{1}{3}}, \quad \& \quad r_s(z_d) = \frac{55.514 \cdot e^{[72.3(\Omega_v h^2 + 0.0006)^2]}}{(\Omega_M h^2)^{0.25351} (\Omega_b h^2)^{0.12807}} Mpc. \quad (17)$$

The value z_d corresponds to the decoupling of photons in the comoving sound horizon scale $r_s(z_d)$ using the fitting formula from [Sharov & Vasiliev \(2018\)](#).

For this approach we combine the likelihoods and write the logarithm-ed equation as:

$$\begin{aligned} \mathcal{L}(GRBs + SNeIa + BAO) = & \sum_i \left[\log \left(\frac{1}{\sqrt{2\pi}\sigma_{\mu,i}} \right) - \frac{1}{2} \left(\frac{\mu_{th,GRB,i} - \mu_{obs,GRB,i}}{\sigma_{\mu,i}} \right)^2 \right] \\ & - \frac{1}{2} [(\mu_{th,SNe} - \mu_{obs,SNe})^T \times C_{inv} \times (\mu_{th,SNe} - \mu_{obs,SNe}) + (\Delta d_z)^T \times C_{inv}^{BAO} \times \Delta d_z], \end{aligned} \quad (18)$$

where the first term relates to GRBs' distance moduli ([Dainotti et al. 2013a](#); [Amati et al. 2019](#)), the second to the SNe Ia's, where C_{inv} is the inverse of the covariance matrix of the SNe Ia data taken from [Scolnic et al. \(2018\)](#), and the third to the BAO, where C_{inv}^{BAO} is the inverse of the covariance matrix of the BAO data taken from [Sharov & Vasiliev \(2018\)](#) and the Δd_z is defined as: $\Delta d_{z,i} = d_z^{obs}(z_i) - d_z^{th}(z_i)$; $d_z^{obs}(z_i)$ is taken from the data, while $d_z^{th}(z_i)$ is computed with the Equation 16.

We have also computed the cosmological parameters using only SNe Ia data as well as SNe Ia+BAO, to verify if adding GRBs would confirm the results and to what extent we could enhance the precision on the cosmological parameters.

6 RESULTS

The results presented here are divided in three major steps. First, we show the capability of GRBs as alone standardizable candles with the fundamental plane using Equations 6 and 7, as well as the Equation for μ_{GRB} , 12, without calibration using Gaussian priors based on the values of SNe Ia in [Scolnic et al. \(2018\)](#) (see 6.1). Then, we show the calibration on SNe Ia using Gaussian priors (see 6.2). Then, we derive the cosmological parameters with uniform priors, both with and without calibrating GRBs on the SNe Ia (see 6.3) and we compare with the results with Gaussian priors. The analysis has the scope of showing the precision of GRBs in constraining cosmological parameters in a flat Λ CDM model. Second, we use GRBs together with SNe Ia and BAO to verify the usefulness of GRBs in combination with other probes, see 6.4). These results will entail both the observational data of GRBs with no correction for evolution as well as accounting for these corrections. The third step is instead the analysis of the open cosmological model with the GRB fundamental plane relation both corrected and uncorrected for selection biases and redshift evolution (see 6.6).

6.1 GRBs alone with no calibration with Gaussian priors

We here clarify that in all computations we do not minimize the relation of the evolutionary parameters as a function of Ω_M , but we use the evolutionary function $k(\Omega_M)$. This indeed is an independent computation, see sec. 4, which shows how the evolutionary functions depend on Ω_M . There is no minimization involved in this computation.

We have tested two approaches to derive the cosmological parameters with GRBs. For each approach we vary a) both Ω_M and H_0 , b) only Ω_M , c) only H_0 and d) only w . For our computations related to GRBs we consider the Gaussian priors of 3σ based on the results and the uncertainties computed in [Scolnic et al. \(2018\)](#). Although this procedure does not allow to test if there are deviations beyond the 3σ limit, it still allows us to understand the role and the impact of GRBs as standalone cosmological probes, and what are the uncertainties we can achieve considering the current state of the art. We use the following likelihoods:

- (i) We assume a likelihood with Equations 2 and 6 without evolution, see Fig. 8.
- (ii) We assume a likelihood with Equation 7 with the evolution considering fixed values of $k_{L_{peak}}$, k_{L_a} and k_{T_X} , see Fig. 9.
- (iii) We assume a likelihood with Equation 7 and considering a function for the evolutionary parameters $k_{L_{peak}}$ and k_{L_a} , since they vary together with the cosmological parameters, and we fix the k_{T_X} , since it does not depend on the cosmological models, see Fig. 10.
- (iv) The likelihood from Equation 12, μ_{GRB} , without evolution, see Fig. 11.
- (v) The likelihood from Equation 12, μ_{GRB} , for the fixed evolutionary parameters, see Fig. 12.

No calibration on SNe Ia, parameters varied Equation 12		Model	Ω_M	H_0	w	$z - score_{SN}$	$z - score_{SN+BAO}$
without evolution	Ω_M	Λ CDM	0.316 ± 0.063	70	-1	0.268	0.190
without evolution	H_0	Λ CDM	0.30	73.225 ± 3.307	-1	0.984	0.987
without evolution	Ω_M and H_0	Λ CDM	0.320 ± 0.068	73.149 ± 3.026	-1	0.307, 1.025	0.137, 1.09
without evolution	w	w CDM	0.30	70	-0.673 ± 0.717	0.460	0.484
with fixed evolution	Ω_M	Λ CDM	0.308 ± 0.063	70	-1	0.142	0.063
with fixed evolution	H_0	Λ CDM	0.30	72.869 ± 2.921	-1	0.988	0.992
with fixed evolution	Ω_M and H_0	Λ CDM	0.304 ± 0.064	73.128 ± 3.008	-1	0.089, 1.024	0.109, 1.10
with fixed evolution	w	w CDM	0.30	70	-0.977 ± 0.620	0.037	0.064
with $k = k(\Omega_M)$	Ω_M	Λ CDM	0.295 ± 0.062	70	-1	0.064	0.144
with $k = k(\Omega_M)$	Ω_M and H_0	Λ CDM	0.297 ± 0.065	73.036 ± 3.139	-1	0.015, 0.955	0.214, 1.02
No calibration on SNe Ia, parameters varied Equations 6 and 7		Model	Ω_M	H_0	w	$z - score_{SN}$	$z - score_{SN+BAO}$
without evolution	Ω_M	Λ CDM	0.302 ± 0.061	70	-1	0.049	0.033
without evolution	H_0	Λ CDM	0.30	73.152 ± 3.113	-1	1.021	1.024
without evolution	Ω_M and H_0	Λ CDM	0.302 ± 0.064	73.074 ± 3.145	-1	0.163, 0.99	0.031, 1.09
without evolution	w	w CDM	0.30	70	-1.133 ± 1.048	0.127	0.111
with fixed evolution	Ω_M	Λ CDM	0.299 ± 0.065	70	-1	0.000	0.077
with fixed evolution	H_0	Λ CDM	0.30	73.073 ± 3.126	-1	0.992	0.995
with fixed evolution	Ω_M and H_0	Λ CDM	0.294 ± 0.065	72.785 ± 3.049	-1	0.058, 0.900	0.260, 0.971
with fixed evolution	w	w CDM	0.30	70	-0.978 ± 0.662	0.033	0.059
with $k = k(\Omega_M)$	Ω_M	Λ CDM	0.305 ± 0.063	70	-1	0.095	0.016
with $k = k(\Omega_M)$	Ω_M and H_0	Λ CDM	0.305 ± 0.064	73.126 ± 3.101	-1	0.103, 0.996	0.093, 1.065

Table 1. Results of the fitting of the cosmological parameters without calibration on SNe Ia, using GRBs alone and using Gaussian priors with μ_{GRB} (first part) and with the Fundamental plane Equation, 6 (2nd part) without evolution correction, with fixed evolution, and with evolution correction as a function of Ω_M . In the first column we define the studied case and the type of evolution correction. In the second column we define which cosmological parameters are left free to vary. In the subsequent columns we present the values of parameters with error bars obtained in the computation for the corresponding cases. The fixed values are presented in bold. In the last column we present a comparison of each of the case results with the ones obtained with SNe Ia alone, present in Table 5. For this purpose we compute the z-score given by: $z = \frac{|X_{SN} - X_{GRB}|}{\sqrt{\sigma_{X,SN}^2 + \sigma_{X,GRB}^2}}$, where X is a computed value of the considered cosmological parameter for SNe Ia and GRBs, respectively, while σ_X is its error.

(vi) The likelihood from Equation 12, μ_{GRB} , for the evolutionary parameters k_{L_a} and $k_{L_{peak}}$ as functions of Ω_M , see Fig. 13.

The Gaussian priors are justified by the fact that the underlying physics of the fundamental plane is not expected to vary within any given cosmology since it relies on a fundamental physical process, the magnetar emission, which gives rise to the plateau and, in turn, naturally drives the anti-correlation between L_X and T_a (Rowlinson et al. 2014; Rea et al. 2015; Stratta et al. 2018), and the prompt kinetic energy is positively correlated with the kinetic power in the afterglow (Dainotti, Ostrowski, & Willingale 2011; Dainotti et al. 2015b), as it is predicted within the standard fireball model assuming microphysical variations (van Eerten 2014a,b).

6.2 GRBs alone calibrated with SNe Ia with Gaussian priors

When it comes to observational cosmology, one can set up a standard candle by calibrating it with other well-known cosmological probes. This method is widely used in the literature with different approaches (it is, indeed, the main procedure to build the

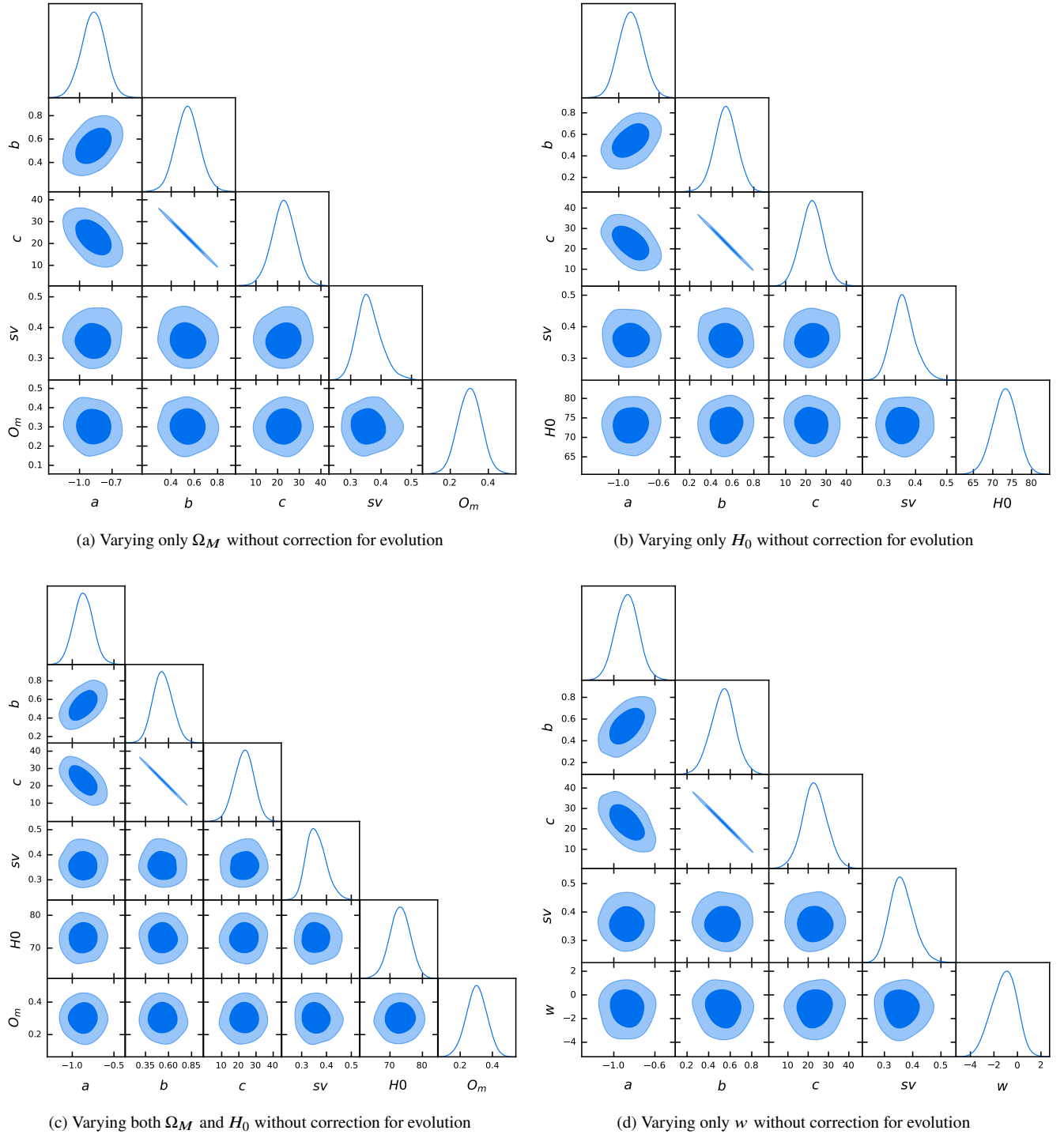


Figure 8. Cosmological results for the GRBs alone (with no calibration) without evolution using the equation of the fundamental plane, Equation 6 and using the 3σ Gaussian priors on the cosmological results reported in Scolnic et al. (2018). We derive in the sub-panels *a*, *b*, *c* and *d* the values of Ω_M , H_0 , Ω_M and H_0 contemporaneously, and w , respectively.

so-called cosmological ladder on which the most updated cosmological late-type results are based upon). To investigate the case of GRBs calibrated with SNe Ia we performed the following procedure:

- (i) First we fit a set of a , b , c , and σ_{int} parameters related to the GRBs fundamental plane with the part of our GRBs sample whose redshift overlaps with the redshift range of SNe Ia (up to $z = 2.25$), which corresponds to 25 GRBs. We fix the H_0 and Ω_M parameters considering the values obtained using SNe Ia alone (for simplicity, we use $H_0 = 70 \text{ km s}^{-1} \text{ Mpc}^{-1}$ and $\Omega_M = 0.3$), but using Gaussian priors with 3σ based on the values of Scolnic et al. (2018).

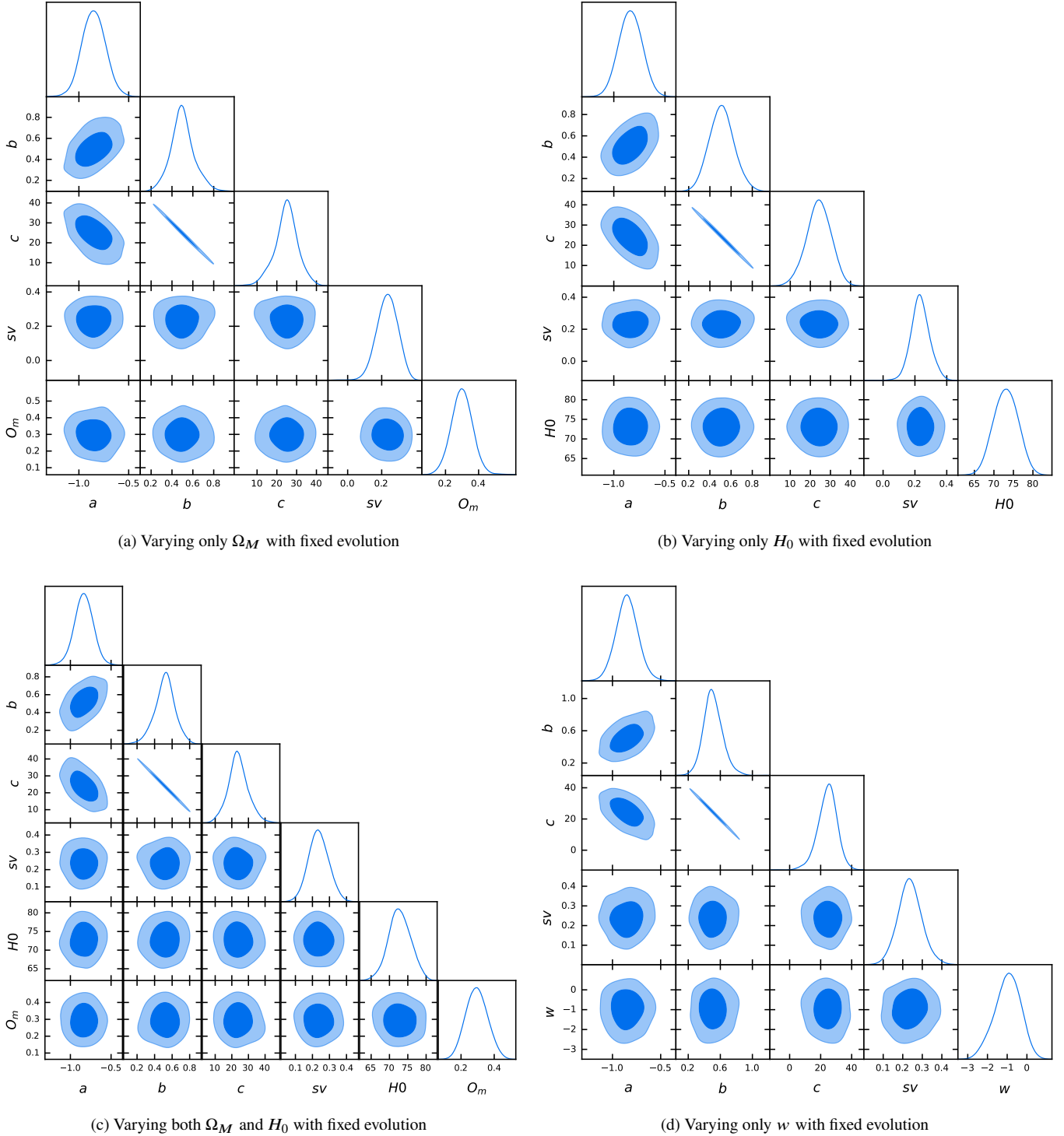


Figure 9. Cosmological results for the GRBs alone with no calibration with Fundamental Plane using fixed evolution on 3σ Gaussian priors on the cosmological parameters investigated following Scolnic et al. (2018). Panels a), b) c) and d) show the contours from the case (ii) for the case of Ω_M , H_0 , Ω_M and H_0 together, and w .

(ii) We have then performed the same steps i)-vi) as in the previous Sec. 6.1 with the only difference that the parameters of the plane are fixed to the sample of the 25 GRBs with $z < 2.25$ overlapping with the SNe Ia.

The results for this analysis are presented without the corrections for evolution in Figs. 15 and 19; with the correction for the evolutionary effects and selection biases in Figs. 16 and 20; and considering these corrections, but with the evolutionary parameter computed as a function of Ω_M , $k = k(\Omega_M)$, in Figs. 17 and 21.

Calibration with SNe Ia, Equation 12	parameters varied	Model	Ω_M	H_0	w	$\Delta_{GRB}^{GRB-C} / \Delta_{GRB}^{GRB-NO-C} \%$	$z - score_{SN}$	$z - score_{SN+BAO}$
without evolution	Ω_M	Λ CDM	0.292 ± 0.068	70	-1	7.94	0.102	0.176
without evolution	H_0	Λ CDM	0.30	73.286 ± 3.007	-1	-9.07	1.102	1.105
without evolution	Ω_M and H_0	Λ CDM	0.295 ± 0.064	73.358 ± 3.006	-1	-5.88, -0.66	0.044, 1.103	0.249, 1.176
without evolution	w	w CDM	0.30	70	-1.094 ± 0.673	-6.13	0.140	0.114
with fixed evolution	Ω_M	Λ CDM	0.316 ± 0.068	70	-1	7.94	0.249	0.176
with fixed evolution	H_0	Λ CDM	0.30	72.762 ± 3.227	-1	10.48	0.864	0.868
with fixed evolution	Ω_M and H_0	Λ CDM	0.306 ± 0.060	73.264 ± 3.082	-1	-6.25, 2.46	0.125, 1.046	0.083, 1.116
with fixed evolution	w	w CDM	0.30	70	-0.743 ± 0.694	11.94	0.370	0.395
with $k = k(\Omega_M)$	Ω_M	Λ CDM	0.298 ± 0.063	70	-1	1.61	0.016	0.095
with $k = k(\Omega_M)$	Ω_M and H_0	Λ CDM	0.295 ± 0.064	73.159 ± 3.134	-1	-1.54, -0.16	0.044, 0.996	0.249, 1.064
Calibration with SNe Ia, Equations 6 and 7	parameters varied	Model	Ω_M	H_0	w	$\Delta_{GRB}^{GRB-C} / \Delta_{GRB}^{GRB-NO-C} \%$	$z - score_{SN}$	$z - score_{SN+BAO}$
without evolution	Ω_M	Λ CDM	0.306 ± 0.069	70	-1	13.11	0.101	0.029
without evolution	H_0	Λ CDM	0.30	73.519 ± 3.119	-1	0.19	1.137	1.140
without evolution	Ω_M and H_0	Λ CDM	0.301 ± 0.065	73.089 ± 3.251	-1	1.56, 3.37	0.044, 0.939	0.083, 1.004
without evolution	w	w CDM	0.30	70	-0.906 ± 0.697	-33.49	0.159	0.159
with fixed evolution	Ω_M	Λ CDM	0.295 ± 0.060	70	-1	-7.69	0.066	0.149
with fixed evolution	H_0	Λ CDM	0.30	73.272 ± 3.143	-1	0.54	1.050	1.140
with fixed evolution	Ω_M and H_0	Λ CDM	0.296 ± 0.066	73.201 ± 3.062	-1	1.54, 0.43	0.029, 1.033	0.226, 1.103
with fixed evolution	w	w CDM	0.30	70	-0.959 ± 0.631	-4.68	0.065	0.0918
with $k = k(\Omega_M)$	Ω_M	Λ CDM	0.300 ± 0.073	70	-1	15.87	0.014	0.055
with $k = k(\Omega_M)$	Ω_M and H_0	Λ CDM	0.296 ± 0.064	73.024 ± 3.073	-1	0, -0.90	0.030, 0.972	0.233, 1.042

Table 2. Cosmological parameters obtained using GRB alone calibrated on SNe Ia (indicated with the subscript C) using Gaussian priors with distance modulus equation (first part) and with the Fundamental plane equation (2nd part) without evolution, with evolution with fixed parameters, and with evolution correction as a function of Ω_M . In the first column we define the studied type of the correction for the evolution. In the second column we define which cosmological parameters are left free to vary, while in the third column we define the investigated cosmological model. In the next three columns we present the values of parameters with error bars obtained in computation for each given case, namely with the fixed cosmological parameters present in bold. In the 7th column, we show the percentage increase/decrease between the uncertainties of GRBs alone without calibration (indicated with No-C) and with Gaussian priors from Table 1 (the Δ_{GRB}^{GRB-C}) vs the results from this Table with calibration (indicated with C) and with Gaussian priors. The formula for the percentage change is: $\frac{\Delta_{comparing} - \Delta_{reference}}{\Delta_{reference}}$, where $\Delta_{reference}$ is the error obtained with GRBs without calibration. With the negative sign we indicate a percentage decrease in the error, while with the positive one, we indicate a percentage increase in the error. Finally, in the last two columns we show the z-scores computed with respect to the SNe Ia alone and SNe Ia+ BAO results, respectively.

We find that all the results of GRBs alone without calibration lie within 1σ with respect to the cosmological results obtained with calibration on SNe Ia. The percentage change in the uncertainty values of the cosmological parameters is shown in the seventh column of Table 2. We also compare cosmological parameters obtained by GRBs alone with calibration using Gaussian priors and the results obtained with SNe Ia alone. We have found out that the results, both using Equation regarding μ_{GRB} , 12, as well as the Fundamental plane Equations 6 and 7 fall within 1σ as shown by the z-score in Table 2. The only exception to this result is the case of GRBs calibrated with SNe Ia using the fundamental plane for the case without evolution and with fixed evolution varying H_0 . Indeed, we note that the z-score for this case is slightly larger than 1 ($z = 1.140$). All the z-score with respect to the GRB results are shown in the last two columns of Table 2.

6.3 GRBs alone with and without calibration with the SNe Ia with uniform priors

The aim of the previous sections is to explore the possibility of using GRBs as standalone standard candles up to redshift 5. Indeed, the aim is not to explore parameter spaces which may lead to exotic scenarios, but rather to consider the reliability of GRBs as cosmological probes. This is the reason why Gaussian priors up to 3σ around the best-fit values of the SNe Ia computations have been investigated. It is clear that given the sample size and the large scatter, the applicability of GRBs as cosmological probes nowadays is not definitive, but one of our goals is to show that the complementarity of using GRBs in combination with SNe Ia is beneficial for exploring the cosmological setting at high-z. This can allow access to the universe in

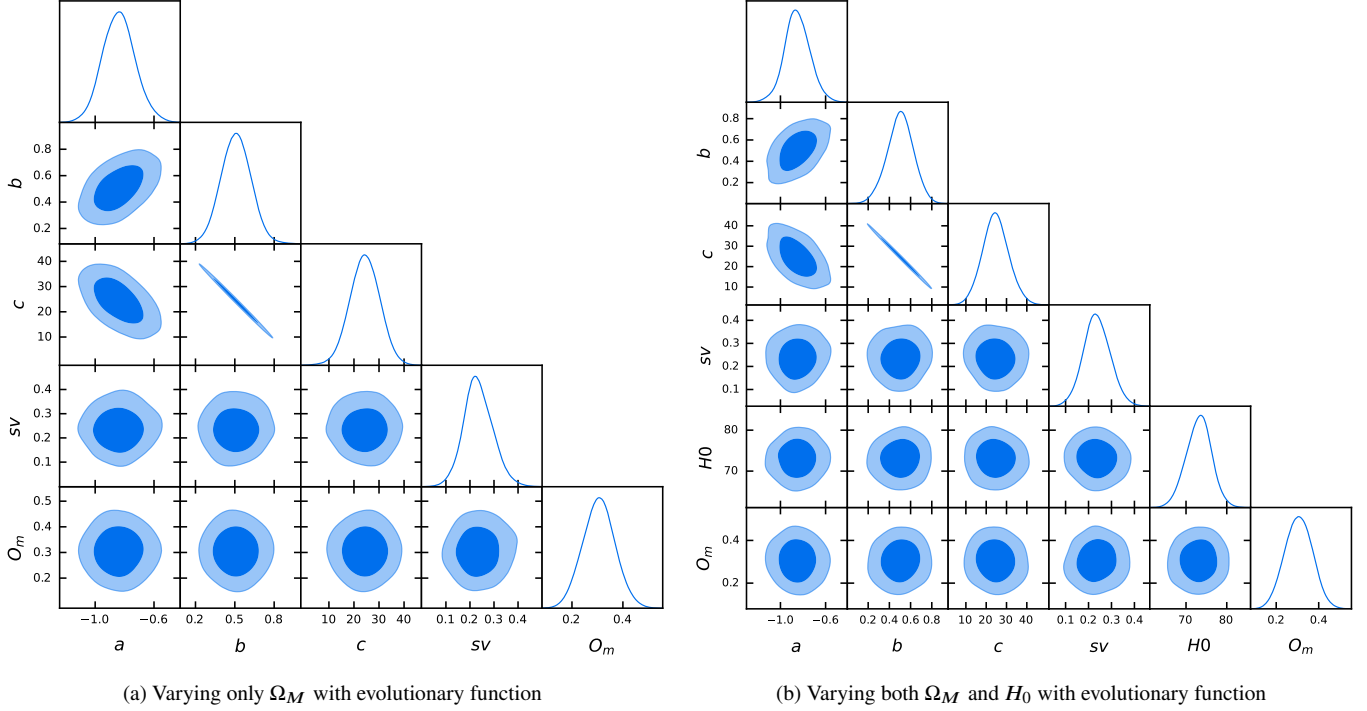


Figure 10. Cosmological results for the GRBs alone (with no calibration) with Fundamental Plane using evolutionary functions and the assumptions of 3σ Gaussian priors on the cosmological parameters investigated following Scolnic et al. (2018). Panels a) and b) show the contours from case (iii) for the case of Ω_M and the case of Ω_M and H_0 together, respectively.

principle up to $z = 9.4$, which is the redshift of the furthest GRB ever detected, and, in our case regarding the platinum sample, up to $z = 5$. If we consider Gaussian priors, we can recover similar results without the need of exploring the full parameter space. However, to explore how strong the impact of the Gaussian priors on our results is, and for comparing also with the results of GRBs and SNe Ia+BAO together, in which uniform priors have been used, we consider the steps i)-vi) with Gaussian priors as well. We here vary Ω_M , w , and H_0 alone to appreciate the differences of the parameters computing them one by one, with the only difference that the priors are uniform and are the following : $0.0 \leq \Omega_M \leq 1$, $50 \leq H_0 \leq 100$ and $-2 \leq w \leq 0$. We have repeated each MCMC run 100 times, and plotted the distribution of Ω_M , w , and H_0 both by calibrating the results on SNe Ia for μ_{GRB} , see Fig. 22 and Fig. 23 for Equations 6 and 7, respectively. The same MCMC run 100 times is adopted without calibration on SNe Ia for μ_{GRB} , see Fig. 24 and Fig. 25 for Equations 6 and 7, respectively.

We consider the scenarios of no evolutionary correction (upper panels of Figs. 22, 23, 24, 25), with evolution correction using fixed parameters (middle panel of Figs. 22, 23, 24, 25), and with evolutionary functions (bottom panels of Figs. 22, 23, 24, 25). Both without and with calibration on SNe Ia using μ_{GRB} , the Ω_M and H_0 uncertainty values tend to be higher by 328.57%, 327.58% (without evolution and calibration); 328.57%, 384.42% (with fixed evolution and without calibration); 326.47%, 348.29% (without evolution and with calibration); 297.06%, 306.57% (with fixed evolution and calibration), respectively, than the results obtained using Gaussian prior of 3σ . Also, without and with calibration on SNe Ia using μ_{GRB} , uncertainties on the value of Ω_M using the $k(\Omega_M)$ evolutionary function are higher by 335.48% and 328.57%, respectively, than the results obtained using Gaussian priors of 3σ .

Now, considering Fundamental plane Equations 6 and 7, the uncertainties on the values for both Ω_M and H_0 obtained by GRBs alone are higher by 359.01%, 355.19% (without evolution and calibration); 315.38%, 356.49% (with fixed evolution and without calibration); 305.80%, 337.32% (without evolution and with calibration); 366.67%, 338.11% (with fixed evolution and calibration), respectively, than the results obtained using Gaussian prior of 3σ . Also, without and with calibration on SNe Ia using Equations 6 and 7, uncertainties on the value of Ω_M using the $k(\Omega_M)$ evolutionary function are higher by 328.57% and 283.56%, respectively, than the results obtained using Gaussian priors of 3σ .

Surprisingly, the uncertainty values of w using uniform priors are always smaller for both without and with calibration on SNe Ia and both with μ_{GRB} and Equations 6 and 7 by 19.11% (without evolution and calibration), 6.45% (with fixed evolution and without calibration), 16.42% (without evolution and with calibration), 16.43% (with fixed evolution and calibration), compared to the values obtained with Gaussian priors. Considering the Fundamental plane Equations 6 and 7, the uncertainties on the

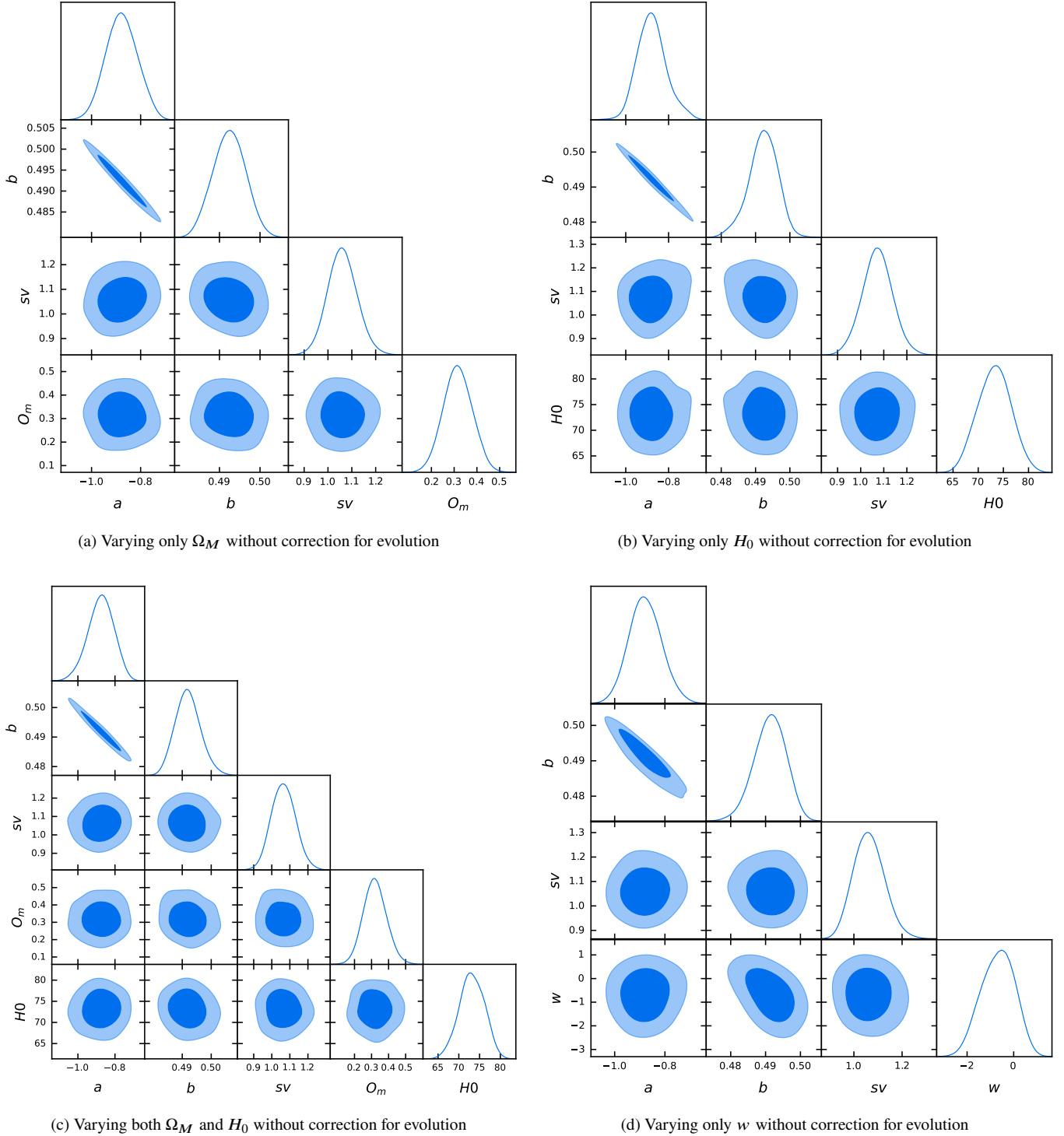


Figure 11. Cosmological results for the GRBs alone (with no calibration) with μ_{GRB} , see Equation 12, without evolution and the assumptions of 3σ Gaussian priors on the cosmological parameters investigated following Scolnic et al. (2018). Panels a), b), c) and d) show the contours from the case (iv) for the case of Ω_M , H_0 , Ω_M and H_0 together, and w , respectively.

value of w using uniform priors for the case of no evolution and fixed evolution for no calibration are smaller than the values of w with Gaussian priors by 44.65% and 12.39%, respectively, and in the case of calibration on SNe Ia they are smaller in the cases of without evolution (18.22%) and with evolution (9.67%).

We note that the values of Ω_M and H_0 obtained considering the Gaussian priors are generally larger than the respective computations taking into account uniform priors. However, as we have pointed out this is not the case for w , thus it is not clear yet why the uniform priors would enlarge the uncertainties only on Ω_M and H_0 . On the other hand, the values of w have narrow

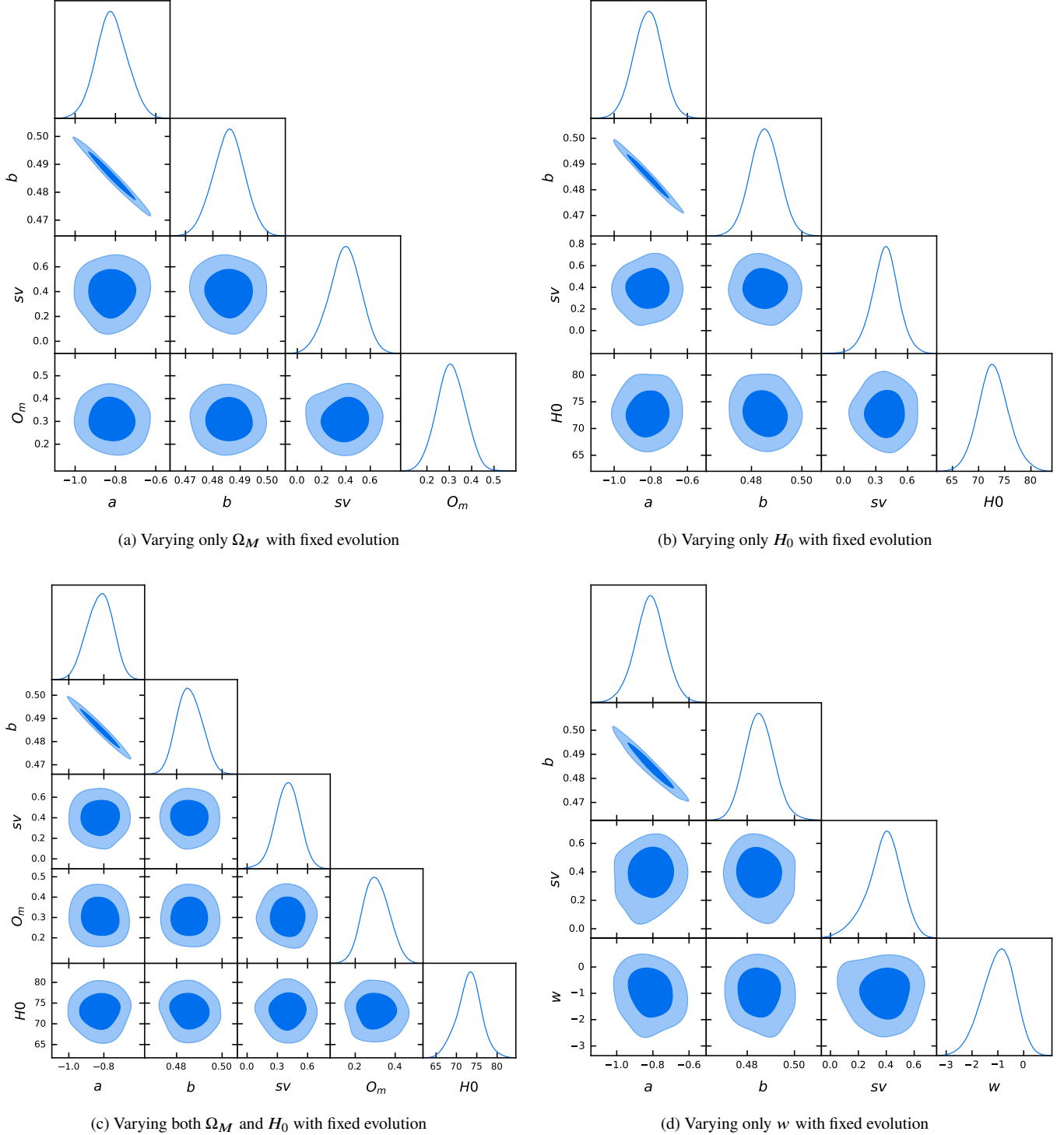


Figure 12. Cosmological results for the GRBs alone (with no calibration) with μ_{GRB} , see Equation 12, using fixed evolution and the assumptions of 3σ Gaussian priors on the cosmological parameters investigated following Scolnic et al. (2018). Panels a), b), c) and d) show the contours from case (v) for the case of Ω_M , H_0 , Ω_M and H_0 together, and w , respectively.

ranges and the difference between Gaussian and uniform priors may be less appreciable. This trend is slightly mitigated when we correct for the evolution and with the evolutionary functions, but the large uncertainties prevent to see a net difference. In the future, when we have more data with smaller uncertainties, the trend noted using the evolutionary functions can be important to reduce such a bias against higher values of Ω_M . On the other hand, we have seen a trend of increasing values for Ω_M when we consider cosmological computations with other high redshift probes (Colgàin et al. 2022). This trend, however, does not appear when we simulate many GRBs based on the features of the 10 closest GRBs to the fundamental plane (Dainotti et al. 2022c).

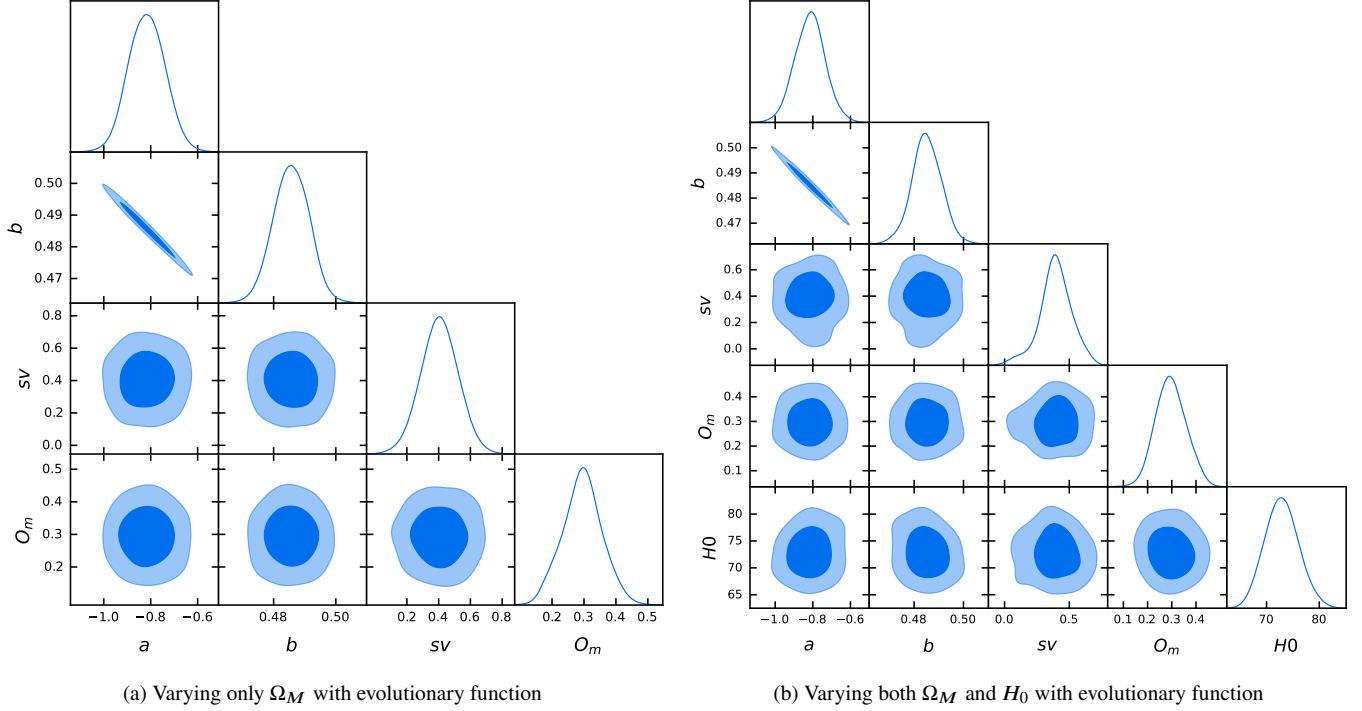


Figure 13. Cosmological results for the GRBs alone (with no calibration) with μ_{GRB} using evolutionary functions and the assumptions of 3σ Gaussian priors on the cosmological parameters investigated following Scolnic et al. (2018). Panels a) and b) show the contours from the case (vi) for the case of Ω_M and the case of Ω_M and H_0 together, respectively.

Results are shown in Sec. 8. All averaged cosmological results over 100 MCMC runs using uniform priors lie within 1σ with respect to the cosmological results obtained using Gaussian priors, both considering calibration and no-calibration on the SNe Ia, see Table 3 and 4.

6.4 GRBs in combination with SNe Ia and BAO with and without the correction for selection biases and redshift evolution

Results for the cosmological computations using GRBs+BAO+SNe Ia are shown in Fig. 26 and for SNe Ia alone and SNe +BAO are shown in 27. All results are summarized in Table 5. We show the cosmological parameters obtained using: 1) SNe Ia alone 2) SNe Ia+BAO 3) SNe Ia+BAO+GRBs without correction for evolutionary effects; 4) SNe Ia+BAO+GRBs with these corrections. The contour plots at 68% (dark blue) and 95% (light blue) are computed for each case. In all figures, the following fiducial values (at which the parameters are fixed) have been taken into account: $\Omega_M = 0.30$, $H_0 = 70 \text{ km s}^{-1} \text{ Mpc}^{-1}$ and $w = -1$ (bold-faced in Table 5).

In Fig. 26 we present the cosmological results of SNe Ia+GRBs+BAO both with (panels d, e, f, h) and without evolution (panels a, b, c, and g) for GRBs. When we consider SNe Ia vs SNe Ia+BAO+GRBs with evolution, we observe smaller computed uncertainties for the cosmological values (see Table 5) once more probes are taken into account. More specifically, we see a decrease of 14.3% for Ω_M , and 16.7% for w . When Ω_M and H_0 are varied contemporaneously, we obtain a decrease in the scatter of 68.2%, and 52.9%, respectively. When we compare SNe Ia+BAO vs SNe Ia+BAO+GRBs with evolution, we reproduce the precision on Ω_M with no reduction of the uncertainties. However, we note an increase of the scatter on H_0 of 14.3% when both Ω_M and H_0 are varied contemporaneously. Furthermore, we see an increase of the scatter when H_0 and w are varied alone of 7.7% and 7.1%, respectively. For completeness, all the percentage variations with respect to the SNe Ia and SNe Ia+BAO results are shown in the last two columns of Table 5. We stress that to check the numerical errors on the computation of the MCMC chain, we ran the computation of H_0 100 times and we found that the uncertainty on the scatter on H_0 is 0.004, which is two orders of magnitude smaller than the error in the results. Similarly, we find the scatter is two orders of magnitude smaller for w (0.0006), while it is one order smaller for Ω_M (0.0002).

When we treat $k_{L_{peak}}$ and k_{L_a} as a function of Ω_M , the results remain unchanged. Both the best fit value and the uncertainties on parameters do not change within the computation accuracy of the MCMC algorithm in both cases, varying Ω_M alone and together with H_0 .

In Fig. 27 we show the results obtained using SNe Ia (panels a, b, c and g) and SNe Ia+BAO (panels d, e, f and h), to quantify

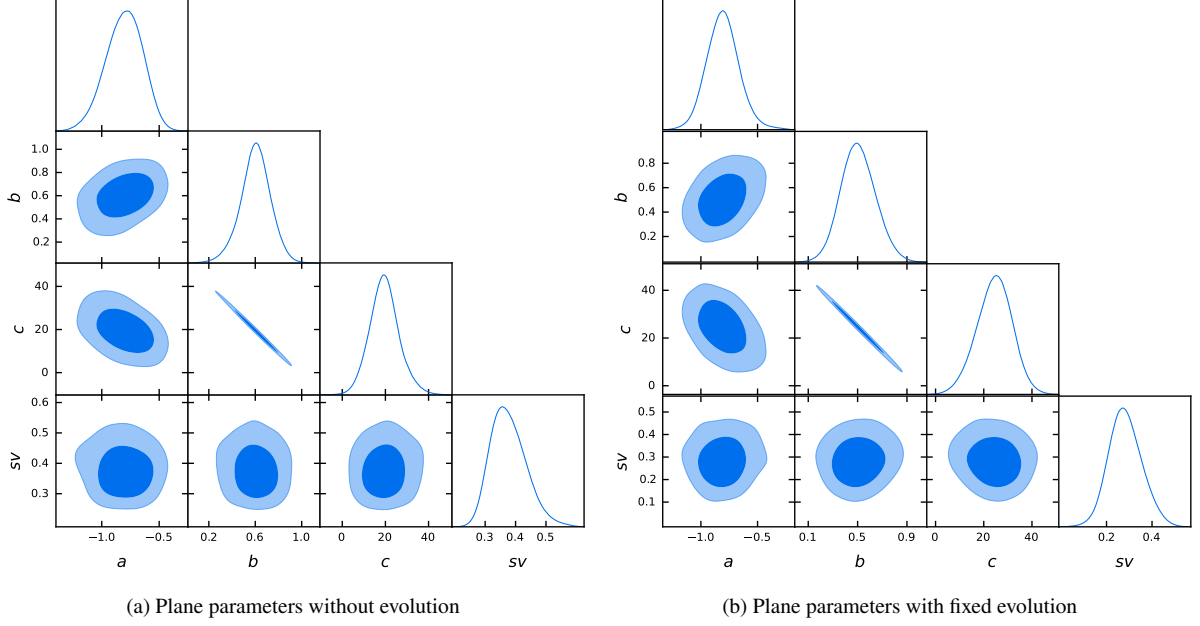


Figure 14. The Fundamental plane relation parameters with the nearest 25 GRBs used to calibrate them on SNe Ia using μ_{GRB} , Equation 12. Panels a) and b) show the contours of the plane fitting parameters without evolution and with fixed evolution respectively.

No calibration with SNe Ia with uniform priors, Equation 12	parameters varied	Model	$\langle \Omega_M \rangle$	$\langle H_0 \rangle$	$\langle w \rangle$	$\Delta_{GRB}^{GRBU\%}$	$z - score_{SN}$	$z - score_{SN+BAO}$
without evolution	Ω_M	Λ CDM	0.58 ± 0.27	70	-1	328.57	1.040	1.022
without evolution	H_0	Λ CDM	0.30	77.51 ± 14.14	-1	327.58	0.533	0.534
without evolution	w	w CDM	0.30	70	-0.91 ± 0.58	-19.11	0.155	0.184
with fixed evolution	Ω_M	Λ CDM	0.56 ± 0.27	70	-1	328.57	0.966	0.948
with fixed evolution	H_0	Λ CDM	0.30	77.48 ± 14.15	-1	384.42	0.531	0.531
with fixed evolution	w	w CDM	0.30	70	-0.93 ± 0.58	-6.45	0.121	0.150
with $k = k(\Omega_M)$	Ω_M	Λ CDM	0.56 ± 0.27	70	-1	335.48	0.966	0.948
No Calibration with uniform priors, Equation 6 and 7	parameters varied	Model	$\langle \Omega_M \rangle$	$\langle H_0 \rangle$	$\langle w \rangle$	$\Delta_{GRB}^{GRBU\%}$	$z - score_{SN}$	$z - score_{SN+BAO}$
without evolution	Ω_M	Λ CDM	0.53 ± 0.28	70	-1	359.01	0.825	0.807
without evolution	H_0	Λ CDM	0.30	75.00 ± 14.17	-1	355.19	0.355	0.356
without evolution	w	w CDM	0.30	70	-0.98 ± 0.58	-44.65	0.034	0.064
with fixed evolution	Ω_M	Λ CDM	0.53 ± 0.27	70	-1	315.38	0.855	0.837
with fixed evolution	H_0	Λ CDM	0.30	74.99 ± 14.27	-1	356.49	0.352	0.352
with fixed evolution	w	w CDM	0.30	70	-0.98 ± 0.58	-12.39	0.034	0.064
with $k = k(\Omega_M)$	Ω_M	Λ CDM	0.55 ± 0.27	70	-1	328.57	0.929	0.911

Table 3. Averaged cosmological parameters of 100 runs with no calibration using GRBs alone assuming uniform priors (indicated with the subscript U) and with μ_{GRB} (first part of the Table) and with Fundamental plane equation, see Equation 6 (2nd part) without evolution, and with the evolution correction as a function of Ω_M . In the header we use the notation: " $\langle \rangle$ " to distinguish results obtained in this analysis from the ones for which Gaussian priors have been considered. The third column before the last corresponds to the percentage change in errors computed comparing the current results obtained with the GRBs alone with Gaussian priors (indicated with the subscript G) without calibration taking as a reference point GRB values from Table 1. The last column represents the z-score from the SNe Ia taking the SNe Ia as a reference point.

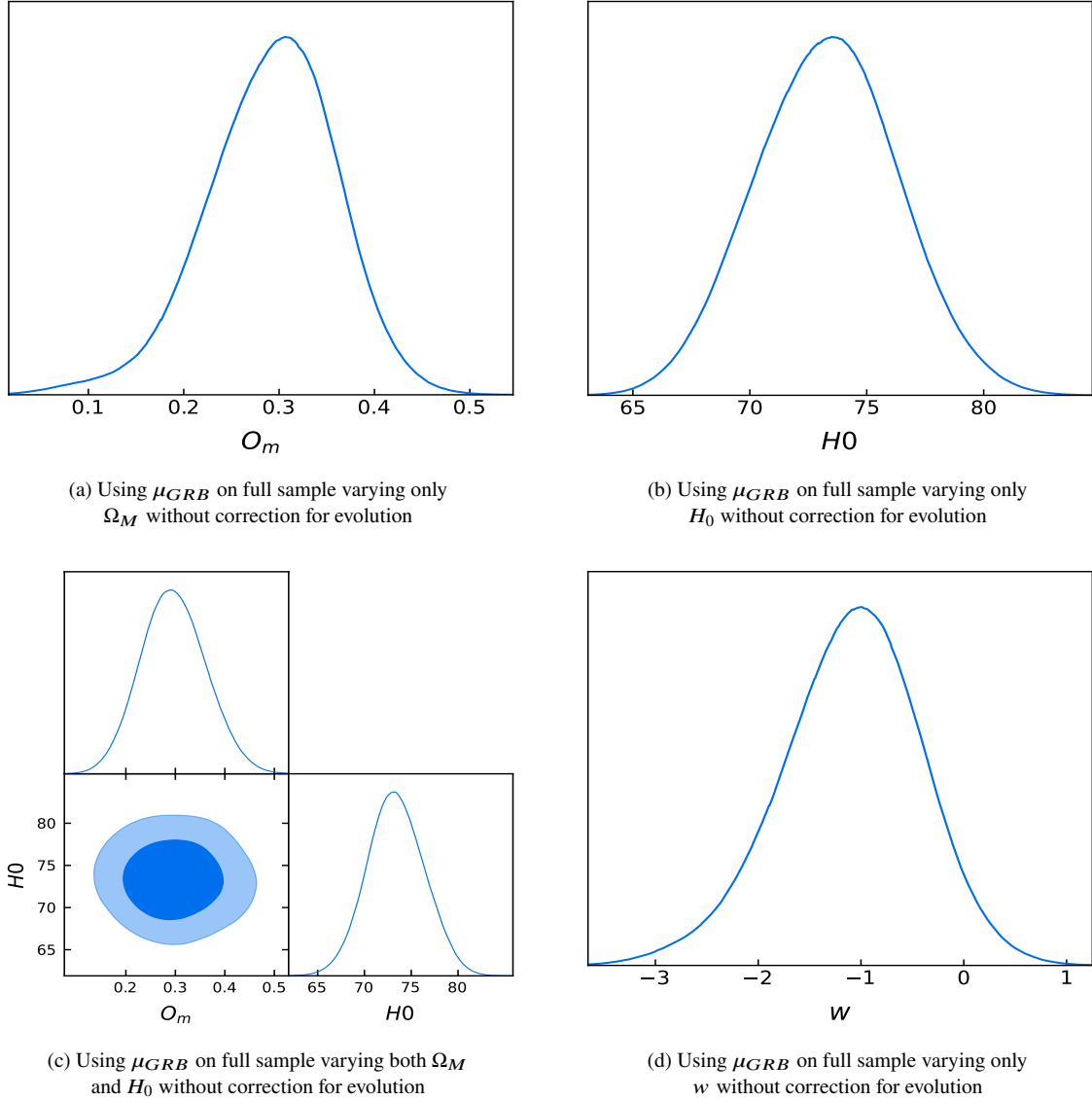


Figure 15. Cosmological results for the GRBs alone (with calibration on SNe Ia) with μ_{GRB} using no correction for the evolution and the assumptions of 3σ Gaussian priors on the cosmological parameters investigated following Scolnic et al. (2018). Panels a), b), c) and d) show the contours from the case (vi) for the case of Ω_M , H_0 , Ω_M and H_0 together, and w , respectively.

how much the uncertainties on the cosmological parameters are changed when we add BAO. In the a) panel, we use SNe Ia only. We vary H_0 fixing Ω_M and w ; in the b) panel we vary Ω_M and fix H_0 and w ; in the c) panel we vary H_0 and Ω_M with w fixed; in the d) panel we vary w for the w CDM model and fix H_0 and Ω_M . In the bottom panels, the figures show the same quantities, considering BAO+SNe Ia. The constraints derived when GRBs are added to the SNe Ia +BAO samples lead to a reduction or a confirmation of the scatter when using SNe Ia only, with the additional advantage that GRBs span up to $z = 5$ in our sample.

6.5 Comparing our results to the other cosmological computations with GRBs in the literature

Many scientists have tried to address the problem of using GRBs as cosmological tools for almost two decades from now and we here discuss only a few papers which are more closely related to the fundamental plane relation or when a similar study about the comparison with and without the calibration on SNe Ia has been performed. As an example, cosmological computations have been performed in Moresco et al. (2022) involving GRBs both with and without calibration against SNe Ia considering uniform priors based on the Amati correlation between the peak energy in the νF_ν of the prompt emission spectrum and the isotropic prompt emission (Amati et al. 2008). For their sample composed of 70 GRBs without calibration, they have found $\Omega_M = 0.27^{+0.38}_{-0.18}$. To compare their results to ours, we symmetrize their results and obtain: $\Omega_M = 0.27 \pm 0.28$, which is similar to the variance obtained by us for an analogous case in Table 3. In particular, for the case without correction for evolution and

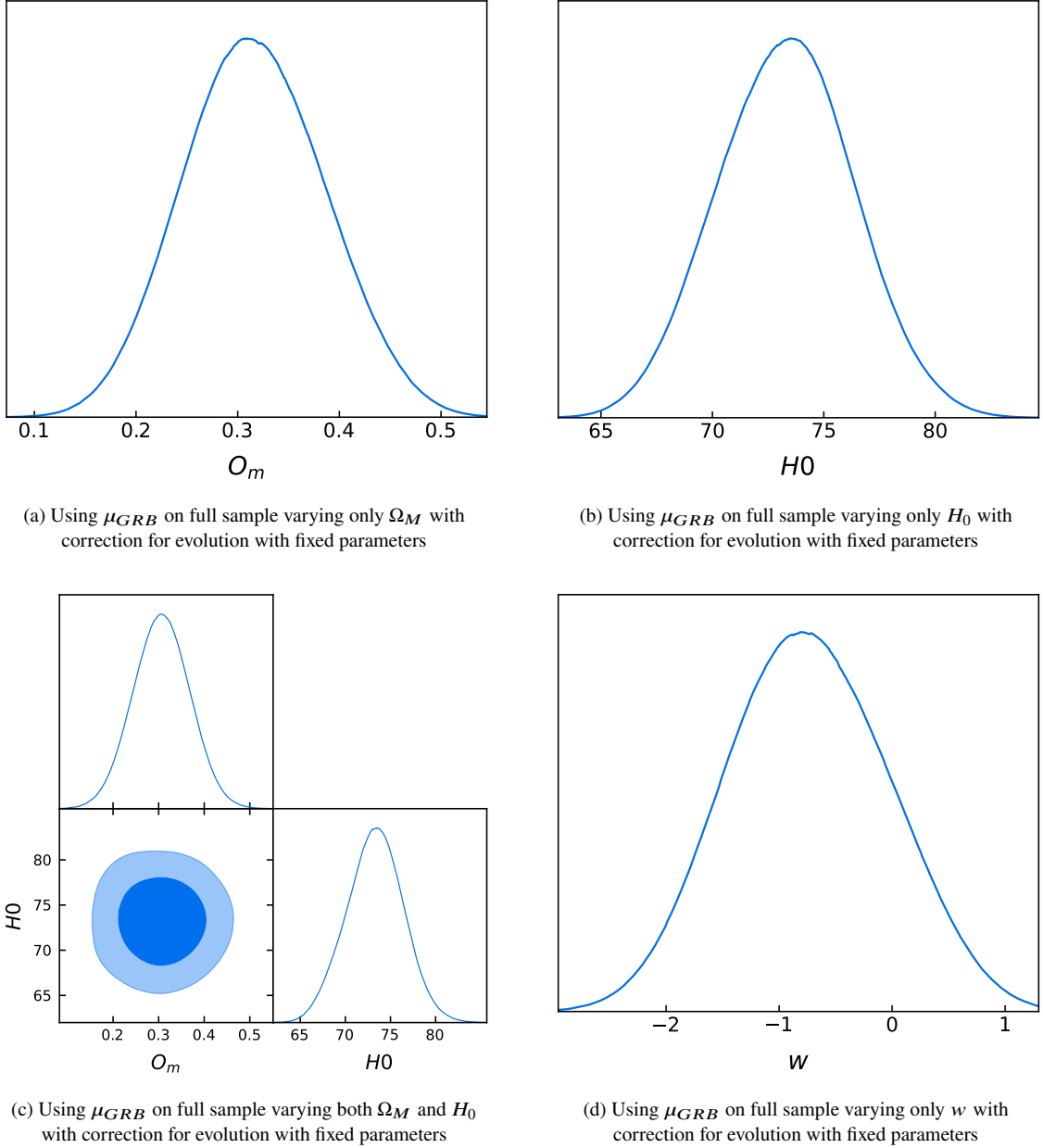


Figure 16. Cosmological results for the GRBs alone (with calibration on SNe Ia) with μ_{GRB} using correction for evolution and the assumptions of 3σ Gaussian priors on the cosmological parameters investigated following Scolnic et al. (2018). Panels a), b), c) and d) show the contours from the case (vi) for the case of Ω_M , H_0 , Ω_M and H_0 together, and w , respectively.

with the likelihood based on the Equation 6 without calibration and with uniform priors, we reproduce the same precision (line 10 in Table 3 and the Figures 25, 23), while for all the other cases we have slightly smaller variance (0.27). For the sample of 208 GRBs, whose size is four times bigger than the one of our sample, they found $\Omega_M = 0.26^{+0.23}_{-0.12}$ and $\Omega_M = 0.30^{+0.06}_{-0.06}$ for the cases without and with calibration, respectively. Both results hold a higher precision than our computations. We remind that our results without evolution and without and with calibration yield $\Omega_M = (0.53 \pm 0.28)$ and $\Omega_M = (0.52 \pm 0.28)$. In Liu et al. (2022b), cosmological computations have been performed with 220 GRBs calibrated with SNe Ia considering uniform priors based on the Amati correlation (Amati et al. 2008) and improved the Amati correlation (Liu et al. 2022a) using the copula function, a multivariate cumulative distribution function. They have found $\Omega_M > 0.651$ with the Amati correlation and $\Omega_M = 0.308 \pm 0.192$ with the improved Amati correlation. The result with the improved Amati correlation is consistent with the ones obtained by us for GRBs alone calibrated with SNe Ia using uniform priors and the distance modulus Equation, 12, see Table 4. Though in this paper, the variance of the measurement is smaller than ours (without evolution: 0.28, with evolution fixed and $k = k(\Omega_M) : 0.27$) it is probably due to the fact that their GRB sample size is more than four times the size of our sample.

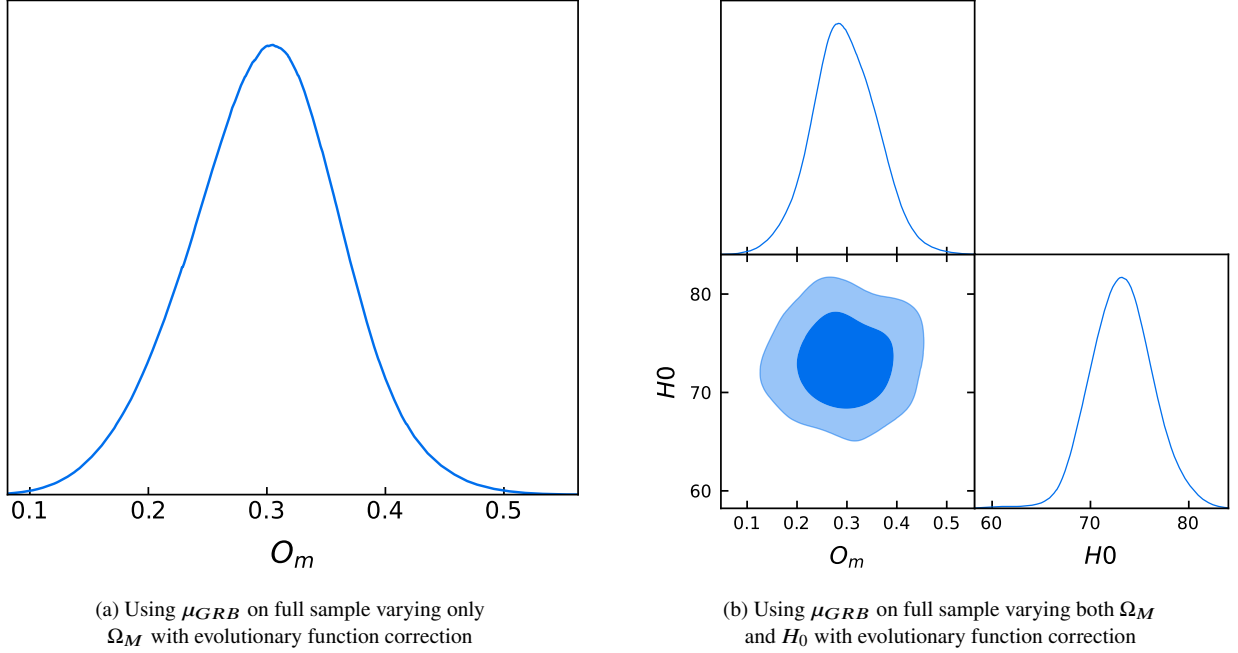


Figure 17. Cosmological results for the GRBs alone (with calibration on SNe Ia) with μ_{GRB} correcting with the evolutionary functions and the assumptions of 3σ Gaussian priors on the cosmological parameters investigated following Scolnic et al. (2018). Panels a) and b) show the contours from the case (vi) for the case of Ω_M and the case of Ω_M and H_0 together, respectively.

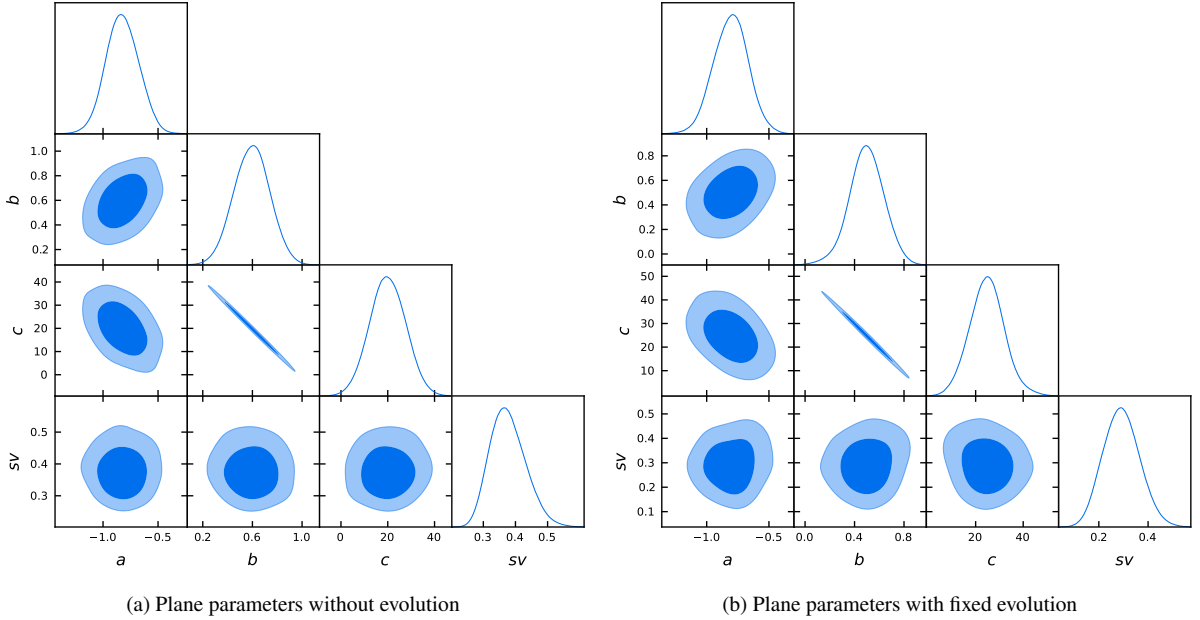


Figure 18. The Fundamental plane relation parameters obtained with the nearest 25 GRBs used to calibrate them on SNe Ia using the Equation 6. Panels a) and b) show the contours of the plane fitting parameters without evolution and with fixed evolution respectively.

Wang, Dai, & Zhu (2007) performed cosmological computations with 69 GRBs without calibration on SNe Ia using the distance modulus Equation, 12, and χ^2 minimization technique to obtain $\Omega_M = 0.34 \pm 0.10$. Their results are consistent with the ones we obtained for GRBs alone without calibration using uniform priors and the distance modulus Equation, 12, see Table 3. The variance in their measurements is smaller than the one in our cosmological calculations as in the comparisons above (without evolution: 0.28, with evolution fixed and $k = k(\Omega_M)$: 0.27).

Cao, Khadka, & Ratra (2022) performed a set of computations involving GRBs using the Dainotti Fundamental plane correlation with 3 different sets consisting of 60 events altogether (one set of 5 GRBs only, one of 24, and the other composed of 31 GRBs)

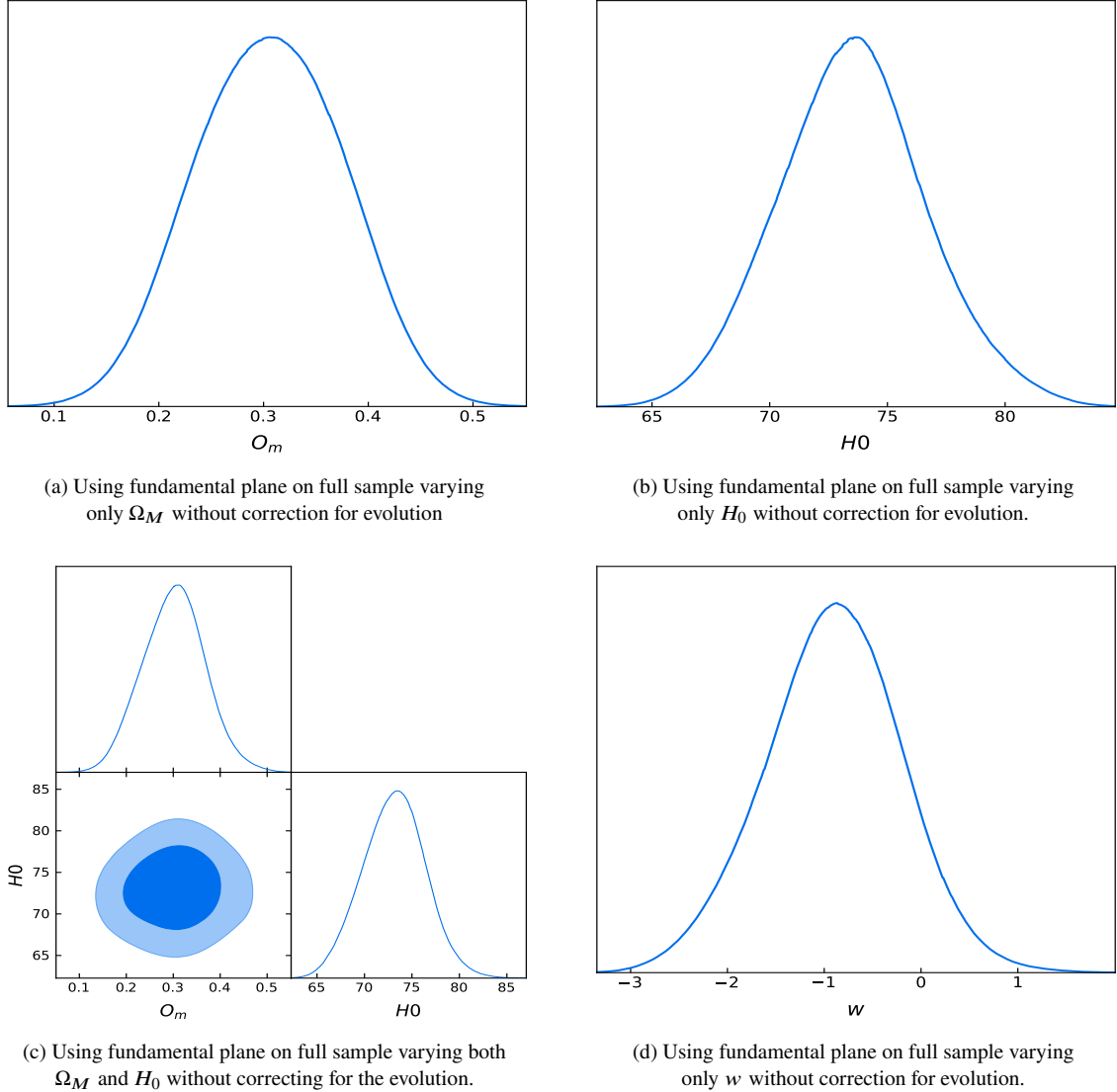


Figure 19. Cosmological results for the GRBs alone (with calibration) using the fundamental plane, Equation 6 with no evolution and the assumptions of 3σ Gaussian priors on the investigated cosmological parameters following Scolnic et al. (2018). Panels a), b), c) and d) show the contours from the case (vi) for the case of Ω_M , H_0 , Ω_M and H_0 together, and w , respectively.

and using also the Amati relation for 118 GRBs. The considered likelihood corresponds to the one derived from equation 6. In the analysis uniform priors were applied. Cao, Khadka, & Ratra (2022) obtained closed contours for only two cases: 115 GRBs (3 events are removed due to the overlap with the other sample) and for 5 GRBs. They obtained using the Fundamental plane alone: $\Omega_M = 0.630^{+0.352}_{-0.135}$ and $\Omega_M = 0.520^{+0.379}_{-0.253}$ for the two samples, respectively. We symmetrize those results in order to compare them with ours, obtaining: $\Omega_M = 0.630 \pm 0.244$ and $\Omega_M = 0.520 \pm 0.316$. In the first case the results are slightly more precise than the one obtained by us in Table 3, but the considered sample is more than 2 times larger, while the others are slightly less precise, but for a very small sample size of GRBs. In the newer paper Cao, Dainotti, & Ratra (2022) used the Platinum sample for the Dainotti Fundamental plane correlation and 118 events using Amati correlation, out of which 17 overlap with the Platinum sample, thus using 101 events in addition to the Platinum sample and obtained: $\Omega_M > 0.411$ using the Platinum sample alone, $\Omega_M > 0.256$ using the 118 GRBs sample alone, and $\Omega_M = 0.614 \pm 0.255$ using both samples together (101 + 50). The variance of those measurements (0.255) is slightly smaller than the ones of our results (0.28 – 0.27) when both the Amati and the Dainotti relations are combined. The difference in the results when the only Platinum sample is used is due to the fact that we run the analysis 100 times and we average our results, instead in the mentioned paper the results are computed only one time.

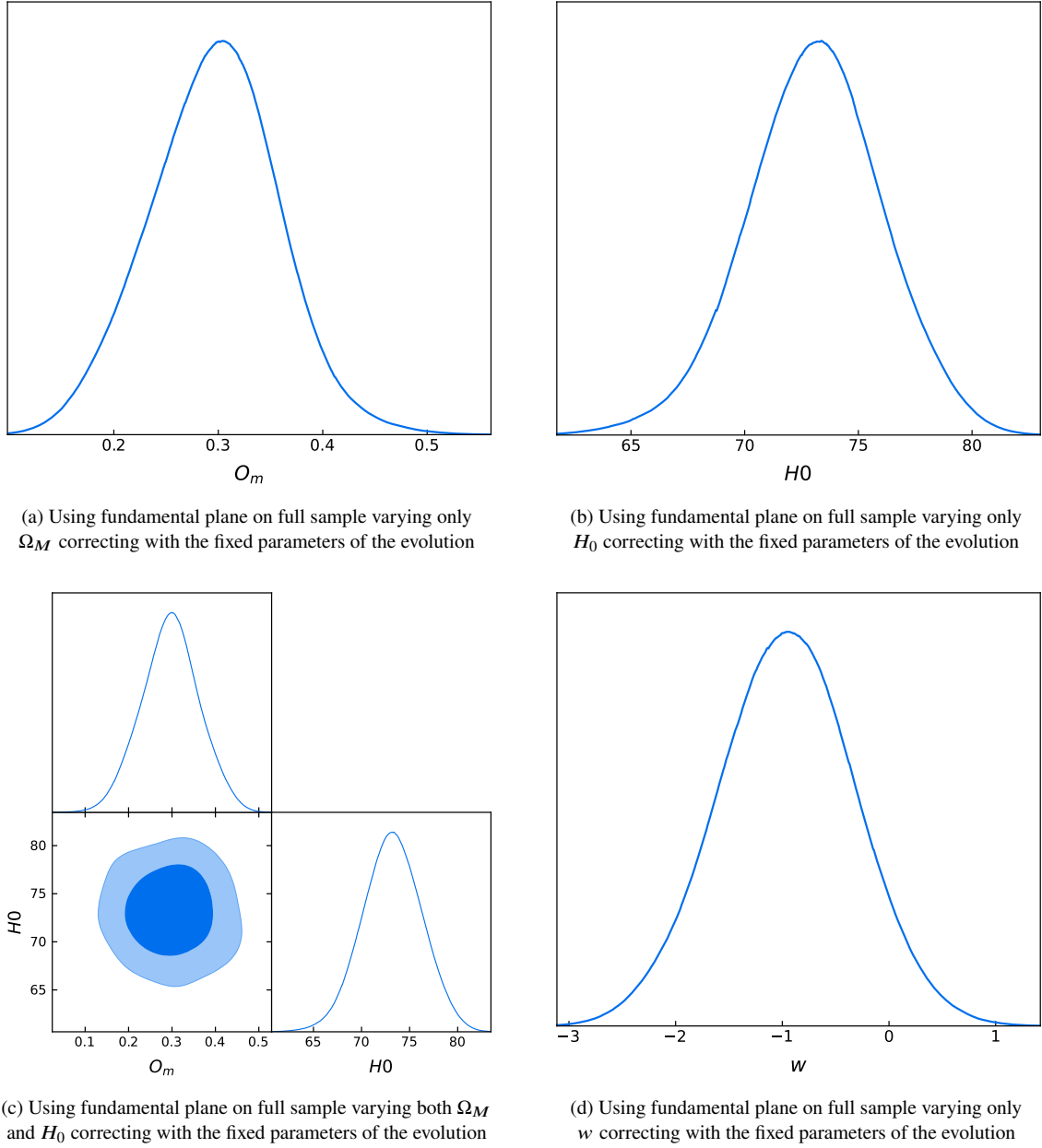


Figure 20. Cosmological results for the GRBs alone (with calibration on SNe Ia) using Fundamental plane, Equation 6 with fixed evolution and the assumptions of 3σ Gaussian priors for the cosmological parameters investigated following Scolnic et al. (2018). Panels a), b), c) and d) show the contours from the case (vi) for the case of Ω_M , H_0 , Ω_M and H_0 together, and w , respectively.

6.6 The flatness of the universe

Due to the recent results in which the flatness of the universe is questioned by Di Valentino et al. (2020) and several other authors we also consider scenarios accounting for its curvature. To consider not-flat universe models we use the appropriate formula for the distance luminosity which reads as follows:

$$d_L = (1 + z) \times d_M, \quad (19)$$

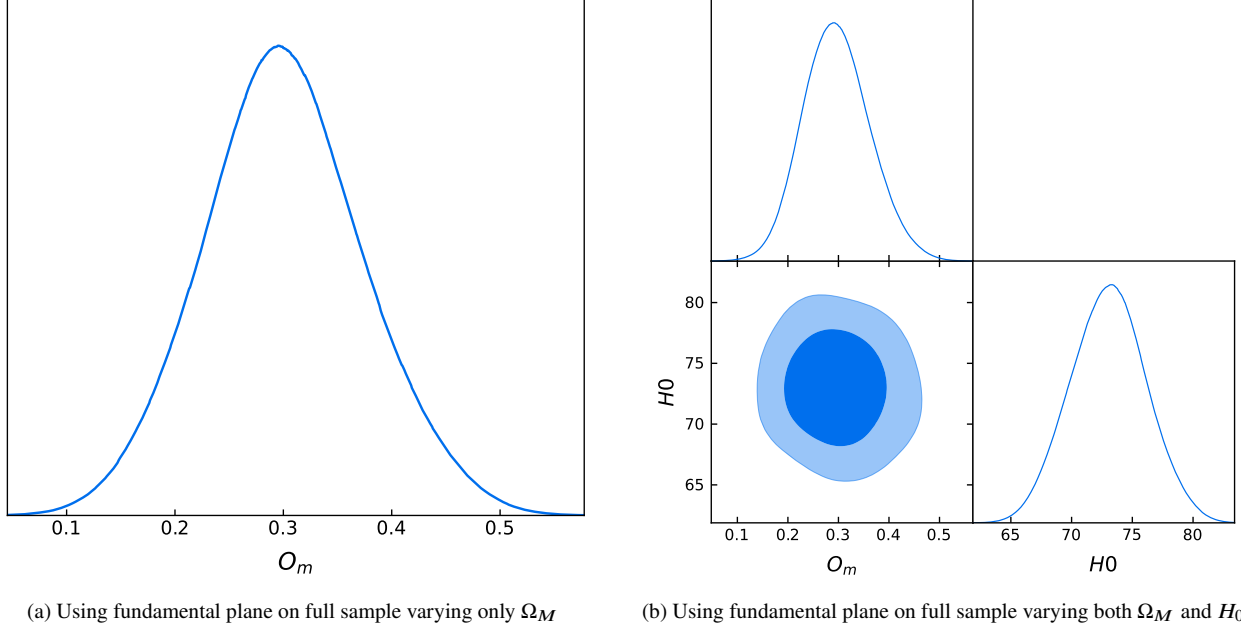


Figure 21. Cosmological results for the GRBs alone (with calibration on SNe Ia) using Fundamental plane, Equation 6 with evolutionary functions and the assumptions of 3σ Gaussian priors on the cosmological parameters investigated following Scolnic et al. (2018). Panels a) and b) show the contours from the case (vi) for the case of Ω_M and the case of Ω_M and H_0 varied together respectively.

Calibration with SNe Ia with uniform priors, Equation 12	parameters varied	Model	$\langle \Omega_M \rangle$	$\langle H_0 \rangle$	$\langle w \rangle$	$\Delta_{GRB}^{GRBU} \%$	$z - score_{SN}$	$z - score_{SN+BAO}$
without evolution	Ω_M	Λ CDM	0.50 ± 0.28	70	-1	326.47	0.718	0.700
without evolution	H_0	Λ CDM	0.30	74.11 ± 13.48	-1	348.29	0.307	0.308
without evolution	w	w CDM	0.30	70	-1.01 ± 0.56	-16.42	0.018	0.012
with fixed evolution	Ω_M	Λ CDM	0.59 ± 0.27	70	-1	297.06	1.077	1.059
with fixed evolution	H_0	Λ CDM	0.30	79.04 ± 13.12	-1	306.57	0.691	0.692
with fixed evolution	w	w CDM	0.30	70	-0.88 ± 0.58	-16.43	0.207	0.236
with $k = k(\Omega_M)$	Ω_M	Λ CDM	0.54 ± 0.27	70	-1	328.57	0.892	0.874
Calibration with SNe Ia with uniform priors, Equations 6 and 7	parameters varied	Model	$\langle \Omega_M \rangle$	$\langle H_0 \rangle$	$\langle w \rangle$	$\Delta_{GRB}^{GRBU} \%$	$z - score_{SN}$	$z - score_{SN+BAO}$
without evolution	Ω_M	Λ CDM	0.52 ± 0.28	70	-1	305.80	0.789	0.771
without evolution	H_0	Λ CDM	0.30	75.70 ± 13.64	-1	337.32	0.420	0.421
without evolution	w	w CDM	0.30	70	-0.97 ± 0.57	-18.22	0.053	0.082
with fixed evolution	Ω_M	Λ CDM	0.52 ± 0.28	70	-1	366.67	0.789	0.771
with fixed evolution	H_0	Λ CDM	0.30	75.71 ± 13.77	-1	338.11	0.417	0.418
with fixed evolution	w	w CDM	0.30	70	-0.97 ± 0.57	-9.67	0.053	0.082
with $k = k(\Omega_M)$	Ω_M	Λ CDM	0.52 ± 0.28	70	-1	283.56	0.789	0.771

Table 4. Averaged Cosmological parameters over 100 runs of the MCMC derived from the calibration on the SNe Ia using GRBs alone assuming uniform priors (indicated with the subscript U) and with μ_{GRB} (first part of the Table) and with Fundamental plane equation, see Equation 6 (2nd part) without evolution, and with the evolution correction, see Equation 7 and as a function of Ω_M . Columns' content is analogous to Table 2. The third column before the last corresponds to the percentage change in errors computed comparing the current results obtained with the GRBs alone with Gaussian priors (indicated with the subscript G) with no calibration taking as reference point values from Table 2. The last two columns represent the z-score from the SNe Ia taking the SNe Ia as a reference point.

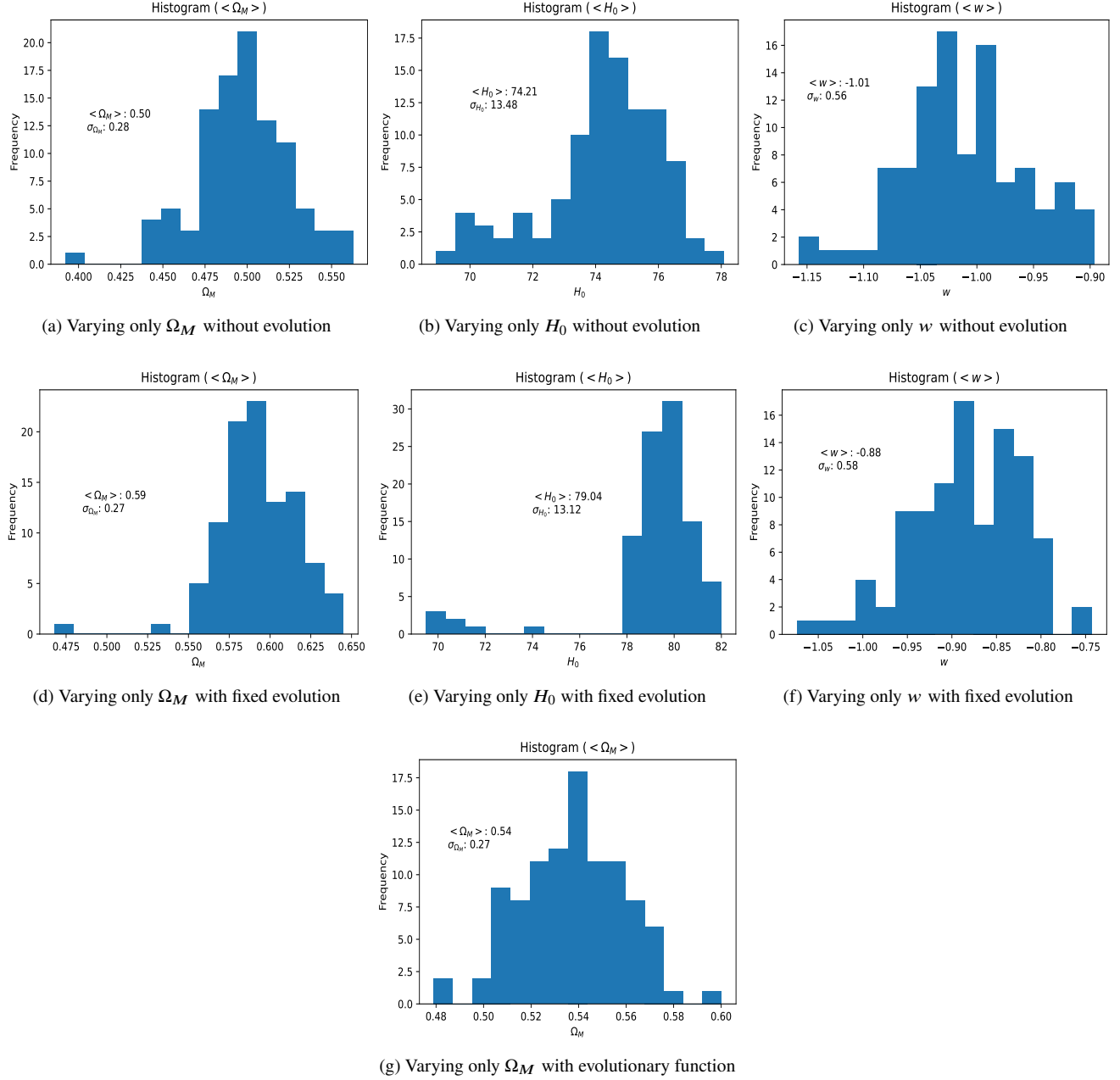


Figure 22. The distributions of the cosmological parameters for the GRBs with calibration and with μ_{GRB} using the assumptions of uniform priors of 100 runs of MCMC. Panels a), b), c) show the contours from case with no evolution (upper panel), evolution with fixed parameters (central panel) and with the evolutionary functions (lower panel) for the case of Ω_M , H_0 , and w , respectively.

where d_M is the transverse comoving distance given by the formula:

$$d_M = \begin{cases} \frac{c}{H_0 \sqrt{\Omega_k}} \sinh \left(\sqrt{\Omega_k} \times \int_0^z \frac{dz'}{\sqrt{\Omega_M (1+z')^3 + \Omega_k (1+z')^2 + \Omega_\Lambda}} \right) & \Omega_k > 0 \\ \frac{c}{H_0} \times \int_0^z \frac{dz'}{\sqrt{\Omega_M (1+z')^3 + \Omega_k (1+z')^2 + \Omega_\Lambda}} & \Omega_k = 0 \\ \frac{c}{H_0 \sqrt{|\Omega_k|}} \sin \left(\sqrt{|\Omega_k|} \times \int_0^z \frac{dz'}{\sqrt{\Omega_M (1+z')^3 + \Omega_k (1+z')^2 + \Omega_\Lambda}} \right) & \Omega_k < 0. \end{cases} \quad (20)$$

The results shown in Table 6 correspond to the computation of Ω_k parameter with the other parameters fixed: $\Omega_M = 0.30$, $H_0 = 70 \text{ km s}^{-1} \text{ Mpc}^{-1}$. All the obtained values are compatible within 1.5σ with $\Omega_k = 0$ corresponding to the flat universe. To

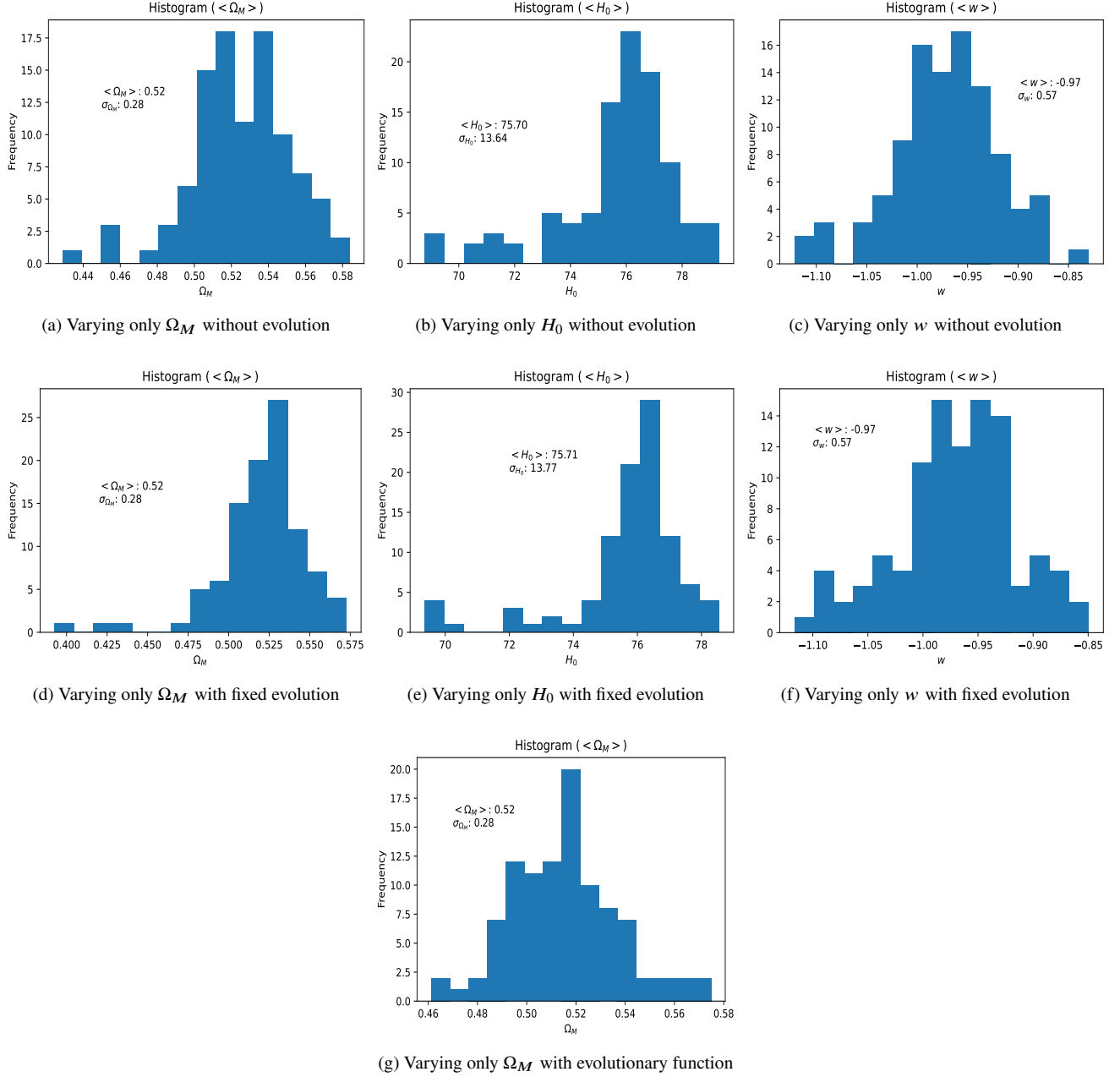


Figure 23. The distributions of the cosmological parameters for the GRBs with calibration and with L_X , Equations 6 and 7 using the assumptions of uniform priors and over 100 runs of MCMC. Panels a), b), c) show the contours from case with no evolution (upper panel), evolution with fixed parameters (central panel) and with the evolutionary functions (lower panel) for the case of Ω_M , H_0 , and w , respectively.

compare the results we use the z-score, defined as:

$$z = \frac{|\Omega_{k,flat} - \Omega_k|}{\Delta\Omega_k} = \frac{|\Omega_k|}{\Delta\Omega_k}. \quad (21)$$

The z-score results are presented in the last column of Table 6. We note an interesting trend. When we add more probes to the SNe Ia sample, the value of Ω_k becomes less close to $\Omega_k = 0$ (the flat universe). The addition of the correction for evolution is indeed leading to a more compatible value (1.18 for z-score) with the flat universe. We present the results of the following computation in Fig. 28.

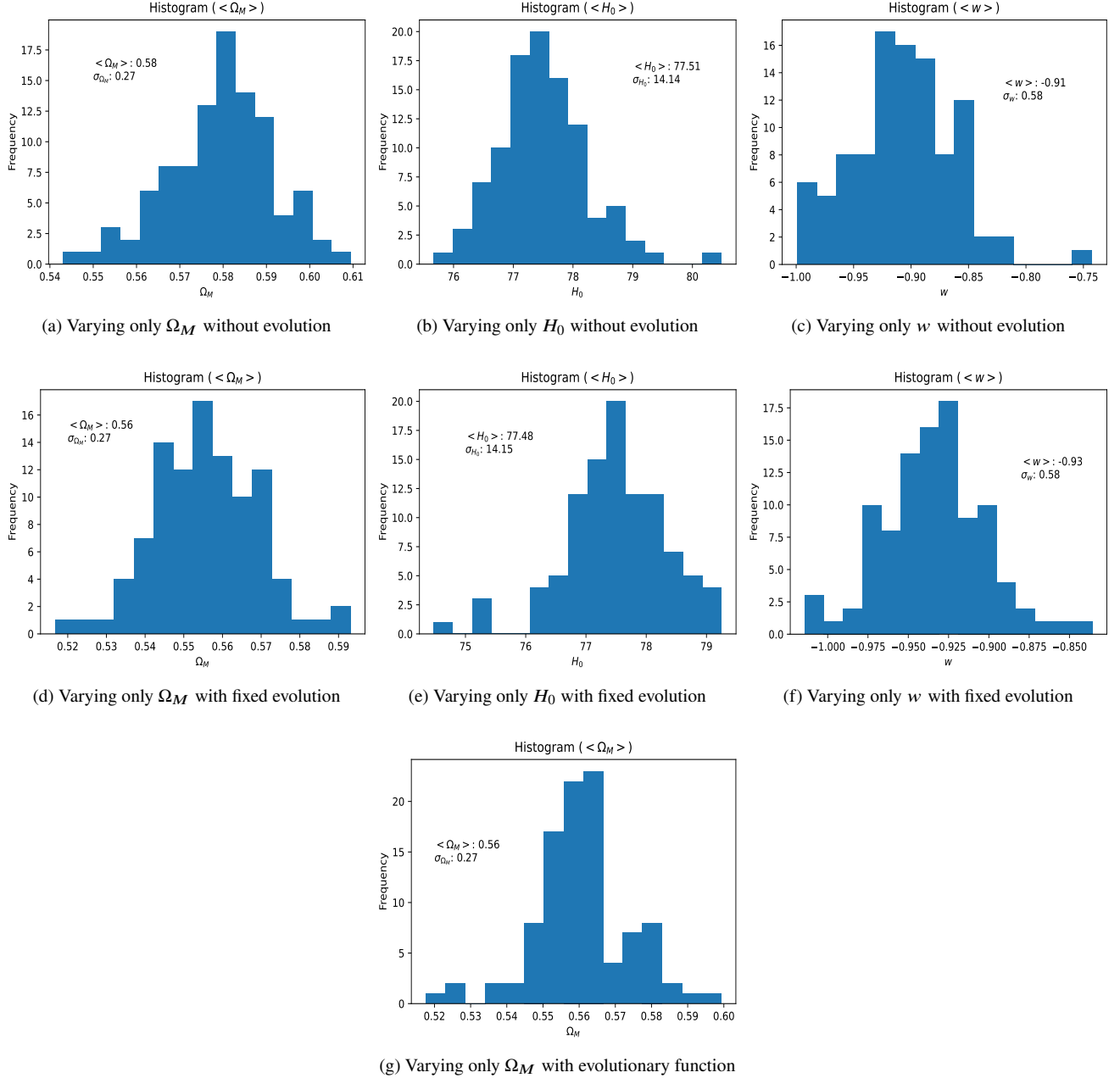


Figure 24. The distributions of the cosmological parameters for the GRBs without calibration and with μ_{GRB} using the assumptions of uniform priors of 100 runs of MCMC. Panels a), b), c) show the contours from case with no evolution (upper panels), evolution with fixed parameters (central panels) and with the evolutionary functions (lower panel) for the case of Ω_M .

7 THE COMPARISON OF GRBS ALONE AND SNE IA ALONE AND SNE IA+BAO

In this section, we evaluate the comparison between the cosmological parameters and their uncertainties of GRBs alone with the SNe Ia alone, and then SNe Ia + BAO. This analysis is done using GRBs for which we consider Gaussian priors of 3σ on the values of the cosmological parameters from SNe Ia taken from [Scolnic et al. \(2018\)](#). We divide our comparison between GRBs without and with calibration on SNe Ia, see Tables 7 and 8, respectively. Specifically, we compare the results in the i)-vi) cases as detailed in Sec. 6.1 without calibration, and in Sec. 6.2 for i)-vi) cases with the calibration. In this way, it will be clear which analysis brings smaller uncertainties. Looking specifically at the distance in terms of σ to the SNe Ia and SNe Ia+BAO, we refer to Table 1 for the comparison of GRBs without calibration with the Gaussian priors.

We first consider the comparison with SNe Ia alone. All the cosmological parameter results, except for the H_0 one when the likelihood of μ_{GRB} (see the upper part of Table 1) is considered in the cases of no evolution and fixed evolution, fall within 1σ . For the cases with and without evolution the z-score is 1.024 and 1.025, respectively, when varying both Ω_M and H_0 .

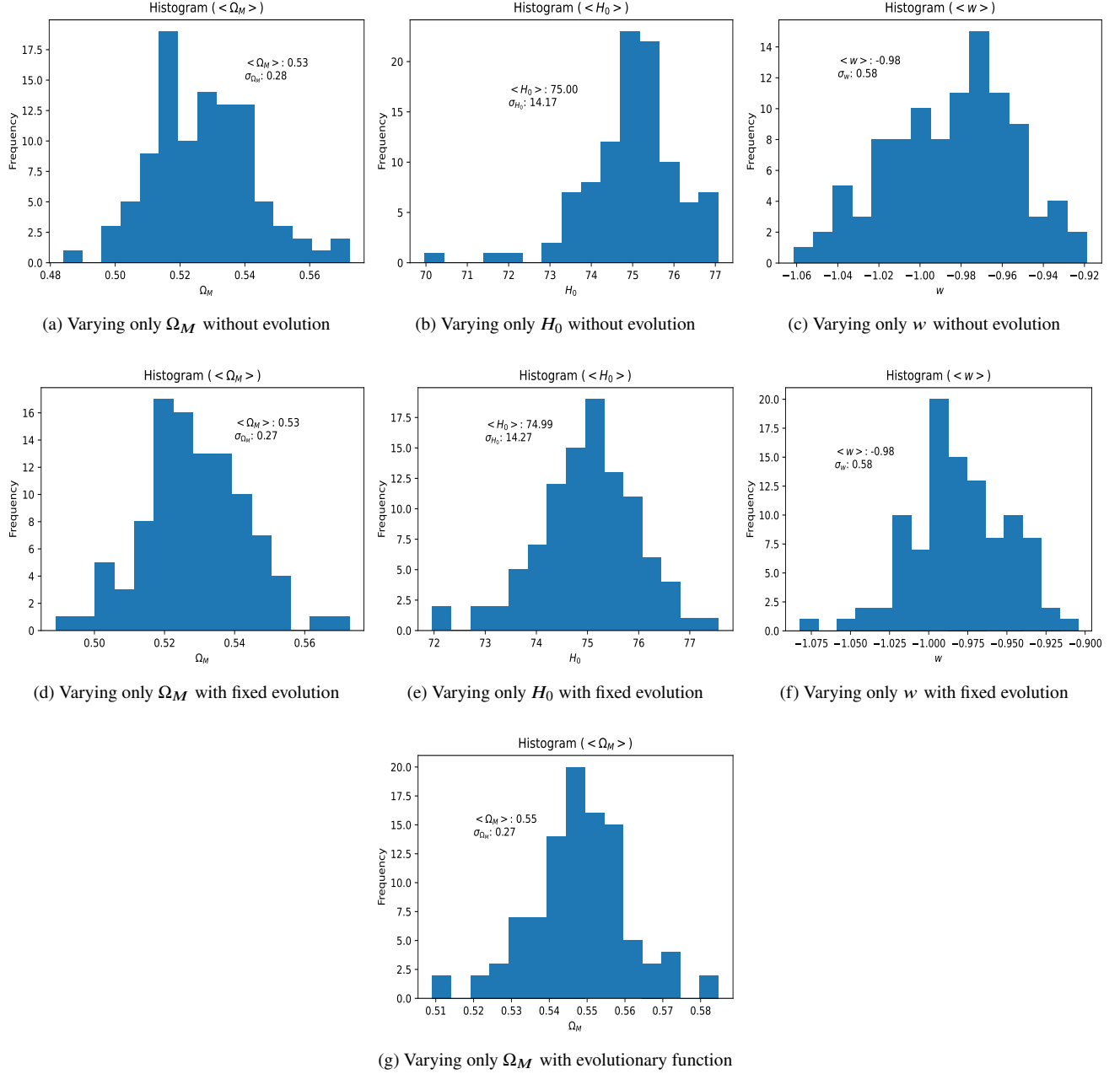


Figure 25. The distributions of the cosmological parameters for the GRBs without calibration and with L_X , Equations 6 and 7 using the assumptions of uniform priors and over 100 runs of MCMC. Panels a), b), c) show the contours from case with no evolution (upper panels), evolution with fixed parameters (central panels) and with the evolutionary functions (lower panel) for the case of Ω_M .

When we look instead at the second part of Table 1 we consider the likelihood for Equations 6 and 7, and the only case that fall outside 1σ is the one for which H_0 is computed without accounting for the evolution (z-score = 1.021).

When comparing with SNe Ia + BAO and considering the likelihood of GRBs with μ_{GRB} , all cases fall within 1σ with the exception again of H_0 without evolution (z-score = 1.09), with fixed evolution (z-score = 1.10) and with the $k = k(\Omega_M)$ evolutionary function (z-score = 1.02). When comparing with SNe Ia + BAO and considering the likelihood for Equations 6 and 7, all cases fall within 1σ with the exception again of H_0 without evolution when varying only H_0 (z-score = 1.024) and when varying both Ω_M and H_0 (z-score = 1.09), and with $k = k(\Omega_M)$ evolutionary function (z-score = 1.065).

In Table 2, we show results obtained for GRBs alone calibrated with SNe Ia with Gaussian priors compared with SNe Ia alone and SNe Ia + BAO. We start the comparison with the SNe Ia only first. We see that the results which are not compatible within 1σ with the likelihood of μ_{GRB} (upper part of Table 2) are the following: H_0 varied alone without correction for evolution is compatible in 1.102σ , H_0 varied together with Ω_M without correction for evolution is compatible in 1.103σ , and H_0 varied

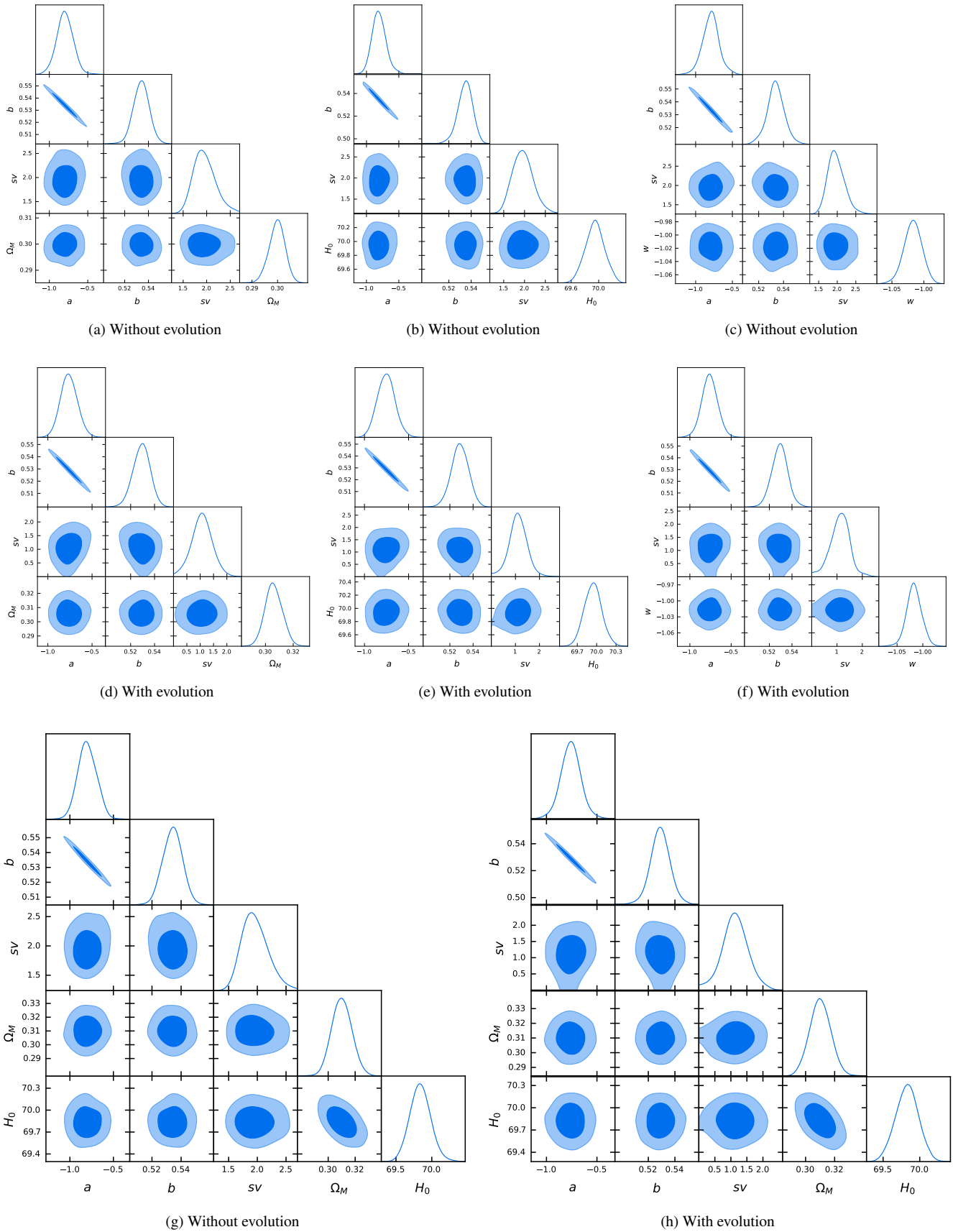


Figure 26. Cosmological results for the GRBs and SNe Ia data with the BAO constraints with uniform priors.

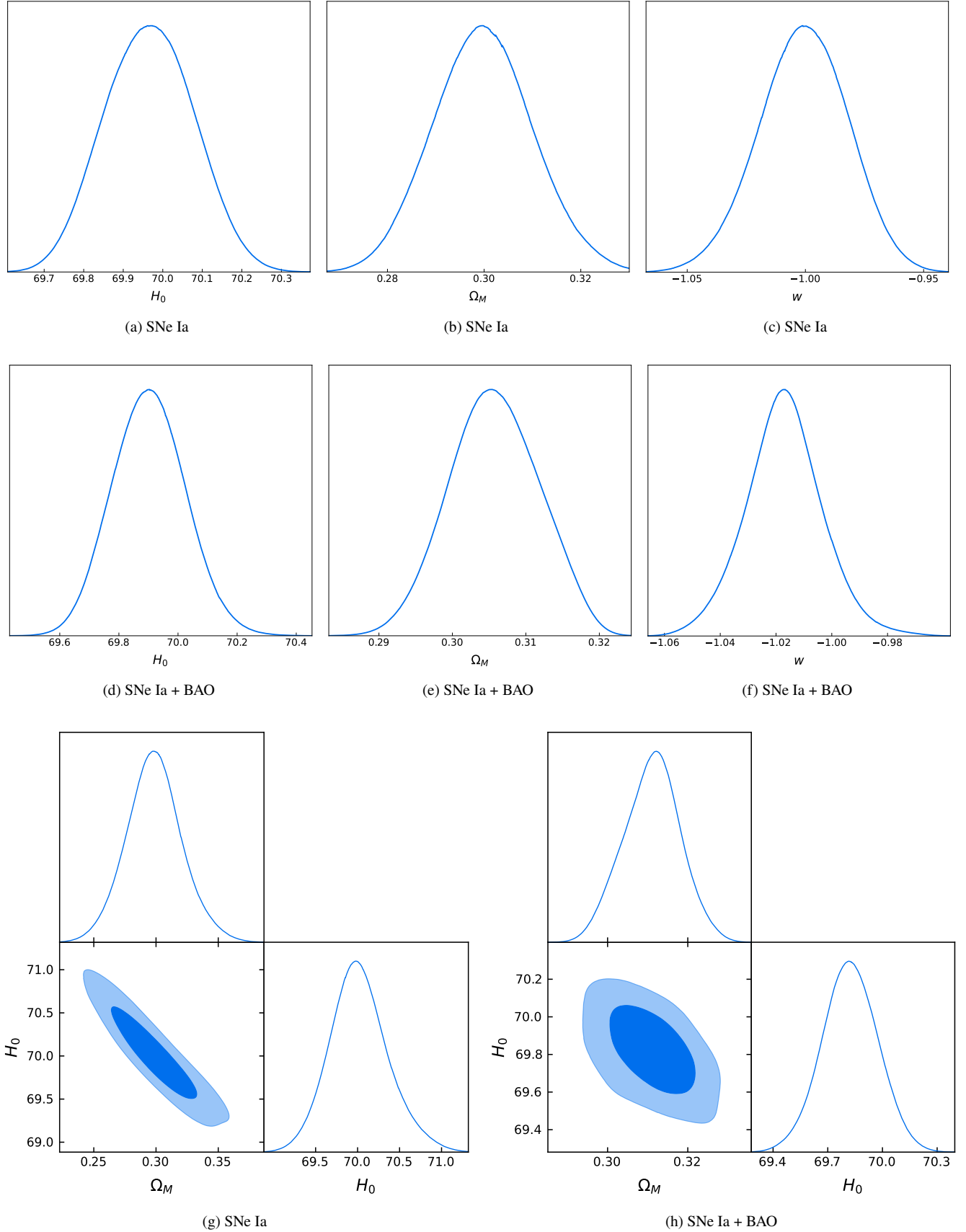


Figure 27. Cosmological results considering only SNe Ia and SNe Ia+BAO using uniform priors. In a) we fix H_0 , in b) we fix Ω_M in c) we fix Ω_M and H_0 . The central panel is the same as the upper panel but adding BAO.

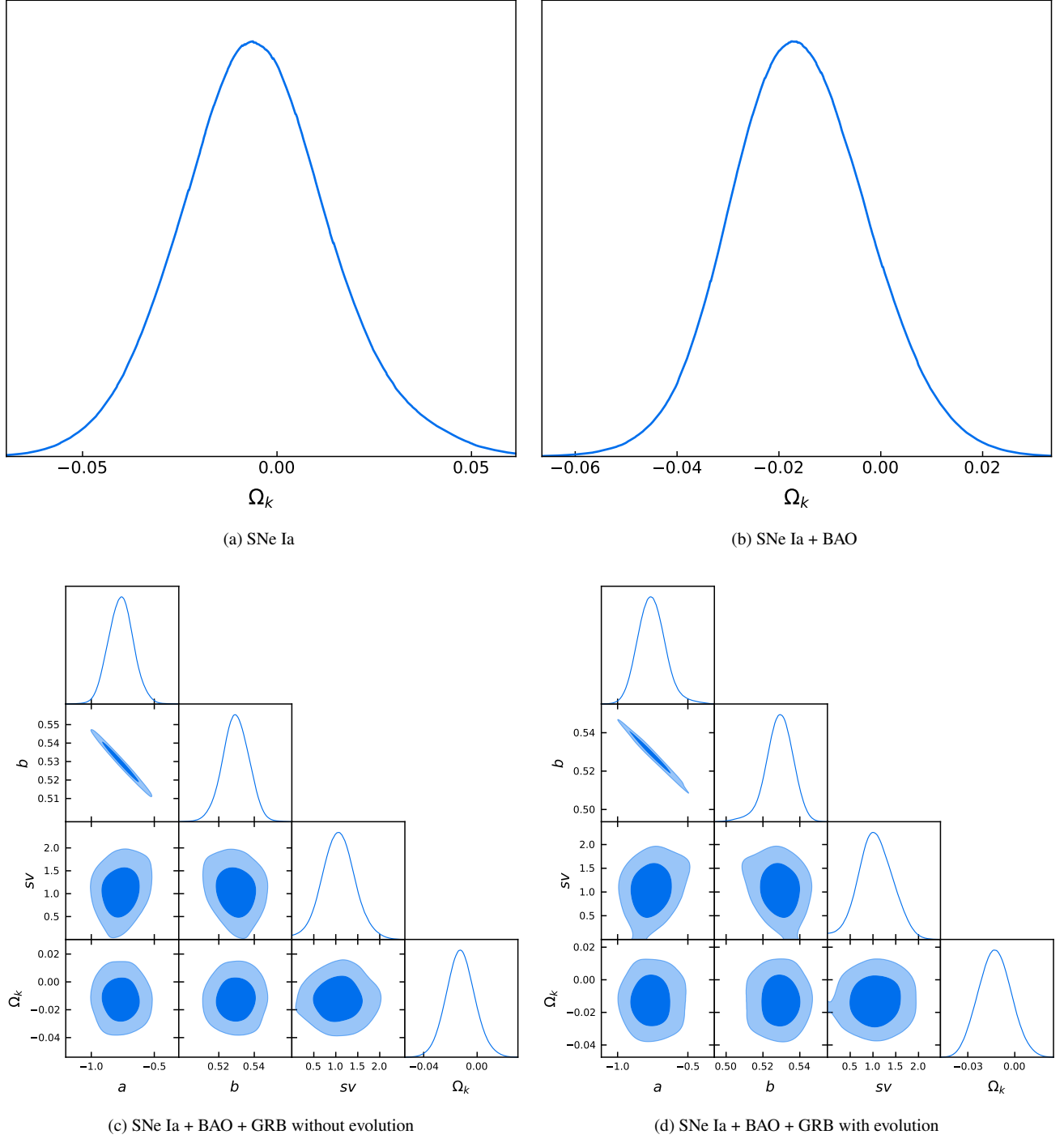


Figure 28. The upper left and right panels show the values of Ω_k fixing H_0 and Ω_M for the SNe Ia and SNe Ia+BAO, respectively. The lower right and left panel shows again the values of Ω_k , but for the SNe Ia+BAO+GRBs with no evolution and SNe Ia+BAO+GRBs with evolution with fixed parameters, respectively. The priors on all probes are uniform.

together with Ω_M with fixed correction for evolution is compatible in 1.046σ . Results that are not compatible in 1σ with SNe Ia when we consider again calibrated GRBs alone with Gaussian priors, but using instead the likelihood derived from the Fundamental plane equation (Equations 7 and 6) (see the lower part of Table 2), are the following: H_0 varied alone without correction for evolution is compatible in 1.137σ , H_0 varied alone with fixed correction for evolution is compatible in 1.050σ , and H_0 varied together with Ω_M with fixed correction for evolution is compatible in 1.033σ .

When we compare SNe Ia + BAO results with the ones obtained with calibrated GRBs alone using the likelihood of μ_{GRB} (see the upper part of Table 2) we obtain that the following are not compatible in 1σ : H_0 varied alone without correction for

SNe Ia sample	Model	w	Ω_M	H_0	–	$\Delta_{SNe+BAO}^{SNe} \%$
varying Ω_M	Λ CDM	-1	0.299 ± 0.007	70	-	16.7
varying H_0	Λ CDM	-1	0.30	69.97 ± 0.13	-	0%
varying Ω_M and H_0	Λ CDM	-1	0.298 ± 0.022	70.02 ± 0.34	-	214.3 %, 142.3 %
varying w	w CDM	-1.000 ± 0.018	0.30	70	-	28.6 %
SNe Ia + BAO sample	Model	w	Ω_M	H_0	$\Delta_{SNe+BAO}^{SNe+BAO} \%$	–
varying Ω_M	Λ CDM	-1	0.304 ± 0.006	70	-14.3 %	-
varying H_0	Λ CDM	-1	0.30	69.96 ± 0.13	0 %	-
varying Ω_M and H_0	Λ CDM	-1	0.311 ± 0.007	69.82 ± 0.14	-68.2 %, -58.8 %	-
varying w	w CDM	-1.017 ± 0.014	0.30	70	-22.2 %	-
SNe Ia + BAO + GRB sample NO EV	Model	w	Ω_M	H_0	$\Delta_{SNe+BAO+GRBNOEV}^{SNe+BAO+GRBNOEV} \%$	$\Delta_{SNe+BAO}^{SNe+BAO+GRBNOEV} \%$
varying Ω_M	Λ CDM	-1	0.306 ± 0.006	70	-14.3 %	0 %
varying H_0	Λ CDM	-1	0.30	69.94 ± 0.13	0 %	0 %
varying Ω_M and H_0	Λ CDM	-1	0.310 ± 0.007	69.84 ± 0.15	-68.2%, -55.9 %	0%, 7.1 %
varying w	w CDM	-1.017 ± 0.014	0.30	70	-22.2 %	0%
SNe Ia + BAO + GRB sample EV	Model	w	Ω_M	H_0	$\Delta_{SNe+BAO+GRBEV}^{SNe+BAO+GRBEV} \%$	$\Delta_{SNe+BAO}^{SNe+BAO+GRBEV} \%$
varying Ω_M	Λ CDM	-1	0.306 ± 0.006	70	-14.3 %	0 %
varying H_0	Λ CDM	-1	0.30	69.94 ± 0.14	7.7 %	7.7%
varying Ω_M and H_0	Λ CDM	-1	0.310 ± 0.007	69.83 ± 0.16	-68.2 %, -52.9 %	0%, 14.3 %
varying w	w CDM	-1.017 ± 0.015	0.30	70	-16.7 %	7.1%

Table 5. Results of the fitting of the cosmological parameters using the SNe Ia (the upper part of the Table), SNe Ia+BAO (the second part), and SNe Ia+BAO+GRBs using GRBs without calibration on SNe Ia and with uniform priors without (the third part) and with (the bottom) the correction for the evolution indicated with EV, using together the platinum sample, the Pantheon sample for SNe Ia and the BAO measurements of [Sharov & Vasiliev \(2018\)](#). The values in bold are fixed at fiducial values. We also show two columns with the percentage increase/decrease between the uncertainties of SNe Ia only (the $\Delta_{SNe}^{considered\ sample} \%$) versus the other results, and the BAO+SNe Ia ($\Delta_{SNe+BAO}^{considered\ sample} \%$) versus the other results. The formula is: $\frac{\Delta_{comparing} - \Delta_{reference}}{\Delta_{reference}}$, where $\Delta_{reference}$ is the uncertainty obtained with SNe Ia (6th column) and SNe Ia + BAO (7th column) samples. With the negative sign we indicate a percentage decrease on the uncertainty compared to the reference sample (indicated with a lower subscript), while with the positive one a percentage increase.

Sample	Ω_k	z-score
SNe Ia sample	-0.003 ± 0.018	0.17
SNe Ia + BAO sample	-0.016 ± 0.012	1.33
SNe Ia + BAO + GRB sample NO EV	-0.017 ± 0.012	1.42
SNe Ia + BAO + GRB sample EV	-0.013 ± 0.011	1.18

Table 6. Results of the fitting of the Ω_k parameter for different samples and probes. All the obtained values are compatible within 1.5σ with $\Omega_k = 0$ corresponding to the flat universe. To compare the results with the flat cosmology we use the z-score, defined as: $z = \frac{|\Omega_{k,flat} - \Omega_k|}{\Delta_{\Omega_k}} = \frac{|\Omega_k|}{\Delta_{\Omega_k}}$.

evolution is compatible in 1.105σ , H_0 varied together with Ω_M without correction for evolution is compatible in 1.176σ , H_0 varied together with Ω_M with fixed correction for evolution is compatible in 1.116σ , H_0 varied together with Ω_M with the correction for evolution as $k = k(\Omega_M)$ is compatible in 1.064σ .

When we compare SNe Ia + BAO results with the ones obtained with calibrated GRBs alone using the likelihood derived from the Fundamental plane equation (Equations 7 and 6) (see the lower part of Table 2) we obtain, that the following results are not compatible in 1σ : H_0 varied alone without correction for evolution is compatible in 1.140σ , H_0 varied together with Ω_M without correction for evolution is compatible in 1.004σ , H_0 varied alone with fixed correction for evolution is compatible in 1.140σ , H_0 varied together with Ω_M with fixed correction for evolution is compatible in 1.103σ , H_0 varied together with Ω_M with the correction for evolution as $k = k(\Omega_M)$ is compatible in 1.042σ .

Likelihood based on μ_{GRB} , Equation 12	parameters varied	Model	$\Delta_{SN}^{GRB} \%$	$\Delta_{SN+BAO}^{GRB} \%$
without evolution	Ω_M	Λ CDM	800.00	950.00
without evolution	H_0	Λ CDM	2443.85	2443.85
without evolution	Ω_M and H_0	Λ CDM	209.09, 790.00	871.43, 2061.43
without evolution	w	w CDM	3883.33	5021.43
with fixed evolution	Ω_M	Λ CDM	800.00	950.00
with fixed evolution	H_0	Λ CDM	2146.92	2146.92
with fixed evolution	Ω_M and H_0	Λ CDM	190.91, 784.71	814.29, 2048.57
with fixed evolution	w	w CDM	3344.44	4328.57
with $k = k(\Omega_M)$	Ω_M	Λ CDM	785.71	933.33
with $k = k(\Omega_M)$	Ω_M and H_0	Λ CDM	195.46, 823.24	828.57, 2142.14
Likelihood based on L_X , Equations 6 and 7	parameters varied	Model	$\Delta_{SN}^{GRB} \%$	$\Delta_{SN+BAO}^{GRB} \%$
without evolution	Ω_M	Λ CDM	771.43	916.67
without evolution	H_0	Λ CDM	2294.62	2294.62
without evolution	Ω_M and H_0	Λ CDM	190.91, 825.00	814.29, 2146.43
without evolution	w	w CDM	5722.22	7385.71
with fixed evolution	Ω_M	Λ CDM	828.57	983.33
with fixed evolution	H_0	Λ CDM	2304.62	2304.62
with fixed evolution	Ω_M and H_0	Λ CDM	195.46, 796.77	828.57, 2077.86
with fixed evolution	w	w CDM	3577.78	4628.57
with $k = k(\Omega_M)$	Ω_M	Λ CDM	800.00	950.00
with $k = k(\Omega_M)$	Ω_M and H_0	Λ CDM	190.91, 812.06	9042.86, 2115.00

Table 7. The table of comparison between the cosmological parameters derived from SNe Ia and from SNe Ia + BAO with GRBs alone using Gaussian priors without calibration on SNe (Table 1). The table is divided into two parts. The first part compares SNe Ia and SNe Ia + BAO with GRBs alone with no calibration (in particular, the percentage decrease of the errors on the measurements) when the computation of the cosmological parameters with GRBs has been performed using Equations 6 and 7. The second part is related to the comparison with SNe Ia and SNe Ia + BAO with GRBs alone, but using μ_{GRB} , Equation 12. The uncertainty percentage change is computed with formulas: $\Delta_{SN}^{GRB} \%$ = $\frac{\Delta_{GRB} - \Delta_{SN}}{\Delta_{SN}}$ and $\Delta_{SN+BAO}^{GRB} \%$ = $\frac{\Delta_{GRB} - \Delta_{SN+BAO}}{\Delta_{SN+BAO}}$. Those quantities measure how much SNe Ia alone and SNe Ia+BAOs have smaller scatter than the GRBs alone. With the negative sign we indicate a percentage decrease on the uncertainty compared to the reference sample (indicated with a lower subscript), while with the positive one a percentage increase. References for comparisons are SNe Ia and SNe Ia + BAO.

We now check the compatibility of the results obtained with GRBs alone with uniform priors in Tables 3, 4. In Table 3 where GRBs have not been calibrated with SNe Ia and with the likelihood based on μ_{GRB} , the only case that exceeds 1σ limit for both SNe Ia alone and SNe Ia + BAO is when we vary Ω_M only without correction for the evolution. The z-scores for SNe Ia alone and SNe Ia + BAO in this case are 1.040 and 1.022, respectively.

In Table 4 the only case of GRBs alone with calibration with uniform priors and with the likelihood based on μ_{GRB} that exceeds the 1σ limit for both SNe Ia alone and SNe Ia + BAO is the one where we compute Ω_M only with fixed correction for evolution. The z-scores for SNe Ia alone and SNe Ia + BAO in this case are 1.077 and 1.059, respectively. When we look instead at the lower part of Tables 3 and 4 considering the likelihood Equations 6 and 7, all cases for SNe Ia alone and SNe Ia + BAO fall within 1σ .

All the percentage variations of SNe Ia alone and SNe Ia+BAO results with respect to the GRB results (SNe Ia and SNe Ia + BAO are taken as reference in the percentage variation computation, respectively) both without and with calibration on SNe Ia are shown in the last two columns of Tables 7 and 8, respectively. The percentage variation of SNe Ia + BAO with GRBs alone ($\Delta_{SN+BAO}^{GRB} \%$) is in general larger than the one of SNe Ia alone with GRBs ($\Delta_{SN}^{GRB} \%$). More specifically, looking at Table 7 where GRBs have not been calibrated, the minimum percentage increase (190.91 %) is when comparing with SNe Ia results and in two cases 1) when we vary Ω_M and H_0 together with fixed evolution using distance modulus μ_{GRB} , equation 12 and 2) when we

Calibration with SNe Ia, Equation 12	parameters varied	Model	$\Delta_{SN}^{GRB} \%$	$\Delta_{SN+BAO}^{GRB} \%$
without evolution	Ω_M	Λ CDM	871.43	1033.33
without evolution	H_0	Λ CDM	2213.08	2213.07
without evolution	Ω_M and H_0	Λ CDM	190.91, 784.11	814.29, 2047.14
without evolution	w	w CDM	3638.89	4707.14
with fixed evolution	Ω_M	Λ CDM	871.43	1033.33
with fixed evolution	H_0	Λ CDM	2382.31	2382.31
with fixed evolution	Ω_M and H_0	Λ CDM	172.72, 806.47	757.14, 2101.43
with fixed evolution	w	w CDM	3755.56	4857.14
with $k = k(\Omega_M)$	Ω_M	Λ CDM	800.00	950.00
with $k = k(\Omega_M)$	Ω_M and H_0	Λ CDM	190.91, 821.76	814.29, 2138.57
Calibration with SNe Ia, Equation 6 and 7	parameters varied	Model	$\Delta_{SN}^{GRB} \%$	$\Delta_{SN+BAO}^{GRB} \%$
without evolution	Ω_M	Λ CDM	885.71	1050.00
without evolution	H_0	Λ CDM	2299.23	2299.23
without evolution	Ω_M and H_0	Λ CDM	195.45, 856.17	828.57, 2222.14
without evolution	w	w CDM	3772.22	4878.57
with fixed evolution	Ω_M	Λ CDM	757.14	900
with fixed evolution	H_0	Λ CDM	2317.69	2317.69
with fixed evolution	Ω_M and H_0	Λ CDM	200.00, 800.59	842.86, 2087.14
with fixed evolution	w	w CDM	3405.56	4407.14
with $k = k(\Omega_M)$	Ω_M	Λ CDM	942.86	1116.67
with $k = k(\Omega_M)$	Ω_M and H_0	Λ CDM	190.91, 803.82	814.29, 2095.00

Table 8. The Table of comparison between the cosmological parameters derived from SNe Ia and from SNe Ia + BAO with GRBs alone using Gaussian priors with calibration on SNe Ia. The first part compares SNe Ia and SNe Ia +BAO with GRBs alone calibrated with SNe Ia (in particular, the percentage decrease of the uncertainties on the measurements) when the computation of the cosmological parameters with GRBs has been performed using Equations 6 and 7. The second part is related to the comparison with SNe Ia and SNe Ia +BAO with GRBs alone, but using μ_{GRB} , Equation 12. The percentage decrease is computed with formulas: $\Delta_{SN}^{GRB} \%$ = $\frac{\Delta_{GRB} - \Delta_{SN}}{\Delta_{SN}}$ and $\Delta_{SN+BAO}^{GRB} \%$ = $\frac{\Delta_{GRB} - \Delta_{SN+BAO}}{\Delta_{SN+BAO}}$. Those quantities measure how much GRBs alone have a larger scatter than SNe Ia alone and SNe Ia + BAO. With the negative sign we indicate a percentage decrease on the uncertainty compared to the reference sample (indicated with a lower subscript), while with the positive one a percentage increase. References for comparisons are SNe Ia alone and SNe Ia + BAO.

vary Ω_M and H_0 together with evolutionary functions, $k = k(\Omega_M)$ using fundamental plane equations, 6 and 7. The maximum percentage increase (5021.43 %) is when comparing with SNe Ia + BAO results and in the case when we vary w in the case without evolution using distance moduli μ_{GRB} , equation 12.

Now, considering the comparison of calibrated GRBs with SNe Ia and SNe Ia + BAOs (see Table 8), the percentage variation of the uncertainties spans from 172.72% when comparing with SNe Ia only in the case of fixed evolutionary parameters and varying Ω_M and H_0 together using distance moduli μ_{GRB} , equation 12, to almost 4878.57% when comparing with SNe Ia + BAOs and varying w in the case without evolution using fundamental plane equations, 6 and 7. In general, the minimum percentage difference in the uncertainty has been found for the case when both Ω_M and H_0 are varied together, both for the calibration and no-calibration cases, and when comparing with SNe Ia alone results. The maximum percentage difference, instead, is found for the case where w is varied both for the calibration and no-calibration cases, and when comparing with SNe Ia + BAO results. We can conclude that SNe Ia alone and SNe Ia + BAO have tighter constraints on the cosmological parameters than GRBs alone, which in turn has larger uncertainties, as expected.

This conclusion does not undermine the possibility of using GRBs as standalone cosmological probes. Indeed, in the very first papers regarding SNe Ia cosmology, (Riess et al. 1998; Perlmutter et al. 1999), the uncertainties on the Ω_M parameter was 0.28 ± 0.09 , which, compared to the current analysis, is 47.54% larger than the same parameter computed using GRBs for the case

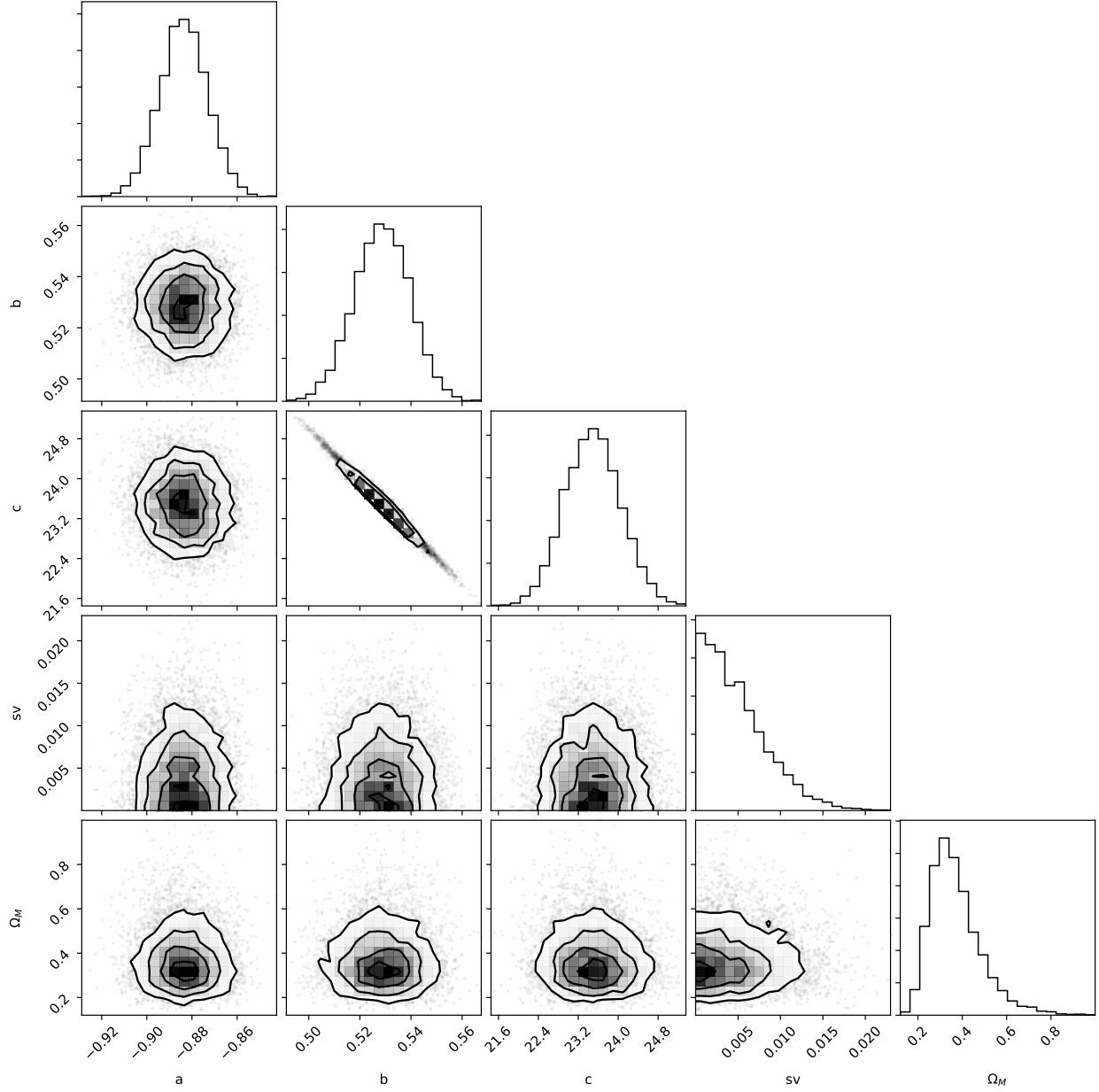


Figure 29. Posterior contours for Ω_M considering 800 simulated GRBs on the platinum fundamental plane.

without evolution and calibration. Further, when we compare this value to GRBs for the case in which evolutionary functions, $k = k(\Omega_M)$ are considered and with calibration on SNe Ia (the largest variance obtained in Tables 1 and 2 $\Omega_M = 0.300 \pm 0.073$), our results have an uncertainty on Ω_M 23.29% smaller. In addition, the current sample of GRBs is 100 times smaller than the current sample of SNe Ia. In the next section indeed we calculate the predictions on the uncertainties on the cosmological parameters if we simulate a sample of 800 GRBs.

8 THE FUTURE USE OF GRB COSMOLOGY AS STANDALONE PROBES

Regarding the use of GRBs as standalone standard candles, in [Dainotti et al. \(2022c\)](#), we studied how many GRBs are required to obtain constraints on the cosmological parameters (in particular on Ω_M) similar to the ones obtained in the literature using SNe Ia, thus giving a realistic forecast of the time required to reach these limits, taking into account present and future telescopes and missions. In order to do so, we simulated different numbers of GRBs starting from the physical features of the platinum sample,

as well as an optical sample of GRBs, opening this studies also to the optical wavelength domain. One of our simulations is shown in Fig. 29, where we note a closed contour for Ω_M for 800 GRBs. The number of 800 GRBs gives a satisfactory precision on Ω_M . Indeed, we have also computed that the number of platinum GRBs which are needed to achieve the same precision reached by Conley et al. (2011) with 472 SNe Ia is 789 if no machine learning and lightcurve reconstructions are involved.

More specifically, in Dainotti et al. (2022c) we have studied, via simulations, the effects that the platinum and the optical samples will have on future studies when the sample size will be increased thanks to 1) new observations by SVOM, Theseus and other ground-based observations 2) the use of machine learning (Dainotti et al. in preparation), 3) the use of lightcurves reconstruction (Dainotti et al. in preparation). Going more-in depth in the analysis performed in the cited paper, the simulations were based on the best-fit fundamental planes obtained by considering different baseline samples. Indeed, not only the entire platinum and optical sets were considered but also subsets built by choosing the closest GRBs to the best-fit planes following two different methods. Then, the simulations were performed by creating GRBs observations lying on the best-fit planes, considering as starting distributions the ones provided by the observed GRBs used as a baseline. We have also run simulations in which we halved the errors on the quantities involved in the best-fit fundamental planes, simulating the increase in the precision which is expected to be achieved by future observations. The goal was to infer how many simulated GRBs are needed to reach pivotal thresholds on the precision on Ω_M achieved by the SNe Ia cosmological literature, namely Conley et al. (2011); Betoule et al. (2014), and Scolnic et al. (2018) results, who found an error on Ω_M equal to 0.10, 0.042, and 0.022, respectively, with the assumption that the ratio of the X-rays and optical plateau will be the same as currently. Indeed, this is a conservative estimate, since we expect to have more GRBs in the future at high redshift and more enhanced sensitivities in X-rays and optical so that more plateaus can indeed be observed. Once we have found the exact number of simulated GRBs necessary to achieve these limits, we have considered both present and future missions and observational campaigns (especially the future SVOM and Theseus missions), to give a realistic time period in which these precisions shall be reached by the standalone GRBs used as cosmological probes. This has been done both considering the current observed data, as well as taking into account machine learning and lightcurve reconstruction methods, which can be used for inferring the redshifts of GRBs observations and decreasing the errors on the observed quantities themselves, respectively. With the analysis of machine learning we will be able to double the optical plateaus, while with the lightcurve reconstruction analysis we will be able to obtain a lightcurve with almost half (47.5 %) of the error carried by the lightcurves not reconstructed. When the machine learning, lightcurve reconstruction and errorbars divided by half will be applied for the optical sample, it is calculated in this analysis that the precision obtained by SNe Ia on Ω_M as the one in Conley et al. (2011) is reachable now, while the precision of Betoule et al. (2014) is reachable in 2026, and the precision of Scolnic et al. (2018) is reachable in 2042. All these results have been gathered in the tables 9 and 10 presented in Dainotti et al. (2022c). This shows the increasing importance the GRBs in the next decades for cosmological applications. Thus, with these two tandem papers we have shown that GRBs have not only the credibility to be used reliably as standard candles, but they can be an important aid and complementary tool together with the SNe Ia to extend the Hubble diagram at high redshifts. For a more complete discussion, we refer to the paper itself (Dainotti et al. 2022c).

9 SUMMARY, DISCUSSION AND CONCLUSIONS

The fundamental plane relation carried a $\sigma_{int} = 0.18 \pm 0.07$ when selection biases and redshift evolution is accounted for, which is the smallest intrinsic scatter in the current literature regarding GRB correlations involving the plateau emission. In this paper, we first investigate the reliability of the 3D fundamental plane as an intrinsic correlation when we correct for selection biases and redshift evolution, then we also study its application as a cosmological tool. To this end, we performed several tests to check the reproducibility of the parameters of the correlation, see Fig. 1, when we consider simulations of the evolutionary coefficients within a 1σ range. We also tested the reliability of the intrinsic scatter on the fundamental plane by showing the distribution of this quantity obtained with the HyperFit online routine, which uses many fitting methods to derive the best-fit parameters of the fundamental plane both with and without the evolutionary corrections, see Fig. 3. Before applying the fundamental plane relation corrected for the evolutionary effects as a cosmological tool, we investigate to which extent the parameters of the evolutionary functions, determined through statistical methods, depend on the cosmological ones, see Fig. 4. We find out that while the evolutionary parameters have no dependence on H_0 , on the other end, they depend on Ω_M , Ω_k and w . This discovery opens the way to the application of the evolution to the fundamental plane both considering fixed parameters for the evolution, as well as the evolutionary function dependent on Ω_M and in the future also on Ω_k and w . Thus, the application of the fundamental plane corrected for selection biases and redshift evolution allows us to estimate cosmological parameters for GRBs alone for the first time considering such correction.

To use GRBs as standalone cosmological probes, we have adopted two methods: the Fundamental plane (Equations 6, 7), and

the distance moduli, μ_{GRB} , variables (Equation 12), taking into account GRBs without calibration on SNe Ia, see 6.1, as well as considering these calibrations on SNe Ia, see 6.2. We have obtained cosmological parameters by GRBs alone using Gaussian priors of 3σ based on the values of SNe Ia, see Tables 1 and 2. We show the percentage change between the uncertainties of GRBs alone without and with calibration on SNe, see the seventh column of Table 2. We find that all the results lie within 1σ when comparing cases i-vi) both with and without calibration.

We, then, explored how strong the impact of the Gaussian priors is on our results and how much the parameter space of GRBs can be constrained. To do so, we obtain averaged cosmological parameter results over 100 runs performed by MCMC by GRBs alone using a uniform prior, see Sec. 6.3. Then, we compare the uncertainties on the results of GRBs alone using both Gaussian and the uniform priors, see the seventh column of Tables 3 and 4. We find that all the results obtained by GRBs alone using uniform priors lie within 1σ with respect to the cosmological ones obtained by GRBs alone using Gaussian priors both with and without the calibration on SNe Ia. We used as Gaussian priors the parameters based on the results of SNe Ia.

The uncertainties on the cosmological parameter values using μ_{GRB} for both Ω_M and H_0 obtained by GRBs alone are higher by 328.57%, 327.58% (without evolution and calibration, the upper part of Table 3); 328.57%, 384.42% (with fixed evolution and without calibration, the upper part of Table 3); 326.47%, 348.29% (without evolution and with calibration, the upper part of Table 4); 297.06%, 306.57% (with fixed evolution and calibration, the upper part of Table 4), respectively, than the uncertainties on the results obtained using Gaussian priors of 3σ .

We then note that the uncertainties on the value of Ω_M using the $k(\Omega_M)$ evolutionary function, both without and with calibration on SNe Ia using μ_{GRB} , are higher by 335.48% and 328.57%, respectively (Table 3) than the ones obtained using Gaussian priors of 3σ .

Surprisingly, the uncertainties on the values of w using μ_{GRB} and uniform priors for the case of no evolution and fixed evolution and for no calibration are smaller than the values of w with Gaussian priors by 19.11% and 6.45% (upper panel of Table 3), respectively, while for the case considering the calibration on SNe Ia they are smaller in both of without evolution (16.42%) and with evolution (16.43%) cases, the upper panel of Table 4. This difference may be due to the fact that the variation in w is smaller than the variation of H_0 ($50 < H_0 < 100$) and Ω_M ($0 < \Omega_M < 1$).

Now, considering the Fundamental plane Equations 6 and 7, the uncertainties on the values for both Ω_M and H_0 obtained by GRBs alone are higher by 359.01%, 355.19% (without evolution and without calibration, the lower part of Table 3); 315.38%, 356.49% (with fixed evolution and without calibration, the lower part of Table 3); 305.80%, 337.32% (without evolution and with calibration, the lower part of Table 4); 366.67%, 338.11% (with fixed evolution and with calibration, the lower part of Table 4), respectively, than the uncertainties on the correspondent results obtained using Gaussian priors of 3σ based on the results of SNe Ia.

Also, when using $k(\Omega_M)$ evolutionary function without and with calibration on SNe Ia using Equations 6 and 7, uncertainties on the value of Ω_M are higher by 328.57% and 283.56%, respectively, than the correspondent results obtained using Gaussian priors of 3σ .

Similarly to the results obtained with the μ_{GRB} , when we compare the values of w using the Fundamental plane Equations 6 and 7 with and without evolution, respectively, in the case without calibration, the uncertainties on w using uniform priors for the case without evolution and fixed evolution are smaller than the values of w with Gaussian priors by 44.65% and 12.39%, respectively (lower part of Table 3). In the case of calibration on SNe Ia, the values of w are smaller in the cases of no evolution (18.22%) and with evolution (9.67%) (lower part of Table 4). We have also computed the percentage change of the uncertainties between the results obtained by GRBs alone with Gaussian priors without calibration and with calibration on SNe Ia, see the last two columns of Tables 7 and 8, respectively, with the results obtained by SNe Ia alone and SNe + BAOs. We have concluded from this analysis that SNe Ia alone and SNe Ia + BAO have tighter constraints on the cosmological parameters than GRBs alone.

To better understand what the advantage of using Gaussian priors is with respect to uniform priors in the comparison with other probes, we have then computed the z-scores of GRBs alone with respect to the SNe Ia alone and SNe Ia + BAO results, see the last two columns of Tables 1, 2, 3, 4. The last two columns of Tables 1 and 2, present GRB results alone using Gaussian priors compared with the SNe Ia and SNe Ia + BAO with no calibration and with calibration, respectively, see Sec. 7 for more details. The last two columns of Tables 3 and 4, present the same comparison among the GRBs alone and SNe Ia and SNe Ia+BAO results, but using uniform priors.

More specifically, we first consider the comparison with SNe Ia using both the μ_{GRB} (upper panels of Tables 1 and 2) and the fundamental plane equations 6 and 7 (lower panels of Tables 1 and 2) using Gaussian priors. In relation to the cases of no calibration, we obtain that all cases have z-score < 1 with the only exception of H_0 , for which the maximum z-score = 1.025 in the case of Ω_M and H_0 varied contemporaneously without considering evolution. In relation to the cases with calibration, we obtain that in all cases z-score < 1 with the only exception of H_0 without evolution varied alone for which the maximum z-score is 1.137.

Now we consider the comparison between SNe Ia+ BAO and GRBs with both μ_{GRB} and the fundamental plane Equations 6 and

7, see Table 1 and Table 2 using Gaussian priors. In relation to the cases of no calibration, we obtain that all cases have z -score < 1 with the only exception of H_0 for which the maximum z -score = 1.10 in the case of Ω_M and H_0 varied contemporaneously with fixed evolution. In relation to the cases considering the calibration, we obtain that in all cases z -score < 1 , with the only exception of H_0 for which the maximum z -score is 1.176 in the case of Ω_M and H_0 varied contemporaneously without considering evolution.

Now, we consider the comparison with SNe Ia using both the μ_{GRB} (upper panels of Tables 3 and 4) and the fundamental plane equations 6 and 7 (lower panels of Tables 3 and 4) using uniform priors. In relation to the cases of no calibration, we obtain that all cases have z -score < 1 with the only exception of Ω_M for which the maximum z -score = 1.040 in the case when Ω_M only is varied without considering evolution. In relation to the cases with calibration, we obtain that in all cases z -score < 1 with the only exception of Ω_M with fixed evolution varied alone for which the maximum z -score is 1.077.

Now we consider the comparison between SNe Ia+ BAO and GRBs with both μ_{GRB} and the fundamental plane Equations 6 and 7, see Table 3 and Table 4 using uniform priors. In relation to the cases of no calibration, we obtain that all cases have z -score < 1 with the only exception of Ω_M for which the maximum z -score = 1.022 in the case when Ω_M only is varied without evolution. In relation to the cases considering the calibration, we obtain that in all cases z -score < 1 , with the only exception of Ω_M for which the maximum z -score is 1.059 in the case when Ω_M only is varied contemporaneously with fixed evolution. The most notable comparison is achieved between SNe Ia, SNe Ia + BAO vs SNe Ia + BAO + GRBs using a uniform prior, for the cases of both without and with correction for evolution, see Table 5. For the case without correction for evolution, we reduced the scatter related to Ω_M by 14.3%, Ω_M and H_0 by 68.2% and 55.9% when varied together, and w by 22.2%, in comparison to the results obtained by SNe Ia alone. For the case of correction for evolution, we reduced the scatter related to Ω_M by 14.3%, Ω_M and H_0 by 68.2% and 52.9% when varied together, and w by 16.7%, in comparison to the results obtained by SNe Ia alone. All our results are consistent at the 68% level with the Λ CDM model. The crucial points of our derivations are: 1) we have obtained cosmological parameters compatible with the Λ CDM model; 2) in all cases, except for H_0 , we obtained a smaller intrinsic scatter by using GRBs + SNe Ia +BAO compared to SNe Ia alone, see subsection 6.4.

From this analysis we have concluded that, even if uncertainties are smaller in the SNe Ia alone and SNe Ia+BAO cases, GRBs alone can still be used to verify if cosmological parameters are compatible with the ones inferred by the SNe Ia. Indeed, we may conclude that GRBs alone can be used as cosmological tools, which carry the great advantage of being observed up to $z = 5$ in the Platinum sample case.

We have also computed the z -scores of GRBs alone using a uniform prior with respect to the SNe Ia alone and SNe Ia + BAO results, see last two columns of Tables 3 and 4, to check the compatibility of the GRBs results using a uniform prior with the SNe Ia and SNe Ia + BAO ones, see Sec. 7. We obtained the maximum z -score of 1.077 for the Ω_M parameter when it is varied with fixed evolution and when we compare SNe Ia results with the ones obtained with calibrated GRBs alone using the μ_{GRB} likelihood. Surprisingly, the average results of GRBs alone using uniform priors do not change even if we correct for evolution, both fixing the parameters as well as using a function for the evolution, see Tables 3 and 4. However, it is very likely that this result is due to the paucity of the sample size, given that when we simulate 800 GRBs starting from the ones closest to the fundamental plane (Dainotti et al. 2022c) we do not recover these results. On the other hand, the closest GRBs to the plane in the simulated data have been built with a given fiducial cosmology. Thus, it is necessary to wait for additional data to come with future missions, such as SVOM and Theseus (Wei et al. 2016; Amati et al. 2018) to cast light on this discrepancy. Very interestingly, also other probes at high redshift, like the quasars, show a tendency to have a higher value of Ω_M (Colgàin et al. 2022). Although this discussion surely deserves much attention, it is far beyond the scope of the current paper.

Although results related to GRB cosmology have been reached by previous studies for the prompt correlation (Amati et al. 2008; Kodama et al. 2008; Wang et al. 2016; Demiansky et al. 2017; Luongo & Muccino 2020) and the Combo relation (Izzo et al. 2015), this is the first time cosmological constraints have been achieved considering a 3D correlation involving the plateau, and it is also the first time the evolutionary parameters have been included in the computation of cosmological ones, thus allowing a road-map for a new methodology to treat selection biases and redshift evolution contemporaneously inside the cosmological setting.

FUNDING

This work is supported by JSPS Grants-in-Aid for Scientific Research “KAKENHI” (A: Grant Number JP19H00693). N.F. acknowledges the support from UNAM-DGAPA-PAPIIT through grant IA102019.

ACKNOWLEDGMENTS

This work made use of data supplied by the UK Swift Science Data Centre at the University of Leicester. We are grateful to E. Rinaldi for helping in the discussion of the constants in the fundamental parameters and useful comments about the manuscript, to B. De Simone for the help in the analysis of the SNe Ia's likelihood, and to G. Srinivasaragavan, R. Wagner, L. Bowden, Z. Nguyen for the help in the fitting of the parameters of the LCs. Z. Kania and J. Fernandez for helping to run our cosmological computations. We are particularly grateful to Dr. Cuellar for managing the SULI program during the summer of 2020. S.N also acknowledges the support from the Pioneering Program of RIKEN for Evolution of Matter in the universe (r-EMU). We thank the RIKEN HOKUSAI BigWaterfall cluster system for the computational time. A. Lenart is grateful for the financial support from the NAOJ Division of Science.

10 DATA AVAILABILITY STATEMENT

The data underlying this article will be shared upon reasonable request to the corresponding author.

REFERENCES

- Abbott, B. P., 2017, *Phys. Rev. Lett.*, 119, 16, id. 161101;
- Ai, S., et al., *ApJ*, 2018, 860, 1, 57;
- Abdalla E., Abellán G. F., Aboubrahim A., Agnello A., Akarsu Ö., Akrami Y., Alestas G., et al., 2022, *JHEAp*, 34, 49. doi:10.1016/j.jheap.2022.04.002
- Amati, L., Frontera, F., Tavani, M., et al., 2002, *A & A*, 390, p.81-89;
- Amati L., Guidorzi C., Frontera F., Della Valle M., Finelli F., Landi R., Montanari E., 2008, *MNRAS*, 391, 577. doi:10.1111/j.1365-2966.2008.13943.x
- Amati, L., et al., 2018, *Advances in Space Research*, 62, 1, 191-244;
- Amati, L., D'Agostino, R., Luongo, O., Muccino, M., & Tantalò, M., 2019, *MNRAS*, 486, 1, L46-L51;
- Betoule M., Kessler R., Guy J., Mosher J., Hardin D., Biswas R., Astier P., et al., 2014, *A&A*, 568, A22. doi:10.1051/0004-6361/201423413
- Bernardini, M. G., Margutti, R., Zaninoni, E., & Chincarini, G., 2012, *MNRAS*, 425, 2, pp. 1199-1204.
- Bernardini, F., de Martino, D., Falanga, M., Mukai, K., Matt, G., Bonnet-Bidaud, J.-M., Masetti, N., & Mouchet, M., *A & A*, 542, id. A22, 18 pp.
- Bloom, J. S., Frail, D., A., & Sari, R., 2001, *ApJ*, 121, 6, pp. 2879-2888;
- Bryant C. M., Osborne J. A., Shahmoradi A., 2021, *MNRAS*, 504, 4192. doi:10.1093/mnras/stab1098
- Cardone, V. F., Dainotti, M. G., Capozziello, S., & Willingale, R., 2010, *MNRAS*, 408, 2;
- Cao S., Khadka N., Ratra B., 2022, *MNRAS*, 510, 2928. doi:10.1093/mnras/stab3559
- Cao S., Dainotti M., Ratra B., 2022, *MNRAS*, 512, 439. doi:10.1093/mnras/stac517
- Colgàin, E. Ó., Sheikh-Jabbari, M. M., Solomon, R., Bargiacchi, G., Capozziello, S., Dainotti, M. G., & Stojkovic, D., 2022, arXiv:2203.10558;
- Conley, A., et al., 2011, *ApJS*, 192, 1, 1;
- Dainotti M. G., Ostrowski M., Willingale R., 2011, *MNRAS*, 418, 2202. doi:10.1111/j.1365-2966.2011.19433.x;
- Dainotti M., Petrosian V., Willingale R., O'Brien P., Ostrowski M., Nagataki S., 2015, *MNRAS*, 451, 3898. doi:10.1093/mnras/stv1229;
- Contopoulos, I., & Spitkovsky, A., 2006, *ApJ*, 643, 2;
- Cucchiara, A., et al., 2011, *ApJ*, 736, 1;
- D'Agostini, G., 2005, arXiv:physics/0511182;
- Dainotti, M. G., Cardone, V. F., & Capozziello, S., 2008, *MNRAS*, 391, 1, L79-L83;
- Dainotti, M. G., Willingale R., Capozziello S., Cardone, F. V., Ostrowski, M.; *ApJL*, 2010, 772, pp. L215-L219;
- Dainotti M. G., Ostrowski M., Willingale R., 2011, *MNRAS*, 418, 2202. doi:10.1111/j.1365-2966.2011.19433.x
- Dainotti, M. G., Cardone, V. F., Piedipalumbo, E., & Capozziello, S., 2013a, *MNRAS*, 436, 1, 82-88;
- Dainotti, M. G., Petrosian, V., Singal, J., & Ostrowski, M., 2013b, *ApJ*, 774, 157;
- Dainotti, M. G., Del Vecchio, R., Nagataki, S., & Capozziello, S., 2015, *ApJ*, 800, 31;
- Dainotti, M. G., Petrosian, V., Willingale, R., O'Brien, P., Ostrowski, M., & Nagataki, S., 2015, *MNRAS*, 451, 4;
- Dainotti, M. G., Postnikov, S., Hernandez, X., & Ostrowski, M., 2016, *ApJL*, 825, 2, id L20, 6.
- Dainotti, M. G., & Del Vecchio, R., 2016, *NAR*, 77, pp. 23-61.
- Dainotti, M. G., Nagataki, S., Maeda, K., Postnikov, S., & Pian, E., 2017b, *A&A*, 600A, 98.
- Dainotti, M. G., Hernandez, X., Postnikov, S., Nagataki, S., O'Brien, P., Willingale, R., & Striegel, S. 2017, *ApJ*, 848, 88;
- Dainotti, M. G., & Amati, L., 2018, *PASP*, 130, 987;
- Dainotti, M. G., Del Vecchio, R., & Tarnopolski, M., 2018, *Adast*, 2018, id.4969503;
- Dainotti, M. G., Lenart, A., Sarracino, G., Nagataki, S., Capozziello, S., & Fraija, N., 2020, *ApJ*, 904, 2;
- Dainotti, M. G., De Simone, B., Schiavone, T., Montani, G., Rinaldi, E., & Lambiase, G., 2021, *ApJ* 912, 2, id.150;
- Dainotti, M. G., Petrosian, V., Bowden, L., 2021, *ApJL*, 914, 2, id. L40;
- Dainotti, M. G., Nielson, V., Sarracino, G., Rinaldi E., Nagataki, S., Capozziello, S., Gnedin O. Y., & Bargiacchi, G., 2022, *MNRAS*, 514, 2, pp.1828-1856.
- Dainotti M. G., De Simone B. D., Schiavone T., Montani G., Rinaldi E., Lambiase G., Bogdan M., et al., 2022, *Galax*, 10, 24. doi:10.3390/galaxies10010024
- Dainotti M. G., Bargiacchi G., Lenart A. L., Capozziello S., Ó Colgáin E., Solomon R., Stojkovic D., et al., 2022, *ApJ*, 931, 106. doi:10.3847/1538-4357/ac6593
- Dall'Osso, S., Stratta, G., Guetta, D., Covino, S., De Cesare, G., & Stella, L., 2011, *A & A*, 526, id.A121, 7 pp;
- Della Valle, M., et al., 2006, *Nature*, 444, 7122, pp. 1050-1052;
- Demiansky, M., Piedipalumbo, E., Sawant, D., & Amati, L., 2017, *A&A*, 598, id.A113, 10 pp;
- Di Valentino, E., Melchiorri, A. & Silk, J., 2020, *Nat Astron*, 4, pp. 196-203;
- Djorgovski, S., & Davis, M., 1987, *ApJ*, 313, p59;
- Efron, B., Petrosian, V., 1992, *ApJ*, 399, p.345;

- Eichler, D., Livio, M., Piran, T., & Schramm, D. N., 1989, *Nature*, 340, 126;
- Evans, P. A., Beardmore, A. P., Page, K. L., et al. 2009, *MNRAS*, 397, 3, 1177;
- Evans, P. A., et al., 2010, *A&A*, 519, id.A102;
- Fraija, N. and Veres, P., 2018, *ApJ*, 859, 1, 70;
- Fraija, N., Veres, P., Beniamini, P., Galvan-Gamez, A., Metzger, B. D., Barniol Duran, R., & Becerra, R., L., 2020, arXiv:2003.11252;
- Fraija, N., Laskar, T., Dichiaro, S., Beniamini, P., Barniol Duran, R., Dainotti, M. G., & Becerra, R., L., 2020, *ApJ*, 905, 112;
- Hascoet, R., Daigne, F., & Mochkovitch, R., 2014, *MNRAS*, 442, 1;
- Ghirlanda, G., Ghisellini, G., Lazzati, D., 2004, *ApJ*, 616, 1, p. 331-338; 29
- Izzo, L., Muccino, M., Zaninoni, E., Amati, L., & Della Valle, M., 2015, *EDP Sciences*, 582, A115;
- Jha, et al., 2006, *ApJ*, 131, 1, 527-554;
- Kodama, Y., et al., 2008, *MNRASL*, 391, 1, L1-L4;
- Kouveliotou, C., Meegan, C. A., Fishman, G. J., Bhat, N. P., Briggs, M. S., Kosshut, T. M., Paciesas, W. S., & Pendleton, G., N. 1993, *ApJ*, 413, 2, L101;
- Kumar, P., Zhang, B., 2015, *Physics Reports*, 561, pp 1-109;
- Lattimer, J. M. & Schramm, D. N., 1976, *ApJ*, 210, 1, 54;
- Li, L.-X., & Paczyński, B., 1998, *ApJ*, 507, 1, pp. L59-L62;
- Li L., et al., 2015, *ApJ*, 805, 13;
- Liang, E., & Zhang, B., 2005, *ApJ*, 633, 2, pp. 611-623.
- Liang, E., Yi, S., Zhang, J., Lü, H.-J., Zhang, B.-B., & Zhang, B., 2010, *ApJ*, 725, 2, 2209-2224;
- Liang, L., Wu, X.-F., Lei, W.-H., Dai, Z.-G., Liang, E.-W., & Ryde, F., 2018, *ApJS*, 236, 2, article id. 26, 31 pp;
- Lien, A., et al., 2016, *ApJ*, 829, 1, id. 7;
- Liu, R. X., Kuang, J., Gong, Q., & Hou, X. L., 2003, *Computer Methods and Programs in Biomedicine*, 71, 2;
- Liu Y., Chen F., Liang N., Yuan Z., Yu H., Wu P., 2022, *ApJ*, 931, 50. doi:10.3847/1538-4357/ac66d3
- Liu Y., Liang N., Xie X., Yuan Z., Yu H., Wu P., 2022, arXiv, arXiv:2207.00455
- Livio, M. & Mazzali, P., 2018, *Physics Reports*, 736, pp. 1-123;
- Luongo, O., & Muccino, M., 2020, *A&A*, 641, id.A174, 15pp.
- MacFadyen, A., & Woosley, S. E., 1999, *ApJ*, 524, 1, 262-289;
- Nagataki, Shigehiro and Takahashi, Rohta and Mizuta, Akira and Takiwaki, Tomoya, 2007, *ApJ*, 659, 1, 512-529;
- Nagataki, S., 2009, *ApJ*, 704, 2, 937-950;
- Nagataki, Shigehiro, 2011, *ApJ*, 63,1, 1243-1249;
- MacFadyen, A., Woosley, S. E., Heger A., 2001, *ApJ*, 550, 1, 410;
- Margutti, R., et al., 2013, *MNRAS*, 428, pp. 729-742;
- Komissarov, Serguei S. and Barkov, Maxim V., 2007, *MNRAS*, 382,3, pp. 1029-1040;
- Barkov, Maxim V. and Komissarov, Serguei S., 2008, *MNRAS*, 385,1, pp. L28-L32;
- Ito, Hirotaka and Matsumoto, Jin and Nagataki, Shigehiro and Warren, Donald C. and Barkov, Maxim V., 2015, *ApJ*, 814,2, pp. L29;
- Ito, Hirotaka and Just, Oliver and Takei, Yuki and Nagataki, Shigehiro, 2021, *ApJ*, 918,2, pp. 59;
- Ito, Hirotaka and Matsumoto, Jin and Nagataki, Shigehiro and Warren, Donald C. and Barkov, Maxim V. and Yonetoku, Daisuke, 2019, *NatCo*, 10, pp. 1054;
- Warren, Donald C. and Ellison, Donald C. and Barkov, Maxim V. and Nagataki, Shigehiro, 2017, *ApJ*, 835,2, pp. 248;
- Warren, Donald C. and Barkov, Maxim V. and Ito, Hirotaka and Nagataki, Shigehiro and Laskar, Tanmoy, 2018, *MNRAS*, 480,3, pp. 4060-4068;
- Wang F. Y., Dai Z. G., Zhu Z.-H., 2007, *ApJ*, 667, 1. doi:10.1086/520768
- Mazets, E. P., et al., 1981, *Astrophys. Space Sci.*, 80, 1, 3;
- Meszáros, P. and Rees, M. J., *MNRAS*, 269, 1, L41 - L43;
- Moresco M., Amati L., Amendola L., Birrer S., Blakeslee J. P., Cantiello M., Cimatti A., et al., 2022, arXiv, arXiv:2201.07241
- Morsony, B. J., Workman, J. C., & Ryan, D. M., 2016, *ApJL*, 825, L24;
- Narayan, R., Paczynski, B., & Piran, T. 1992, *ApJ*, 395, L83;
- O'Brien, P. T., et al., 2006, *ApJ*, 647, 2, 1213;
- Perlmutter S., et al., 1999, *ApJ*, 517, 2, 565;
- Paczynski, B., 1986, *ApJ*, 308, L43-L46;
- Panaiteescu, A. & Vestrand, W. T., 2011, *MNRAS*, 414, 4, 3537;
- Perley D. A., et al., 2014, *ApJ*, 781, 37;
- Petrosian, V., Kitanidis, E., & Kocevski, D., 2015, *ApJ*, 806, 1, 44;
- Piran, T., 2004, *Rev. of Modern Physics*, 76, 4;
- Planck Collaboration, Planck 2018 results. VI. Cosmological parameters, 2018, arXiv:1807.06209;
- Postnikov, S., Dainotti, M. G., Hernandez, X., & Capozziello, S., 2014, *ApJ*, 783, 2, 126;
- Rea, N., Gullón, M., Pons, J. A., Perna, R., Dainotti, M. G., Miralles, J. A., & Torres, D. F., 2015, *ApJ*, 813, 92;
- Reichart, D. E., 2001, *ApJ*, 553, pp 235-253;
- Riess, A. G., et al., 1998, *ApJ*, 116, 3, pp- 1009-1038;
- Robotham, A. S. G., & Obreschkow, D., 2015, *Publications of the Astronomical Society of Australia*, 32, id.e033 14 pp.;
- Rodney, S. A., et al., 2015, *ApJ*, 150, 5, id. 156;
- Rowlinson, A., Gompertz, B. P., Dainotti, M. G., O'Brien, P. T., Wijers, R. A. M. J., & van der Horst, A. J., 2014, *MNRAS*, 443, 2, 1779-1787;
- Sakamoto, T., et al., 2007, *ApJ*, 669, 2, 1115;
- Sakamoto, T., et al. 2011, *ApJS*, 195, 2;
- Sari, R., Piran, T., & Narayan, R., 1998, *ApJ*, 497, 1, L17-L20;
- Scolnic, D. M., et al., 2018, *ApJ*, 859, 101;
- Sharov G. S., Vasiliev V. O., 2018, arXiv, arXiv:1807.07323;
- Shun-Kun, S., et al., 2018, *ApJ*, 863, 1, 50;
- Srinivasaragavan, G. P., Dainotti, M. G., Fraija, N., Hernandez, X., Nagataki, S., Lenart, A., Bowden, L. & Wagner, R., 2020, *ApJ*, 903, 1, id. 18;
- Stanek, K. Z., et al., 2003, *ApJ*, 591, 1, L17-L20;
- Stratta, G., Dainotti, M. G., Dall'Osso, S., Hernandez, X., & De Cesare, G., 2018, *ApJ*, 869, 2, 155;

- Tang, C., Huang, Y., Geng, J., & Zhang, Z.-B., 2019, *ApJS*, 245, 1, 1;
- Tanvir N. R., Fox D. B., Levan A. J., Berger E., Wiersema K., Fynbo J. P. U., Cucchiara A., et al., 2009, *Natur*, 461, 1254. doi:10.1038/nature08459
- Troja, E., et al., 2017, *Nature*, 551, 7678, pp. 71-74;
- Usov, V. V., 1992, *Nature*, 357, 6378, pp. 472-474;
- van Eerten, H., J.; 2014, *MNRAS*, 442, 4, p.3495-3510;
- van Eerten, H., J.; 2014, *MNRAS*, 445, 3, p.2414-2423;
- Wei, J., et al., 2016, arXiv:1610.06892;
- Wen, Z., et al., 2020, *ApJ*, 900, 2, 112, P11;
- Wang, J. S., Wang, F., Y., Cheng K., S., & Dai F., G., *A & A*, 585, id. A68.
- Willingale, R., et al., 2007, *ApJ*, 662, 1093;
- Woosley, S. E., Langer, N., Weaver, T. A., 1993, *ApJ*, 405, 1, 273;
- Xiao, L. & Schaefer, B.E. 2009, *ApJ*, 707, 387;
- Xu, M., & Huang, Y. F., 2012, *A & A* 538, A134;
- Yonetoku, D., Murakami, T., Nakamura, T., Yamazaki, R., Inoue, A. K., & Ioka, K., 2004, *ApJ*, 609, 2, pp. 935-951;
- Zaninoni, E., Bernardini, M. G., Margutti, R., & Amati, L., 2016, *MNRAS*, 455, 2, p.1375-1384;
- Zhang, B., Fan, Y. Z., Dyks, J., Kobayashi, S., Mészáros, P., Burrows, D. N., Nousek, J. A., & Gehrels, N., 2006, *ApJ*, 642, 1, 354;
- Zhao, L., Zhang, B., Gao, H., Lan, L., Lü, H., & Zhang, B., 2019, *ApJ*, 883, 1, 97;

AN EXAMPLE OF A RESEARCH NOTE OF THE AMERICAN ASTRONOMICAL SOCIETY (RNAAS)

Ethan Vishniac,^{1,*} Chris Lintott,^{2,†} **Greg J. Schwarz,**³ and August Muench³

¹*Johns Hopkins University*

²*Oxford University*

³*American Astronomical Society
2000 Florida Ave., NW, Suite 300
Washington, DC 20009-1231, USA*

Keywords: editorials, notices — miscellaneous — catalogs — surveys

Research Notes of the American Astronomical Society (RNAAS) is a publication in the AAS portfolio (alongside ApJ, AJ, ApJ Supplements, and ApJ Letters) through which authors can promptly and briefly share materials of interest with the astronomical community in a form that will be searchable via ADS and permanently archived.

The astronomical community has long faced a challenge in disseminating information that may not meet the criteria for a traditional journal article. There have generally been few options available for sharing works in progress, comments and clarifications, null results, and timely reports of observations (such as the spectrum of a supernova), as well as results that wouldn't traditionally merit a full paper (such as the discovery of a single exoplanet or contributions to the monitoring of variable sources).

Launched in 2017, RNAAS was developed as a supported and long-term communication channel for results such as these that would otherwise be difficult to broadly disseminate to the professional community and persistently archive for future reference.

Submissions to RNAAS should be brief communications - 1,000 words or fewer ¹, and no more than a single figure (e.g. Figure 1) or table (but not both) - and should be written in a style similar to that of a traditional journal article, including references, where appropriate, but not including an abstract.

Unlike the other journals in the AAS portfolio, RNAAS publications are not peer reviewed; they are, however, reviewed by an editor for appropriateness and format before publication. If accepted, RNAAS submissions are typically published within 72 hours of manuscript receipt. Each RNAAS article is issued a DOI and indexed by ADS (Kurtz et al. 2000) to create a long-term, citable record of work.

Articles can be submitted in L^AT_EX (preferably with the new "RNAAS" style option in AASTeX v6.2), MS/Word, or via the direct submission in the [Authorea](#) or [Overleaf](#) online collaborative editors.

Authors are expected to follow the AAS's ethics (Kennicutt et al. 2006), including guidance on plagiarism (Vishniac 2012).

Acknowledge people, facilities, and software here but remember that this counts against your 1000 word limit.

Corresponding author: August Muench
greg.schwarz@aaas.org, august.muench@aaas.org

* Editor-in-Chief

† RNAAS Editor

¹ An easy way to count the number of words in a Research Note is to use the `texcount` utility installed with most L^AT_EX installations. The call `texcount -incbib -v3 rnaas.tex` gives 57 words in the front matter and 493 words in the text/references/captions of this template. Another option is by copying the words into MS/Word, and using "Word Count" under the Tool tab.

Topical Corridors

- GALAXIES AND COSMOLOGY
- HIGH-ENERGY PHENOMENA AND FUNDAMENTAL PHYSICS
- STARS AND STELLAR PHYSICS
- THE SOLAR SYSTEM, EXOPLANETS, AND ASTROBIOLOGY
- INTERSTELLAR MATTER AND THE LOCAL UNIVERSE
- THE SUN AND THE HELIOSPHERE
- INSTRUMENTATION, SOFTWARE, LABORATORY ASTROPHYSICS, AND DATA

Announcing *The Research Notes of the AAS*

We are pleased to announce a new venue for authors to promptly and briefly share materials of interest with the astronomical community: *The Research Notes of the American Astronomical Society*. Prof. Chris Lintott will be the *Research Notes Editor* and submissions are now being accepted. Research Notes are free to read and currently carry no author publication charges. [Read more](#)

Author Services

- Submit an article to the AAS Journals (*AJ, ApJ, ApJS*)
- Submit a Letter (*ApJL*)
- Submit a Research Note (*RNAAS*)

Access Our Journals

- THE ASTRONOMICAL JOURNAL
- THE ASTROPHYSICAL JOURNAL
- THE ASTROPHYSICAL JOURNAL LETTERS
- THE ASTROPHYSICAL JOURNAL SUPPLEMENT SERIES
- RNAAS RESEARCH NOTES OF THE AAS

Figure 1. Top page of the AAS Journals' website, <http://journals.aas.org>, on October 15, 2017. Each RNAAS manuscript is only allowed one figure or table (but not both). Including the data behind the figure in a Note is encouraged, and the data will be provided as a link in the published Note.

REFERENCES

- Kennicutt, R. C., Jr., Vishniac, E., & Sneden, C. 2006, *ApJ*, 652, 847
- Kurtz, M. J., Eichhorn, G., Accomazzi, A., et al. 2000, *A&AS*, 143, 41
- Vishniac, E. T. 2012, American Astronomical Society Meeting Abstracts #219, 219, 204.04